Assessment of Geochemical Reactivity in Geologic CO_2 Utilization and Storage Systems

By

Chidera O. Iloejesi

A dissertation submitted to the Graduate Faculty of
Auburn University
In partial fulfillment of the
requirements for the Degree of
Doctor of Philosophy

Auburn, Alabama
July 18, 2022

CO_2-brine-mineral reaction, reactive transport modeling, energy storage, CO_2 mineralization and solubility trapping, porous aquifer properties.

Copyright 2022 by Chidera O. Iloejesi

Approved by

Lauren E. Beckingham, Chair, Assistant Professor, Department of Civil and Environmental Engineering
Mark O. Barnett, Professor, Department of Civil and Environmental Engineering
Natalie L. Capiro, Assistant Professor, Department of Civil and Environmental Engineering
Ming-kuo Lee, Professor and Chair, Department of Geosciences
Michael P. Howard, Assistant Professor, Department of Chemical Engineering

Abstract

Increasing atmospheric carbon dioxide concentration is a consequence of increasing energy consumption. As a result, developing ways to manage excess CO_2 emissions has become a vital concern to avert the exacerbating effects of global warming. This has given rise to ideas for the utilization of greenhouse gases like CO_2 as cushion gas for energy storage systems and subsurface sequestration of excess captured greenhouse gases. The potential geochemical reactivity of CO_2 with brine in porous aquifers and corresponding implications on the operational system is uncertain. Additionally, the rate and extent of trapping, including how much of the injected CO_2 will be permanently stored as minerals, is not well understood. To enhance understanding of geochemical reactions in these systems with varying flow conditions and aquifer properties, this study will 1) use micro-continuum scale numerical simulations to assess the potential of utilizing CO_2 as a cushion gas for compressed energy storage and 2) leverage field-scale numerical simulations to evaluate the optimum aquifer properties for maximizing CO_2 sequestration in porous saline aquifers. Core scale reactive transport simulations were used to evaluate the geochemical reactions that occur during injection and extraction flow cycles for a compressed energy system in a porous saline formation using CO_2 as cushion gas. The results of the cyclic flow regime simulation for the energy storage scenario are compared with a model that simulates CO_2 sequestration by considering an injection-only flow regime. Results show that in the injection-only flow regime, larger extents of dissolution occur. The dissolution extent is limited during the continuous cyclic flow of acidified brine. This implies that CO_2 is a viable choice of cushion gas. Further investigation of the CO_2 potential as a cushion involves determining the impact of the operational schedule of a compressed energy system on the geochemical reaction pathway in the system. For this study, the operational schedule which comprises injection, withdrawal, and reservoir

closure was used to simulate the periodic operational schedule. This operational schedule was compared to the continuous injection and extraction cycling operational schedule to understand the impact of the storage duration. The geochemical reaction results show that the operational schedule does not have a significant effect on the geochemical evolution of the formation used for compressed energy storage. In addition, field scale reactive transport simulation is leveraged to enhance the understanding the influence of aquifer properties (porosity, permeability, depth, and carbonate mineralogy) on the overall geochemical reactivity in the reservoir and CO_2 trapping potential. Here, the simulations reveal that the considered aquifer properties impact the sequestration efficiency, defined as the rate at which the CO_2 injected into the aquifer is converted to aqueous or mineralized CO_2. Based on the studied properties, the impact of aquifer properties on CO_2 evolution depends on the stage of the sequestration project. The final study on the heterogeneity of aquifer shows that the potential to accurately estimate the sequestration efficiency of a formation will present more uncertainty during the injection phase which will reduce as the simulation timeline increases.

Acknowledgments

I thank God for this Ph.D. opportunity.

I am extremely grateful for the opportunity for having Dr. Lauren E. Beckingham as my mentor in this program. Dr. Lauren has been patient, available, and resourceful as she helps me to navigate these five years of my program. Her knowledge has not only impacted me as a researcher but as also has provided me with lessons that I can utilize in other areas of my life. Dr. Lauren is truly an inspiration.

I thank my family for their support during this program. To my mother who has been the rock for my brother and sister, I genuinely appreciate you. Being far away from home comes with its challenges that could cause instability. However, my family consistently made effort to present the positives in the situations that they face in their lives to avert distraction. I appreciate all the effort to provide me with the necessary mental and emotional stability to focus on my program.

I had the opportunity to come across great minds while being part of the WRISES research group. Fanqi Qin, Ishan Anjikar, Jeffery Steinwinder, Olivia Brunhoeber, Md. Fahim Salek, Parisa Asadi, Nora Rivera, and Abdullah Al Nahian. Also, I have had the opportunity to work with several undergraduate research students. This group of students is smart, lively, and collaborative. I am thankful for the opportunity to be part of such a collaborative group of talented students.

I am not a self-made individual. The path that has led me to this point in life has been paved by several helpful individuals. I appreciate your support. To my professors at Auburn University and the University of Nigeria, my education advisors at EducationUSA Nigeria, my colleagues and boss at Ove Arup, my students at Auburn University, and friends that I have share life with. Your impacts have made me a better person. Thank you all!

Table of Contents

List of Tables

List of Figures

Chapter 1

1.0 Introduction

Utilization of captured CO_2 and geologic CO_2 sequestration are essential approaches to reducing atmospheric CO_2 emissions. These processes can help make energy production from hydrocarbons more environmentally friendly as flue gases captured from these plants are utilized in an environmentally friendly way or injected into porous saline aquifers for permanent storage. However, one important concern is the geochemical consequences of CO_2. As a result, it will be important to understand the criteria for efficiency in utilizing and sequestering the injected CO_2. Previous studies have investigated various aspects of sequestering and utilizing CO_2 (Kharaka and Cole 2011; Z. Zhang and Huisingh 2017; De Coninck and Benson 2014a). These studies have also applied various experimental and modeling techniques toward this goal (C. I. Steefel et al. 2015; Xu, Apps, and Pruess 2004a).

In a porous saline aquifer, the CO_2-brine reactions create geochemical conditions that may result in mineral dissolution and precipitation reactions (Ahmmed et al. 2016a; Deng et al. 2017). However, the impact of the flow conditions of the CO_2-brine in the porous aquifer is not understood. During the operation of the CO_2 storage system, the added complexity of the flow cycle regime on the overall geochemical reaction in the storage aquifer is not well understood. These geochemical reactions have an impact on sequestration efficiency. Aquifer properties can also impact sequestration efficiency which has largely not been studied. This thesis provides an answer to how aquifer flow conditions and properties impact CO_2 sequestration. The specific flow conditions evaluated in this study include the uni-directional flow condition, bi-directional flow condition, and bi-directional flow condition with storage period. Also, the aquifer properties evaluated include the depth, porosity, permeability, and carbonate mineralogy. The relationship between these aquifer properties and flow conditions is evaluated with a numerical modeling technique to understand how it affects CO_2 sequestration in porous saline aquifers.

1.1 Assessment of Geochemical Limitations to Utilizing CO_2 as a Cushion Gas in Compressed Energy Storage Systems

Compressed Energy Storage (CES) in subsurface formations is a promising means of long-term, large-capacity, energy storage required to increase reliance on renewable energy by eliminating the fluctuation associated with renewable energy production. CES systems store and produce energy through injection and extraction of gas, referred to as a working gas. When energy production exceeds demands, the gas is injected into the storage formation and then extracted and used to drive a turbine and recover energy when demands exceed production. To establish the storage system, a cushion gas that will remain in the formation throughout the system operation is first injected followed by the working gas. CO_2 is a promising choice of cushion gas and previous studies on the utilization of CO_2 as a cushion gas have shown its properties may increase operational efficiency (C. M. Oldenburg, Stevens, and Benson 2004; Laille, Molinard, and Wents 1988; Dussaud 1989). However, the injection of CO_2 in saline aquifers has been studied extensively in the context of geologic CO_2 sequestration. These investigations have revealed dissolution of CO_2 into the formation brine following injection lowers pH and results in the dissolution of carbonate and aluminosilicate minerals, buffering pH and creating conditions favorable for precipitation of secondary minerals(Ketzer et al. 2009; Liu et al. 2013; Ellis et al. 2011; Gharbi et al. 2013; Xiong et al. 2018b; Zou et al. 2018b; Fazeli et al. 2019; Farquhar et al. 2013). In energy storage systems, these reactions may intensify the migration of the cushion gas away from the injection well and further into the formation or enhance the trapping of the cushion gas near the well, depending on if reactions result in increases or decreases in formation permeability.

As the CES system is established, the injection of the cushion gas to develop the gas bubble mimics that of geological CO_2 sequestration systems with unidirectional flow. Following this, however, CES systems deviate with the injection of a potentially

different composition working gas that is cycled over periods of hours to months for energy storage or production(Carden and Paterson 1979; Crotogino et al. 2010; Carr et al. 2014). The geochemical influence of the cyclic flow regime of CES systems on geochemical reactions at the cushion gas-brine interface in the porous aquifer is not well understood and is the focus of this work. This region is selected as it is anticipated to be the region most impacted by mineral dissolution reactions.

A reactive transport simulation for the cyclic flow conditions corresponding to energy storage in porous formations is developed. Simulation results are compared quantitatively and qualitatively to those for a similar system considering geological CO_2 sequestration in the same formation to deduce differences or similarities in potential geochemical reactions due to the flow regimes of the two systems. This work examines:

- The rate, extent, and impact of potential geochemical reactions at the gas dissolution zone under cyclic and uni-directional flow conditions.

- The evolution of formation brine, mineral volume fractions, and mineral porosity in the CO_2 sequestration system compared to the energy storage system.

1.2 Effect of Energy Storage on Geochemical Reactions in Porous Aquifer Energy Storage Systems

The intermittency of renewable energy production requires reliable storage to achieve energy security through renewable energy (van der Linden 2006). Efforts to increase and improve energy storage have included fast discharging, low capacity options like lead-acid batteries to slow discharging, and high capacity options like pumped hydro and compressed energy storage(Dunn, Kamath, and Tarascon 2011). The high-capacity options like compressed energy storage store bulk energy in

megawatts for hours to months, which offers increased reliability in grid-scale applications of renewable energy. The storage mechanism in the compressed energy storage system involves injecting cushion gas into the subsurface to maintain pressure and further injecting a working gas during the period of low energy demand and extracting the gas to power turbines during periods of high energy demand.

A variety of gases including nitrogen (Pfeiffer and Bauer 2015a; Bauer et al. 2015), native methane (Curtis M. Oldenburg 2003), and air (Succar and Williams 2008) have all been considered potential cushion gases. It was in the wake of geologic CO_2 sequestration that studies began to investigate the potential of using CO_2 as a cushion gas. While CO_2 is a favorable choice of cushion gas from its physical property point of view, there could be potential geochemical implications of reactions between CO_2, formation brine, and formation minerals that could pose to be a challenge to system operation (Z. Zhang and Huisingh 2017). A previous study by Iloejesi and Beckingham (2021) has shown that there is no geochemical limitation of continuously cycling of CO_2 as cushion gas for energy storage. The new challenge lies in the fact that there are different types of operational schedule that could result to different in flow conditions in energy storage systems. Operational schedules in most subsurface storage aquifers integrate duration of storage or shut-in which is when the injected gas is allowed to sit in the aquifer with little to no flow in the storage reservoir before it is extracted to meet demand. This operational schedule that includes duration of storage between the injection and extraction flow cycles can be referred to as the periodic schedule. The resulting geochemical reactions and implications for these types of operating conditions have not been considered. This study compares the difference between the already understood geochemical evolutions of porous aquifer–compressed energy storage systems operating with a continuous schedule with the geochemical evolution when the system operates using the periodic operational schedule. Here, reactive transport simulations are developed considering daily cyclic interactions

between CO_2 utilized as a cushion gas, formation brine, and formation minerals over a 15-year study period with the aim to enhance understanding of:

- The rate and extent of potential geochemical reactions in porous saline aquifer utilized for energy storage which operates using a periodic schedule.

- The evolution of major ions in the formation of brine, formation minerals, and porosity for each system is tracked and compared to aid in the understanding of the use of CO_2 as a cushion gas for compressed energy storage systems in porous saline aquifers operating with a periodic schedule.

1.3 Field Scale Insight Towards Understanding Impact of Aquifer Properties on Extent and Timeline of CO2 Trapping.

The geochemical timeline for attaining mineralization of injected CO_2, however, is not well understood. Several factors have been identified in previous studies that affect the efficiency and rate of mineralization in a storage site. This includes the vertical permeability of caprocks, the residual CO_2 saturation in aquifer rocks, the abundance of potential cations, and the reactive surface area of silicate rocks (Bourg, Beckingham, and DePaolo 2015). Core scale evaluation of potential target formations has identified the importance of abundant iron, magnesium, and calcium cations in silicate and oxide minerals which can neutralize acidified brine and eventually mineralize into new carbonates (S. Zhang and DePaolo 2017). It is shown that the ease with which these species can be released by the potential host rock can facilitate the further reaction and hence increase storage efficiency (Kelemen et al. 2011; J. M. Matter et al. 2016; B. Peter McGrail et al. 2017). The mineral reactive surface area has a noted impact on geochemical reactions where higher reactive surface areas increase the rate of mineral reactions (Qin and Beckingham 2021b).

While these nano- and microscale properties have shown to contribute significantly to understanding the storage efficiency, it is also important to understand how field-scale properties correlate to potential geochemical reactivity necessary for CO_2 trapping. Typically, field-scale subsurface characterization is conducted before CO_2 injection to determine aquifer suitability for storage. Most storage site investigations produce data on the porosity, permeability, mineralogy, stratigraphy, and depth and thickness of the storage formation(s). These are used to predict the stress-, and flow state of the subsurface and as indicators for the feasibility of subsurface CO_2 sequestration in the targeted formation. For instance, porosity and permeability are typically used to evaluate the ease of injection. Core samples extracted during borehole drilling can be used to help determine the mineral composition. The stratigraphy evaluation of the borehole log confirms the presence or absence of a caprock formation. The depth of storage is a critical factor to consider in most subsurface storage processes because of its impact in achieving a supercritical state of injected CO_2. Furthermore, depth influences aquifer deliverability (Pfeiffer and Bauer 2015b). Petrologically, the depth is critical in characterizing the texture and compactness of the formation grains. This implies that depth would have an impact on the permeability and porosity of the formation (X. Wang and Economides 2013). The trend typically shows that some deeper formations are less porous or permeable than shallower formations. The disparity in grain size distribution can be accentuated with increasing thickness of the formation. Despite this direct information gained during site investigation, the nano and core scale are typically used to infer the magnitude of potential geochemical reactions and CO_2 mineralization potential of a storage site.

This study conducts a field-scale simulation study of CO_2 sequestration to gain insight into how different aquifer properties could affect CO_2 trapping and the timeline of storage processes. Here, the evaluated aquifer properties include the depth of storage, aquifer thickness, the volume fraction of carbonate minerals, porosity, and permeability.

- The study approach simulates small to large variations of each aquifer property as compared to a base case model to evaluate the impact of each aquifer property on CO_2 trapping.

- This study will provide a metric to understand the relationship between aquifer properties and CO_2 trapping potential.

1.4 Impact of Aquifer Heterogeneity on Simulated CO_2 Trapping Mechanisms in Porous Saline Aquifers

Each time the subsurface is utilized for the development of CO_2 sequestration technology, there are myriads of potential considerations to guarantee the success of the project. Subsurface site investigation is one of the major approaches to ensure that storage aquifers meet these guidelines to guarantee the success of the project and the onsite safety of all concerned stakeholders involved in the project(Doughty et al. 2007). Hence, the site investigation process is initiated before developing a project to evaluate the several conditions that present opportunities and threats to the successful completion of the intended project(Niemi et al. 2017). An intensive subsurface site investigation is one of the major prerequisites to guaranteeing the onsite safety of all concerned stakeholders involved in the project (NETL 2015). The prohibitive cost of these site investigations implies that a select portion of the site is investigated. Hence, the suite of geological wellbore log information and core sample data used for estimating and evaluating the storage capacity and response of the entire formation to CO_2 injection is estimated from select points in the formation. Nevertheless, the borehole logging, geophysical mapping, core sample analysis, well testing, and geological mapping from these select spots still provide meaningful overall insights into the suitability of the target formation to store CO_2 storage.

However, the results from the field-scale site investigation show that the aquifer properties vary at different locations in the same aquifer (Zemke, Liebscher, and Wandrey 2010). Moreover, the heterogeneity of aquifer properties has been found to impact the fluid flow and the variation in aquifer property impacts the geochemical reaction to sequester CO_2 in the target formation (Wardlaw and Petroleum 1976; Weber 1982). This implies that if the aquifer properties that have been understood to control the CO_2-brine interaction vary beyond how it could be sufficiently generalized from field scale site investigation. Thus, an understanding of the impact of geologic heterogeneity encountered during the migration of the injected CO_2 away from the point of injection becomes necessary.

These formation heterogeneities are typically considered to be a result of the evolution in the grain size, geometry, and internal structure of the original sediment composition of the aquifer to the final structural features and diagenetic alterations (Morad et al. 2010). Lithological heterogeneities can result from various features like the alternating presence of good reservoir facie with poor quality facies as seen in Stuggart formation (Förster et al. 2006), or the presence of faults in a formation (Juhlin et al. 2007) which are all critical details that inform the vicinity and depth of injecting CO_2 in the subsurface. These lithological features influence the porosity and permeability of the formation. The lithological influence on the hydrogeological features affects the rate and transport of fluid in the subsurface which have been found to impact the CO_2-migration front to cause fingering effect and ultimately impacting injectivity(Lengler et al. 2010). Consequently, the micro-scale through hecto-scale heterogeneities in the formation exert influence to the formation that needs to be understood.

The model used for the study will simulate the heterogeneity impact on hydrogeology which would be captured by considering spatial heterogeneity of porosity in the model. The other model presented in this study will capture the impact of subsurface heterogeneity on the geochemical process by considering a spatial

heterogeneity of carbonate mineralogy in the model and the variation of aquifer temperature and pressure properties with depth. This study uses numerical modeling to analyze the CO_2 mineralization efficiency by answering the following question:

- What is the geochemical impact of spatial heterogeneity associated with geothermal gradient, porosity, and carbonate mineralogical composition on the sequestration efficiency of a heterogeneous formation?

- How does the heterogeneity impacts the prediction of sequestration efficiency of a formation?

Chapter 2: Assessment of Geochemical Limitations to Utilizing CO_2 as a Cushion Gas in Compressed Energy Storage Systems

Chidera O. Iloejesi; Lauren E. Beckingham*

Department of Civil and Environmental Engineering, Auburn University, Auburn, AL 36849

Published in Environmental Engineering Science 38(3), 2021, pp.115-126.

https://doi.org/10.1089/ees.2020.0345

Abstract

Compressed Energy Storage (CES) of air, CO_2, or H_2 in porous formations is a promising means of energy storage to abate the intermittency of renewable energy production. During operation, gas is injected during times of excess energy production and extracted during excess demands to drive turbines. Storage in saline aquifers using CO_2 as a cushion or working gas has numerous advantages over typical air storage in caverns. However, interactions between CO_2 and saline aquifers may result in potential operational limitations and have not been considered. This work utilizes reactive transport simulations to evaluate the geochemical reactions that occur during injection and extraction operational cycles for CES in a porous formation using CO_2 as cushion gas. Simulation results are compared with similar simulations considering an injection-only flow regime of geologic CO_2 storage. Once injected, CO_2 creates conditions favorable for the dissolution of carbonate and aluminosilicate minerals. However, the dissolution extent is limited in the cyclic flow regime where significantly smaller dissolution occurs after the first cycle such that CO_2 is a viable choice of cushion gas. In the injection-only flow regime, larger extents of dissolution occur as the fluid continues to be undersaturated with respect to formation minerals throughout the study period and porosity increased uniformly from 24.84% to 33.6% throughout the simulation domain. For the cyclic flow conditions, porosity increases non-uniformly to 31.1% and 25.8% closest and furthest from the injection well, respectively.

2.1 Introduction

Compressed Energy Storage (CES) in subsurface formations is a promising means of long-term, large-capacity, energy storage required to increase reliance on renewable energy and eliminate the fluctuation associated with renewable energy production(Succar and Williams 2008; Cavallo 2007; van der Linden 2006; Schoenung and Hassenzahl 2001). Potential geological storage formations include caverns and porous formations, such as depleted gas reservoirs and saline aquifers(Pfeiffer and Bauer 2015a; Ozarslan 2012; Bary et al. 2002; Bo Wang and Bauer 2017). Porous saline aquifers are particularly favorable due to their large potential storage capacity and the ubiquity of potential storage sites(Succar and Williams 2008; Bo Wang and Bauer 2017; Mouli-Castillo et al. 2019; Sopher et al. 2019). Porous saline aquifers, however, have not been previously used for compressed energy storage and involve additional complexities as compared to storage in caverns including multi-phase flow and geochemical reactions that are not well understood and may impact system operation or efficiency(Beckingham and Winningham 2019; R. D. Allen 1981).

CES systems store and produce energy through injection and extraction of a gas, referred to as a working gas. When energy production exceeds demands, the gas is injected into the storage formation and then extracted and used to drive a turbine and recover energy when demands exceed production. To establish the storage system, a cushion gas that will remain in the formation throughout the system operation is first injected followed by the working gas. The cushion gas may be the same or different in composition as the working gas but mainly serves to ensure adequate operational pressure to facilitate extraction(Carden and Paterson 1979). During injection of the cushion gas into the brine saturated porous aquifer, three distinct zones are created as the injected gas pushes brine away from the injection well(Cui et al. 2018). This includes a gas saturated or “dry-out” zone near the well surrounded by a two-phase gas and brine mixing zone and single-phase brine saturated zone furthest from the well (Figure 2.1). The working gas, the same or different in composition to the cushion gas,

is then injected into the porous aquifer and recycled for energy generation. Previous studies have identified that a third of volume of the injected gas is stored in the porous saline aquifer as cushion gas to ensure isobaric extraction during operation(Carden and Paterson 1979). At the gas/brine interface, gas dissolves into the brine phase and water into the gas phase, controlled by their mutual solubilities. Depending on the choice of working or cushion gas and storage formation, the properties of the gas phase may vary from ideality and some phases may even exist as supercritical phases in the storage formation where air, CO_2, H_2 and gas mixtures have been considered as working or cushion gases (Beckingham and Winningham 2019).

CO_2 is a promising choice of cushion gas where previous studies on utilization of CO_2 as a cushion gas have shown its properties may increase operational efficiency(C. M. Oldenburg, Stevens, and Benson 2004; Laille, Molinard, and Wents 1988; Dussaud 1989). At depths of typical storage formations, CO_2 will exist as a supercritical fluid, with a high density and high compressibility that translates to large storage capacity(Suekane et al. 2005; Curtis M. Oldenburg and Pan 2013b). Compressibility is an important property to consider in selecting the gas utilized in CES systems to minimize pressure variability during injection and extraction cycles, particularly for the selection of a cushion gas(Curtis M. Oldenburg 2003), where highly compressible phases will maintain pressures and enhance operational efficiency. The high heat capacity of CO_2(He et al. 2018) is also anticipated to favorably impact operational efficiency in comparison to the utilization of other working gases. Utilization of CO_2 as a cushion gas would provide additional environmental benefits via the reduction in anthropogenic greenhouse gas emissions and economic advantages in the form of the cost of recovering the cushion gas upon the end of project life span as the injected CO_2 can be permenently sequestered in the formation. This is in addition to additional benefits from carbon tax credits, as the cushion gas is injected periodically to sustain operational pressure during the operational lifespan(Metcalf 2009).

Injection of CO_2 in saline aquifers has been studied extensively in the context of geologic CO_2 sequestration. These investigations have revealed dissolution of CO_2 into formation brine following injection lowers pH and results in the dissolution of carbonate and aluminosilicate minerals, buffering pH and creating conditions favorable for precipitation of secondary minerals(Ketzer et al. 2009; Liu et al. 2013; Ellis et al. 2011; Gharbi et al. 2013; Xiong et al. 2018b; Zou et al. 2018b; Fazeli et al. 2019; Farquhar et al. 2013). These geochemical reactions may result in modifications to pore structures and connectivity(Gharbi et al. 2013; Xiong et al. 2018a; Luquot and Gouze 2009; Nogues et al. 2013) that alter permeability(Liu et al. 2013; Zou et al. 2018a),(Ketzer et al. 2009) and widen fractures(Ellis et al. 2011; Fazeli et al. 2019; Deng et al. 2018) in subsurface systems. In energy storage systems, these reactions may intensify the migration of the cushion gas away from the injection well and further into the formation or enhance trapping of the cushion gas near the well, depending on if reactions result in increases or decreases in formation permeability. If the migration of the cushion gas into the formation is promoted, the gas remaining near the well in the desired cushion gas zone that is required to maintain the pressure necessary for efficient cycling of the working gas during operation will decrease, reducing operational efficiency. This would also require more frequent injections of additional cushion gas to establish the pressure plume for operation. If migration of the cushion gas into the formation is further inhibited, operational efficiencies may actually increase as the pressure will be more easily maintained and the need to inject additional cushion gas will be reduced.

CO_2-cushioned CES systems can be carried out in the same porous aquifers as CO_2 sequestration(Kabuth et al. 2017) but the resulting geochemical conditions, reactions, and impact of resulting reactions are unknown. As the CES system is established, the injection of the cushion gas to develop the gas bubble mimics that of geological CO_2 sequestration systems with unidirectional flow. Following this, however, CES systems deviate with injection of a potentially different composition

working gas that is cycled over periods of hours to months for energy storage or production(Carden and Paterson 1979; Crotogino et al. 2010; Carr et al. 2014). The rate, extent, and impact of potential geochemical reactions at the gas dissolution zone under these flow conditions have not been considered. In this work, the geochemical influence of the cyclic flow regime of CES systems on geochemical reactions at the cushion gas-brine interface in the porous aquifer are considered and compared to reactions for a CO_2 sequestration system. This region is selected as it is anticipated to be the region most impacted by mineral dissolution reactions. A reactive transport simulation for the cyclic flow conditions corresponding to energy storage in porous formations is developed and used to examine the evolution of formation brine, mineral volume fractions and mineral porosity. Simulation results are compared quantitatively and qualitatively to those for a similar system considering geological CO_2 sequestration in the same formation to deduce differences or similarities in potential geochemical reactions due to the flow regimes of the two systems.

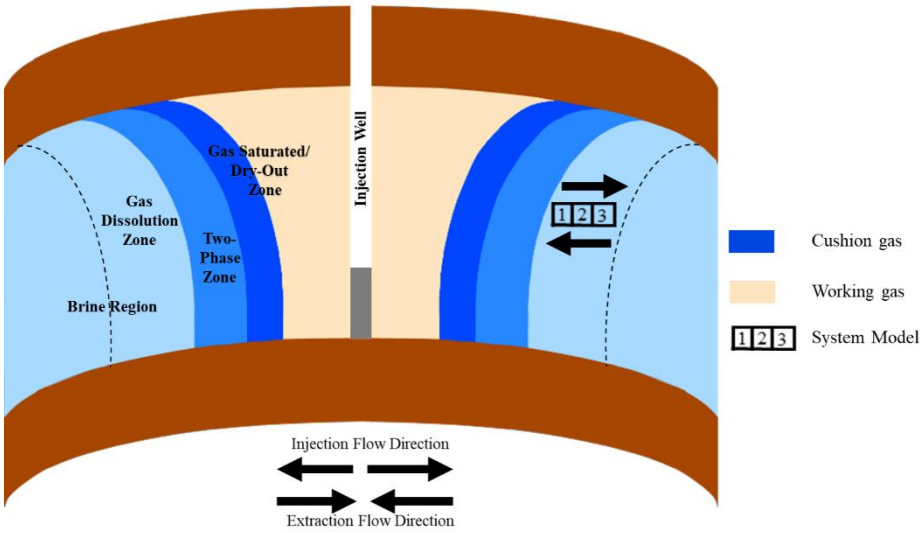

Figure 2.1: Schematic of idealized anticline saline aquifer compressed energy storage system showing the delineation of the working gas, cushion gas, and brine regions. Also shown is the conceptualized location of the simulated reactive transport model grid location of the simulated reactive transport model grid location. The dotted line illustrates the extent of gas dissolution into the brine.

2.2 Materials and Methods

2.2.1 Sample

The sample considered in this study is from the Paluxy formation, a prospective CO_2 storage reservoir at the Kemper Power Plant in Mississippi (Project ECO$_2$S). The formation is stratigraphically located between the Washita-Fredericksburg and Mooringsport formation in the Mississippi Gulf Coast(John Warner 1993). This sample was the subject of previous work in Qin and Beckingham that utilized imaging to characterize sample properties(Qin and Beckingham 2019) and simulated the rate and extent of geochemical reactions in the storage reservoir following CO_2 injection(Qin and Beckingham 2021a). The sample was extracted from a depth of 5048 ft from well MPC 10-4 and is comprised of quartz as the dominant mineral phase, calcite and siderite as the carbonate minerals, K-feldspar, smectite, and minor muscovite. The porosity of the sample is 24.84%. Table 2.1 contains details of the mineral composition.

2.2.2 Reactive Transport Simulations

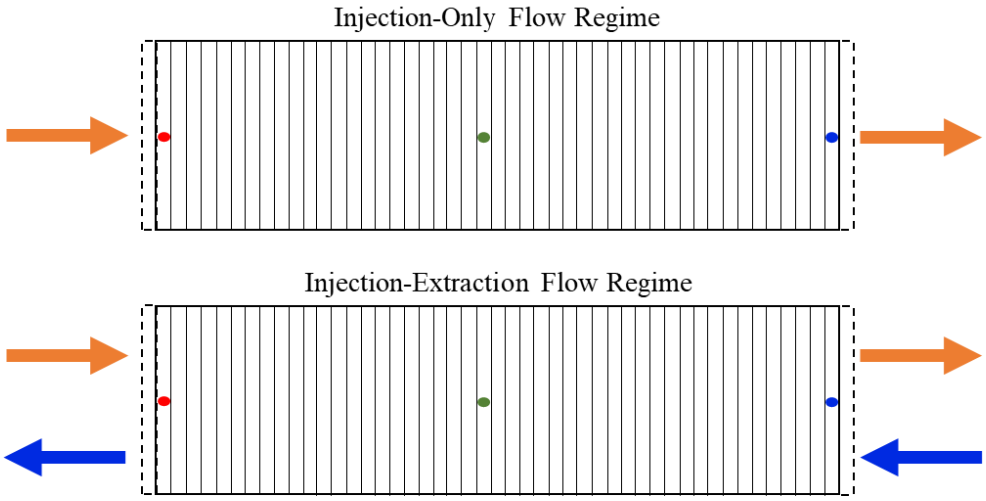

Figure 2.2: Schematic of the model setup for the injection-only flow regime and injection-extraction flow regime showing the direction of injection flow cycle (orange arrow) and extraction flow cycle (blue arrow). Also shown is the conceptualized location of the upstream (red marker), midstream (green marker), and downstream (blue marker) mineral cells which are utilized for comparing reactive transport simulation results. The dotted lines illustrate the boundary conditions.

Coupling of solute transport, flow, and multiple species kinetic evolution for an injection-only and injection-extraction systems were simulated using CrunchFlow, a multicomponent reactive transport simulation code(C. I. Steefel et al. 2015). Here, a one-dimensional transient reactive transport model was developed focusing on the single-phase reactive zone contiguous to the two-phase CO_2-brine zone in the storage aquifer (Figure 2.1). Previous investigation of fluid-rock reactivity in the two-phase(Tutolo et al. 2015) and single-phase(Huq et al. 2015) flooding of acidified brine in core samples demonstrate that the single-phase region is anticipated to be the region with the most extensive geochemical reactions. As such, it was selected as the region of focus for this work.

A forty-seven-cell model system is considered here to define the brine saturated region adjacent to the CO_2 cushion gas bubble. The first cell, the one closest to the injection well, is a 'ghost' cell treated as a boundary condition where the formation brine equilibrates with CO_2 using the improved CO_2 solubility model in aqueous solution by Duan et al. that accounts for high pressure and temperature conditions(Duan et al. 2006). The model assumes a constant partial pressure of CO_2 in this cell. The forty-five internal cells are defined as initially identical porous media cells with a total length of 15 cm. These cells are initialized according to the aquifer mineralogy, mineral surface areas, and porosity characterization results in Qin and Beckingham[33]. The last cell is another 'ghost' cell which is also treated as a boundary condition that serves as the influent fluid source during the extraction cycle. Simulations consider the flow of the acidified brine through the forty-five mineral cells, tracking the concentration of major ion species, mineral volume fractions, and porosity at three mineral cell locations designated as upstream, midstream, and downstream mineral cells as shown in Figure 2.2. The upstream location is in the first internal grid cell, the midstream is the central internal grid cell, while the downstream location is the furthest internal grid cell from the source of injection. Advective dominated flow through the mineral cells is simulated with flux continuity across the boundary using a constant flow rate of 0.489

m/day(Gelhar, Welty, and Rehfeldt 1992). The brine flowrate was estimated based on extrapolation of modeling results from a field scale simulation considering brine velocities at the boundary of an injected CO_2 plume in a sandstone formation(S. Zhang and DePaolo 2017). Based on the geothermal gradient at Kemper, Mississippi and a typical pressure gradient, a reservoir temperature and pressure of 50^oC and 100 bar are used for the simulation, respectively(Reysa 2012; Nathenson and Guffanti 1988; Bachu 2000). The initial brine compositions of major primary species shown in Table 2.1 were determined by simulating the equilibration of 1 M NaCl with quartz, calcite, K-feldspar, siderite, muscovite and smectite (Table 2.2) for ten thousand years under reservoir temperature and pressure(Qin and Beckingham 2021a). The influent brine composition was then determined by equilibration with CO_2 in the 'ghost' cell. The CO_2 concentration and initial pH of the brine after CO_2 equilibration are 1.01 mol/kg and 3.17, respectively. The aqueous activity coefficients of the brine were obtained using the extended Debye-Huckle model.

Simulations consider injection-only and injection-extraction flow cycling for a 24-hour cycle over a four-month study period. The injection-only scenario reflects a CO_2 storage system where CO_2 is injected for a specified period of time and the injected CO_2 remains indefinitely in the formation. The injection-extraction simulation is representative of the operational energy storage system where a cyclic flow pattern is used to cycle between energy storage (injection) and recovery (extraction). The injection-only simulation is modified from a study that investigates the influence of surface area on the rate of mineral reactivity during CO_2 sequestration by Qin and Beckingham(Qin and Beckingham 2021a). In these simulations, a CO_2 acidified brine with constant composition, simulated using initial brine composition equilibrated with CO_2 gas, flows away from the well. The Qin and Beckingham simulations consider geochemical evolution over twenty years in a 3 cm three-grid mineral cell where in this work forty-five mineral cells are considered over 15 cm to investigate the geochemical

reactions adjacent to the cushion gas bubble during the injection-only flow regime and injection-extraction flow regime.

The injection-extraction cycle starts with 12 hours of injection flow away from the well followed by 12 hours of extraction flow towards the well. This corresponds to a continuous operation system comprised of a constant injection and extraction process corresponding to a CES system used daily for power generation(Fleming et al. 2018). It should be noted that there are other CES operational models, including some that include shut-in periods between injection and extraction(Pfeiffer, Beyer, and Bauer 2017; R. D. Allen et al. 1983). During the first cycle, the influent is the initial brine composition equilibrated with CO_2 as discussed above. The composition of the returning fluid, and subsequent influent for the remaining injection periods, is based on the effluent of the preceding flow regime as the brine is recycled through the system. For each injection period, the recycled influent is equilibrated with CO_2 at the brine-cushion gas boundary.

Mineral reactions are simulated in CrunchFlow utilizing parallel rate laws to account for pH dependence and the effects of hydroxyl or electrolyte on the simulated reaction process(Carl I Steefel and Molins 2016). The corresponding rate equation is given by:

$$r_s = -A\left(\sum_{a=1}^{N} K_a \left(\prod_{i=1}^{N_c+N_x} a_i^{p_{ia}}\right)\right)\left(1-\left(\frac{Q_s}{K_s}\right)^{M}\right)^{n} \qquad (1)$$

where r_s is the reaction rate, A is the reactive surface area of a constituting mineral in the rock sample, K_a is the equilibrium dissolution rate constant for the 'a'th parallel reaction, N is number of parallel reactions, p_{ia} is an exponent that gives the dependence of a species i on the 'a'th parallel reaction, $\prod_{i=1}^{N_c+N_x} a_i^{p_{ia}}$ explains the degree of equilibrium effect of ions in solution, n and M are exponents which are experimentally determined to explain nonlinear dependence of the affinity term, K_s is the equilibrium constant, and Q_s is the ion activity product for the rock-water interaction. The rate constants which incorporates all geochemical dependencies relevant to the study were obtained from literature data and extrapolated to the reservoir temperature condition

and reactive surface areas approximated as mineral accessible surface areas in Qin and Beckingham(Qin and Beckingham 2019). The pH of the system was determined via charge balance.

Table 2.1: Simulated initial brine composition of the Paluxy formation.

Primary species	Concentration (Mol/kg_w)
HCO_3^-	7.53E-04
SiO_2(aq)	8.87E-04
Al^{+++}	1.09E-06
Fe^{++}	4.56E-05
Ca^{++}	7.07E-04
Mg^{++}	6.19E-07
K^+	1.07E-04
Na^+	1.00E+00
Cl^-	1.00E+00
SO_4^{--}	1.08E-4

The pH of the system was calculated by using charge balance. The initial pH is 8.82.

Table 2.2: Properties of the Paluxy formation obtained from multi-scale imaging of the sample and used in prior reactive transport simulations(Qin and Beckingham 2019) and rate constants (superscripts) for the respective mineral phases as obtained from the literature([1]Brady and Walther 1990; [2]Knauss and Wolery 1988; [3]Alkattan et al. 1998; [4]Bevan and Savage 1989; [5]Amram and Ganor 2005; [6]Oelkers et al. 2008; [7]Golubev et al. 2009).

Mineral	Ideal Chemical Formula	Abundance (%)(Qin and Beckingham 2019)	Volume Fraction(Qin and Beckingham 2019)	Surface Area (m^2g^{-1})(Qin and Beckingham 2019)	Log Rate Constant (mol s^{-1} m^{-2})
Quartz(Brady and Walther 1990; Knauss and Wolery 1988)	SiO_2	76.45	0.5740	2.59E-2	-11.60
Calcite(Alkattan et al. 1998)	$CaCO_3$	9.63	0.0724	1.42E-3	-4.21
K-Feldspar(Bevan and Savage 1989)	$KAlSi_3O_8$	3.50	0.0263	1.15E-3	-11.65
Smectite(Amram and Ganor 2005)	$(Na,Ca)_{0.33}(Al,Mg)_2(Si_4O_{10})$	8.23	0.0619	1.63E+1	-13.35
Muscovite(Oelkers et al. 2008)	$KAl_2(Si_3AlO_{10})(OH)_2$	0.31	0.0023	1.10E+0	-12.67
Siderite(Golubev et al. 2009)	$FeCO_3$	1.98	0.0141	6.49E-4	-5.69

2.3 Results and Discussion

The evolution of minerals is considered in simulations with an injection-only flow regime, corresponding to geologic CO_2 sequestration, and an injection-extraction flow regime, corresponding to energy storage. Here we present plots for two days and four months of operation that consider the temporal evolution of minerals, major ion concentrations, and porosity at three locations in the domain and the spatial evolution of minerals across the entire domain.

2.3.1 Temporal Mineral Evolution

The simulated evolution of mineral volume fractions at three locations in the simulation domain are shown in Figure 2.3 and 2.4 on individual minerals axis for two days and 120 days, and a combine plot for all minerals for 120 days in Figure 2.5 (120 cycles). Mineral evolution is expressed in terms of mineral volume fraction (Fig. 2.3 and 2.4) and relative volume fractions (Fig. 2.5) that correspond to the ratio of mineral volume fraction over initial mineral volume fraction for each phase. Values of relative volume fractions greater than one signify precipitation and values less than one indicate dissolution.

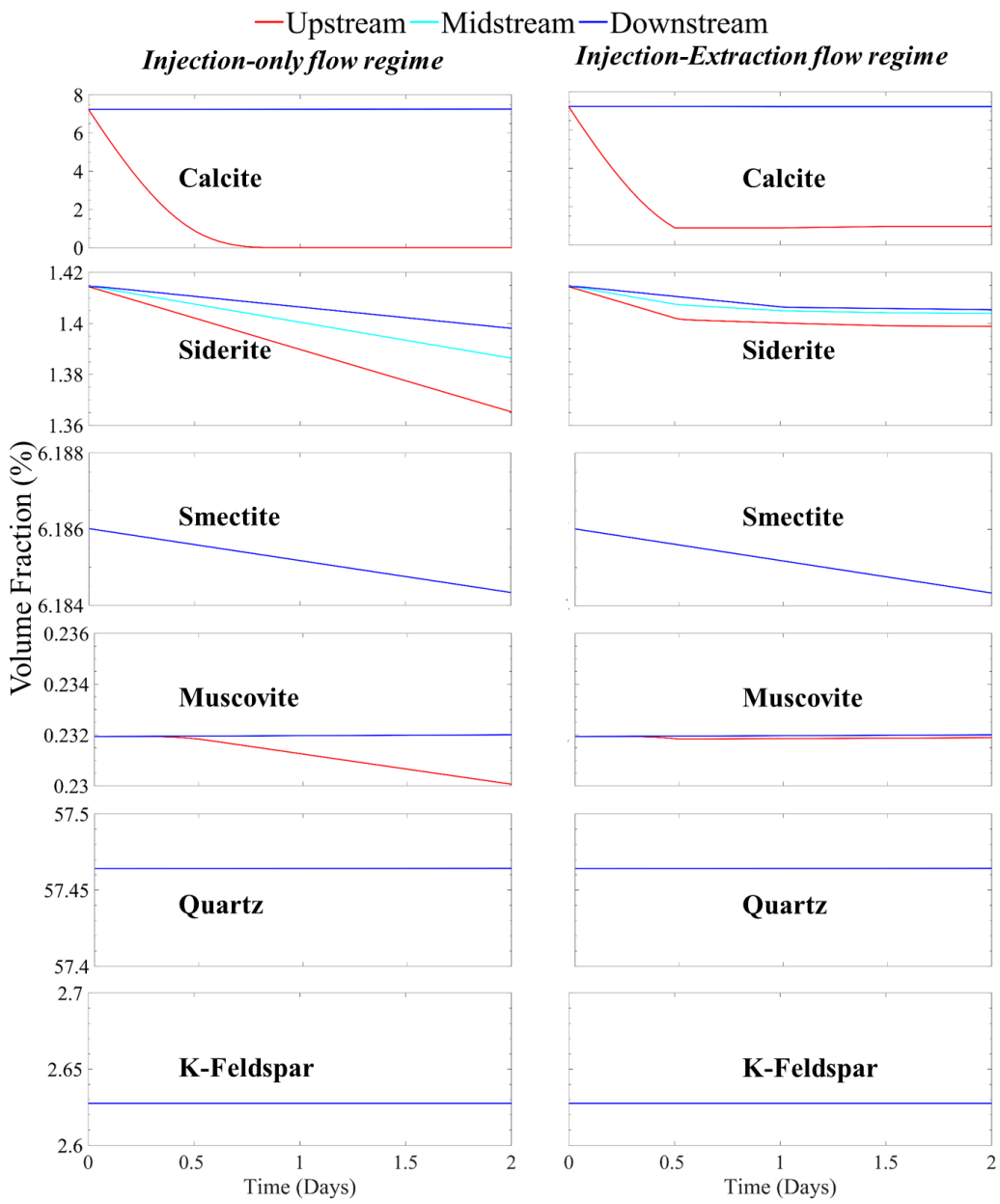

Figure 2.3: The simulated evolution of mineral volume fraction in three different grid cells over the first two cycles for the injection-only flow regimes and injection-extraction flow regimes. Upstream is closest to the source of CO2 injection and downstream is furthest.

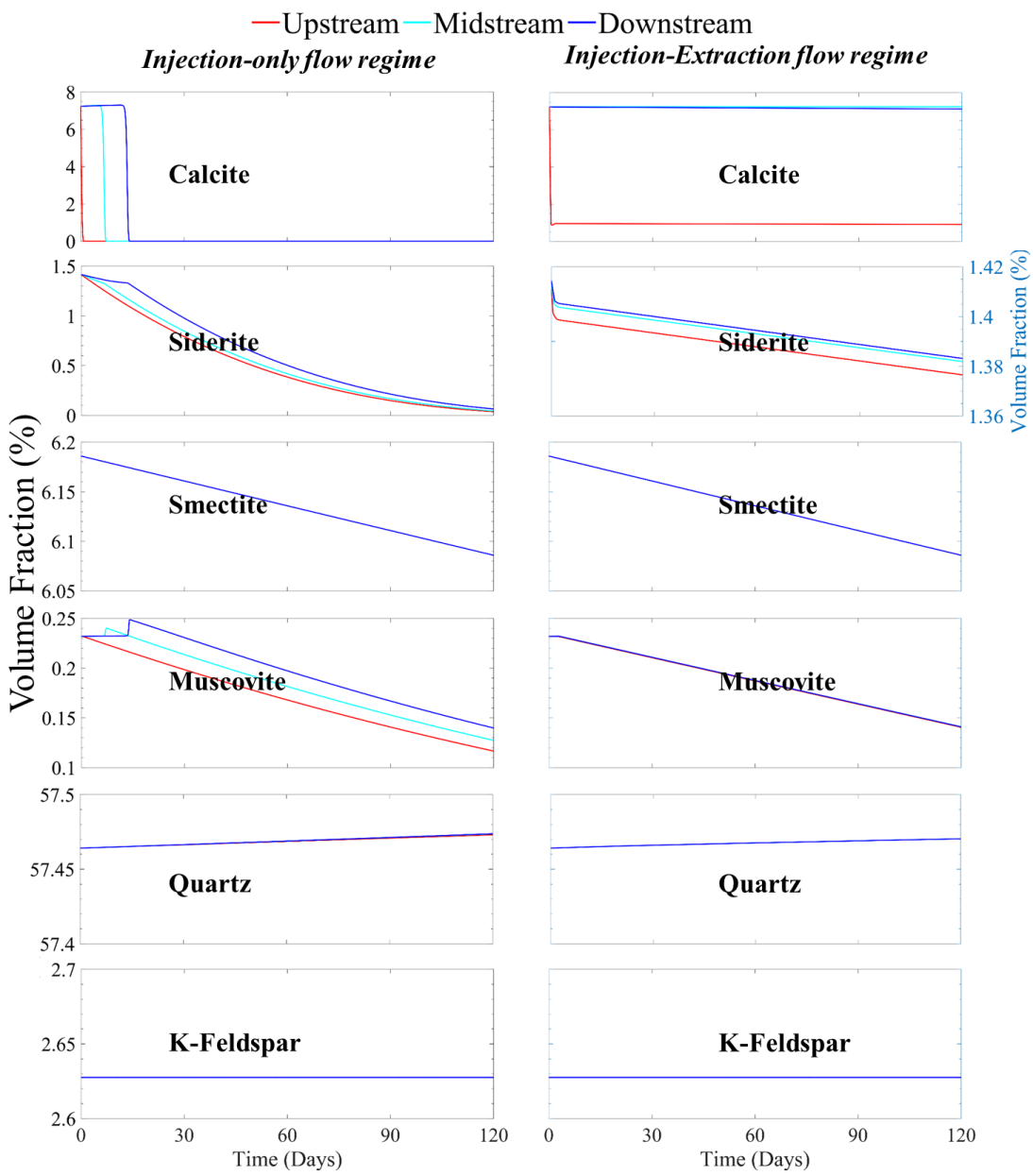

Figure 2.4: The simulated evolution of mineral volume fraction in three different grid cells over the 4 months study period for the injection-only flow regime and injection-extraction flow regime. Upstream is closest to the source of CO2 injection and downstream is furthest.

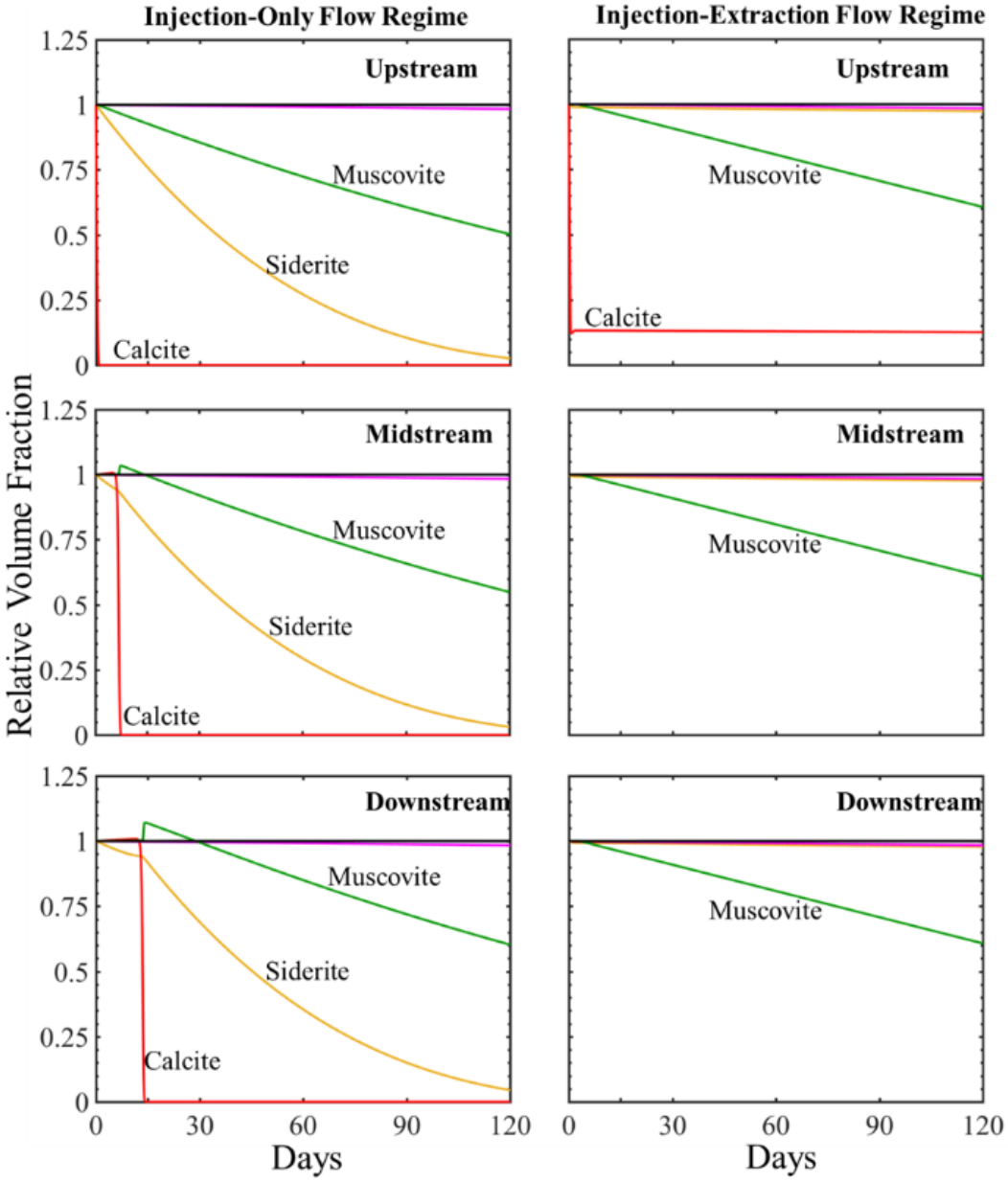

Figure 2.5: The simulated evolution of relative mineral volume fractions at three locations along the simulation domain over 120 days for the injection-only flow regime (left) and injection-extraction flow regime (right). Upstream is the location closest to the injection well and downstream is furthest (Fig. 2.2). The red line represents calcite, yellow siderite, green muscovite, magenta smectite, black quartz and blue K-feldspar.

2.3.1.1 Injection-Only Flow Regime

As the CO_2-saturated brine flows into the system, calcite, siderite, and smectite rapidly begin to dissolve as indicated by the decrease in relative volume fractions of each phase (seen more clearly in 0 - 0.5 day, Fig. 2.3). After 0.5 days, muscovite begins

to dissolve. Calcite and muscovite dissolution only occur in the upstream cell over the first two days while siderite and smectite dissolve throughout the simulation domain where the dissolution rate of siderite is highest closest to the injection well (upstream location) which remains unbuffered. Quartz and K-feldspar remain stable throughout the simulation domain over the first two days.

The simulated evolution of formation minerals for over 120 days (Figure 2.4 and Figure 2.5) follows similar trends to that observed at short times. Calcite dissolution at the inlet initially results in slight calcite precipitation downstream that later dissolves. Complete dissolution of calcite occurs at 23, 181, and 258 hours for the up-, mid- and downstream mineral cells, respectively. Siderite continuously dissolves throughout the simulation domain. The average dissolution rate of siderite increases after complete dissolution of calcite in the system and decreases as siderite nears depletion. At early times, muscovite precipitates then begin dissolving following complete dissolution of calcite in each cell. Muscovite precipitation, however, does not occur in the upstream mineral cell. SiO_2 is predicted to precipitate while K-feldspar remains stable. Precipitation of additional secondary mineral phases was also investigated. Conditions were observed favorable for possible precipitation of albite, chalcedony, chlorite, and kaolinite (Figure 2.6) albeit to very small volume fractions (< 3 orders of magnitude of primary minerals). Throughout the simulation duration, conditions continuously favor chalcedony and chlorite precipitation, indicated by saturation indices greater than one. Conditions favor albite precipitation at early times and dissolution as time progresses. Kaolinite initially precipitates throughout the domain and dissolves closer to the injection well as time progress.

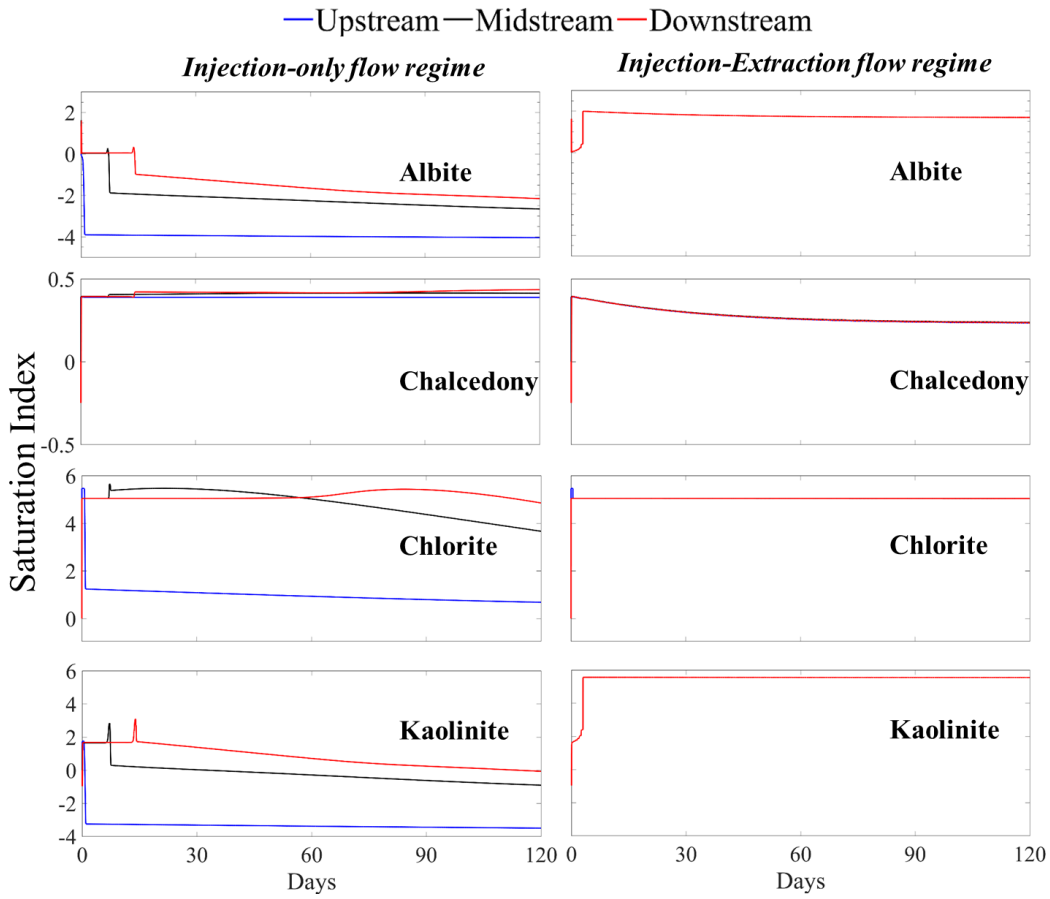

Figure 2.6: The simulated evolution of saturation index of the potential mineral precipitates in three different grid cells over the 4 months study period for the injection-only flow regime and injection-extraction flow regime. Upstream is closest to the source of CO_2 injection and downstream is furthest.

2.3.1.2 Injection-Extraction Flow Regime

The simulated evolution of formation minerals on its individual axis for the injection-extraction flow regime corresponding to energy storage is shown in Figures 2.3 and 2.4 for durations of two days and 120 days. The mineral response is the same during the first 12 hours as the injection-only system. After 12 hours, the system evolves discretely differently as the cyclic flow pattern begins. During the extraction flow regime, brine recycles through the system. In the first extraction flow regime, the higher resolution plots of figure 2.3 shows that between 0.5 days to 1 day, there is little change in calcite mineral volume fraction as the brine is almost in equilibrium with respect to calcite. Siderite and smectite continue to dissolve while muscovite begins to

dissolve in the upstream location and no changes in quartz and K-feldspar volume fractions occur. The dissolution rate of siderite is greatest in the cell furthest from the injection well and decreases in the cells closer to the injection well. After 1 day, the second 12-hour injection cycle begins corresponding to brine recycling with replenished acidity as influent brine is saturated with CO_2. This results in continued dissolution of siderite and smectite but does not result in increased dissolution rates as the ion concentrations in the recycled brine limit reactions. In comparison with the injection-only scenario, initial dissolution rates (Fig. 2.5) in the injection-extraction flow regime are smaller and ultimately reduces the extent of dissolution. The dissolution rate for smectite, however, is the same for both flow conditions.

As time progress, calcite and smectite dissolve continuously throughout the simulation, albeit at slow rates at longer times (higher resolution plots shown in Figure 2.4 and Figure 2.5). Smectite is also dissolving with a rate dissolution similar to that in the injection-only flow conditions (Figure 2.4 and Figure 2.5). As in the injection-only simulation, SiO_2 slowly precipitates and K-feldspar remains stable. The extent of quartz precipitation for the injection-extraction flow regime, however, is slightly less than for the injection-only flow regime (Figure 2.4). Potential additional secondary mineral phases include albite, chalcedony, chlorite, and kaolinite (Figure 2.6). As indicated by saturation indices, conditions favor precipitation throughout the simulation domain, albeit to small volume fractions. The volume fraction of most dominant precipitate is also more than three orders of magnitude less than the primary minerals. Here, continuous precipitation is favored which is distinctly different than that of the injection-only flow conditions where only chlorite and chalcedony were stable throughout the simulation time and domain.

2.3.2 Spatial Mineral Evolution

The evolution of the mineral volume fractions across the domain length for the two flow regimes is discussed below with respect to the number of pore volumes of fluid that have passed through the domain.

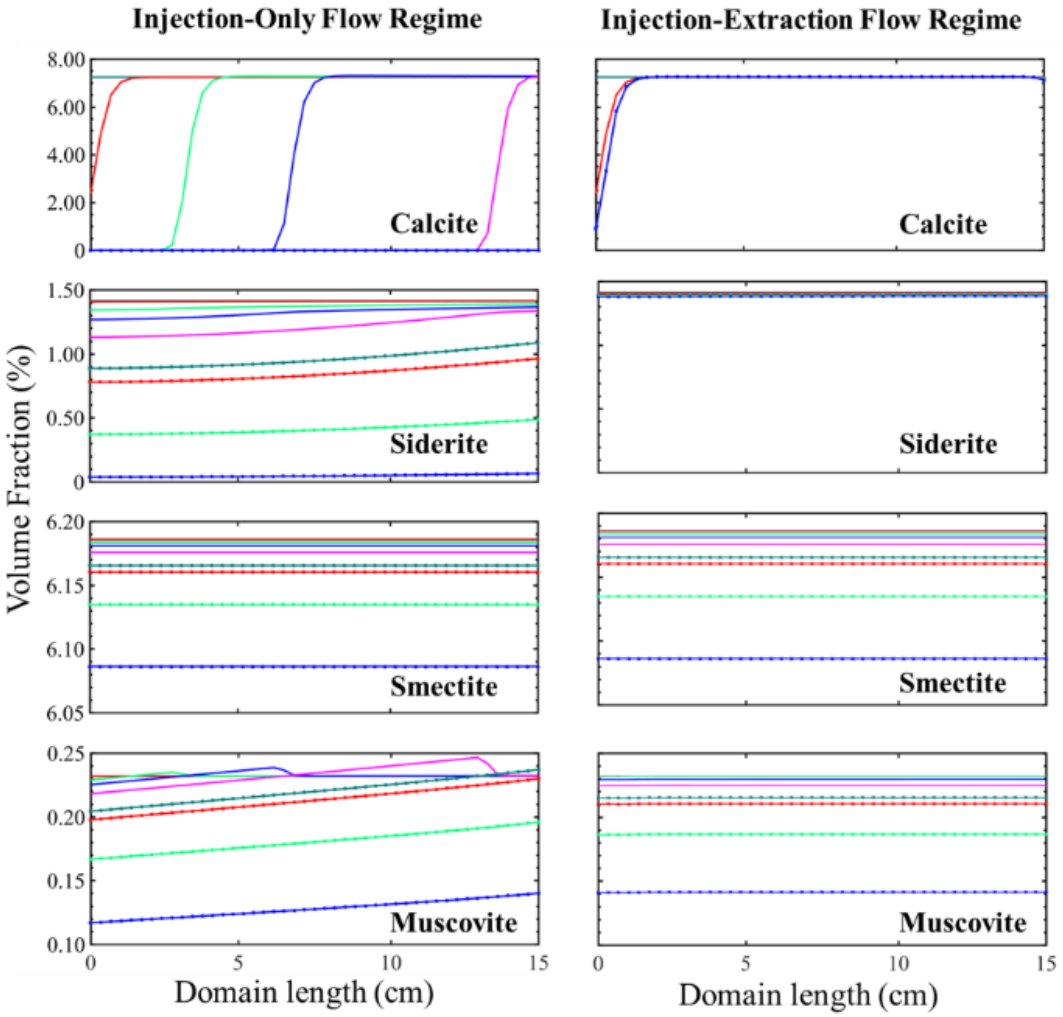

Figure 2.7: The simulated evolution of mineral volume fractions with increasing number of pore volumes (PV) of CO2 acidified brine flowing through the simulation domain over 120 days for the injection-only flow regime (left) and injection-extraction flow regime (right). 0 PV is the initial condition and 391 PV is the last pore volume to flow through the porous media. Dark green represents 0 PV, red 1PV, light green 10PV, blue 20PV, magenta 40PV, dotted dark green 80 PV, dotted red 1PV, dotted light green 200PV, and dotted blue 391PV.

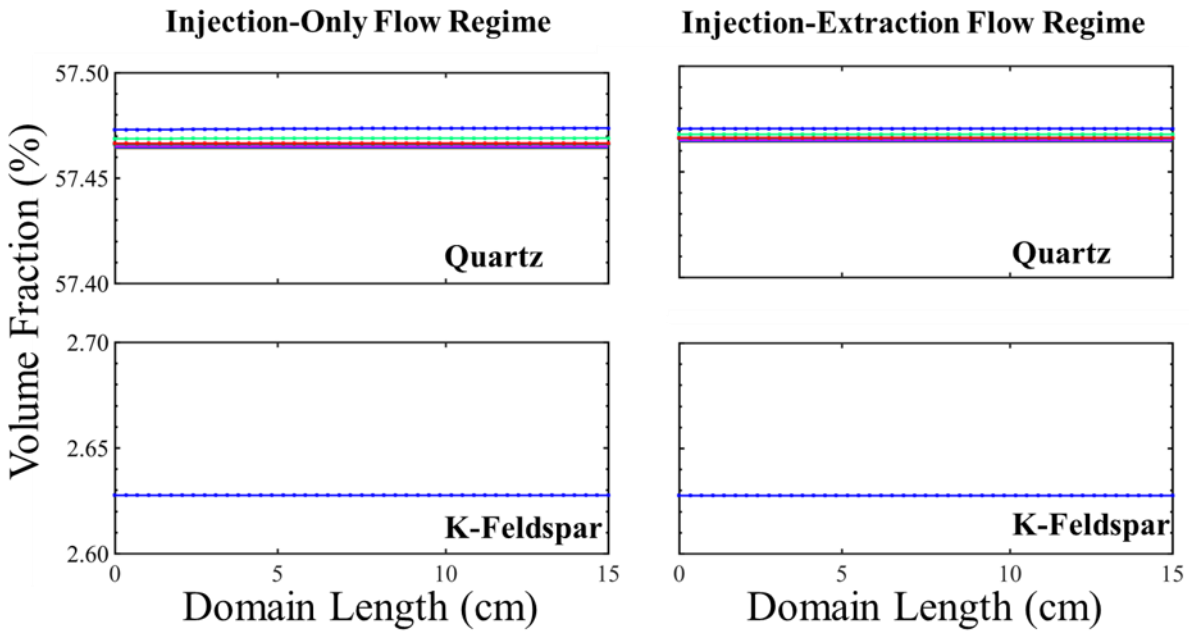

Figure 2.8: The simulated evolution of mineral volume fractions with increasing number of pore volumes (PV) of CO2 acidified brine flowing through the simulation domain over 120 days for the injection-only flow regime (left) and injection-extraction flow regime (right). 0 PV is the initial condition and 391 PV is the last pore volume to flow through the porous media. Dark green represents 0 PV, red 1PV, light green 10PV, blue 20PV, magenta 40PV, dotted dark green 80 PV, dotted red 1PV, dotted light green 200PV, and dotted blue 391PV.

2.3.2.1 Injection-Only Flow Regime

The simulated spatial evolution of formation minerals with respect to pore volumes for the injection-only flow regime is given in Figure 2.7 and shows non-uniform dissolution of calcite and siderite. Variations in calcite dissolution show calcite successively dissolves, and is consumed, from the inlet to the outlet. Siderite dissolution is initially larger near the injection well and becomes more uniform throughout the simulation domain as simulations progress. This non-uniform dissolution pattern of calcite and siderite mineral is expected as dissolution of these minerals buffers the acidity, creating conditions where calcite and siderite are more stable. The high reaction rate of calcite results in rapid depletion of calcite after contact with acidified brine that prevents downstream calcite dissolution until it is completely consumed upstream. This results in non-uniform calcite volume fractions across the domain until all calcite is

consumed, after more than 40 pore volumes. In comparison, the lower dissolution rate of siderite results in siderite dissolution throughout the simulation domain earlier in the simulation. Unlike calcite, siderite dissolution approaches uniform extents across the domain length as simulations progress.

Large variations in muscovite across the simulation domain can also be observed. Initially, muscovite precipitates, coupled with calcite dissolution. As calcite is depleted, muscovite then precipitates. Once calcite is consumed, muscovite dissolves throughout the simulation domain to varying extents with the largest reduction in muscovite volume fraction near the injection well.

Smectite, K-feldspar, and quartz do not vary across the simulation domain. Smectite dissolves continuously throughout the simulation domain as a result of smectite's lower dissolution rate in comparison to calcite and siderite, Quartz precipitates uniformly throughout the simulation domain throughout the duration of the simulations. K-feldspar is constant throughout the simulation (Fig. 2.8).

2.3.2.2 Injection-Extraction Flow Regime

The simulated spatial variation of mineral volume fractions in the injection-extraction flow regime is much less than in the injection-only flow regime, as shown in Figure 2.7. Here, the recycling process significantly reduces the rate and extent at which calcite and siderite dissolve. Some spatial variation is evident for calcite with increased dissolution near the injection well and no dissolution of calcite further in the simulation domain. While CO_2 saturated brine enters the system during each injection half-cycle, the elevated ion concentrations from earlier calcite dissolution limit additional dissolution. Siderite dissolves uniformly in the domain throughout the simulation but to a much lower extent than in the injection-only flow regime. Smectite also uniformly dissolves, facilitated by its slower dissolution rate and the continuous acidic conditions. The rate of smectite dissolution is the same in the injection-only and injection-extraction flow conditions. K-Feldspar is stable throughout the domain and simulation

like the injection-only flow regime. Muscovite dissolves uniformly during cyclic flow conditions with no initial precipitation because of the absence of rapid calcite dissolution. Overall, the extent of muscovite dissolution is less than in the injection-only flow regime, particularly closer to the injection well. Quartz uniformly precipitates throughout the domain to a slightly lesser extent than the injection-only flow regime, a consequence of overall reduced muscovite dissolution (Fig 2.8).

2.3.3 Evolution of Major Ion Concentrations

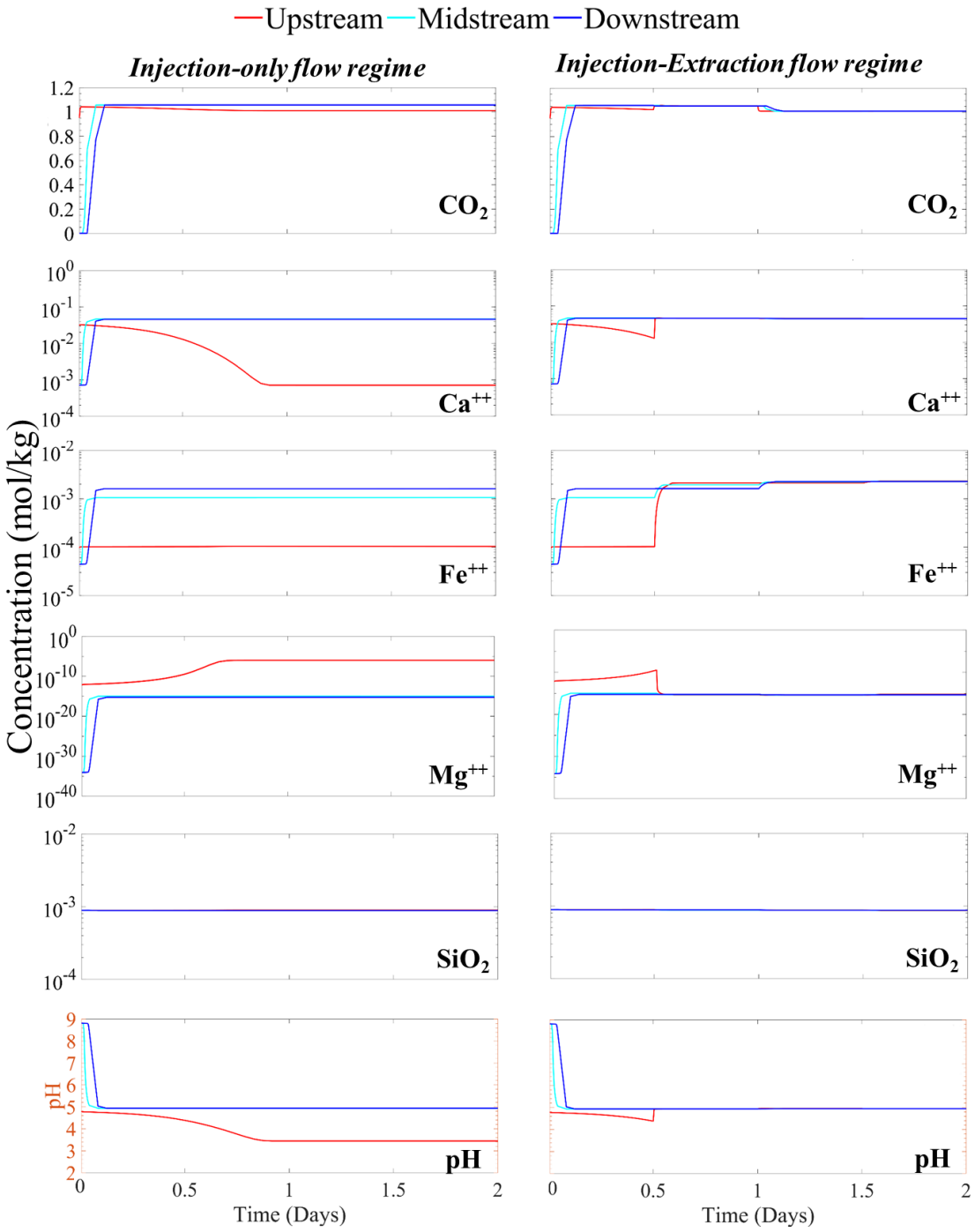

Figure 2.9: The simulated evolution of major ion concentrations and pH of the porous formation in three different grid cells over the first two cycles for the injection-only flow regimes and injection-extraction flow regimes. Upstream is closest to the source of CO_2 injection and downstream is furthest.

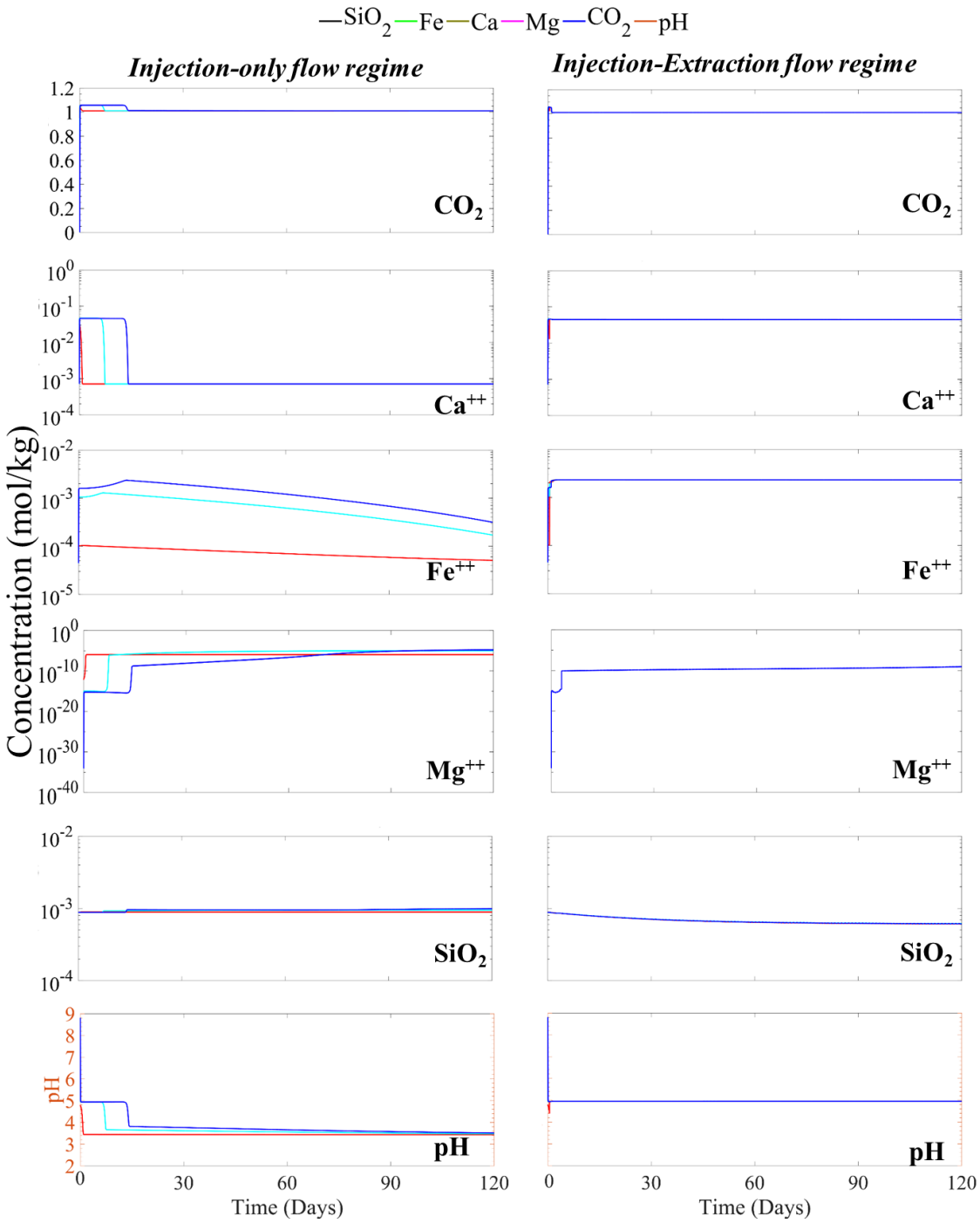

Figure 2.10: The simulated evolution of major ion concentrations and pH in three different grid cells over the 4 months study period for the injection-only flow regime and injection-extraction flow regime. Upstream is closest to the source of CO2 injection and downstream is furthest.

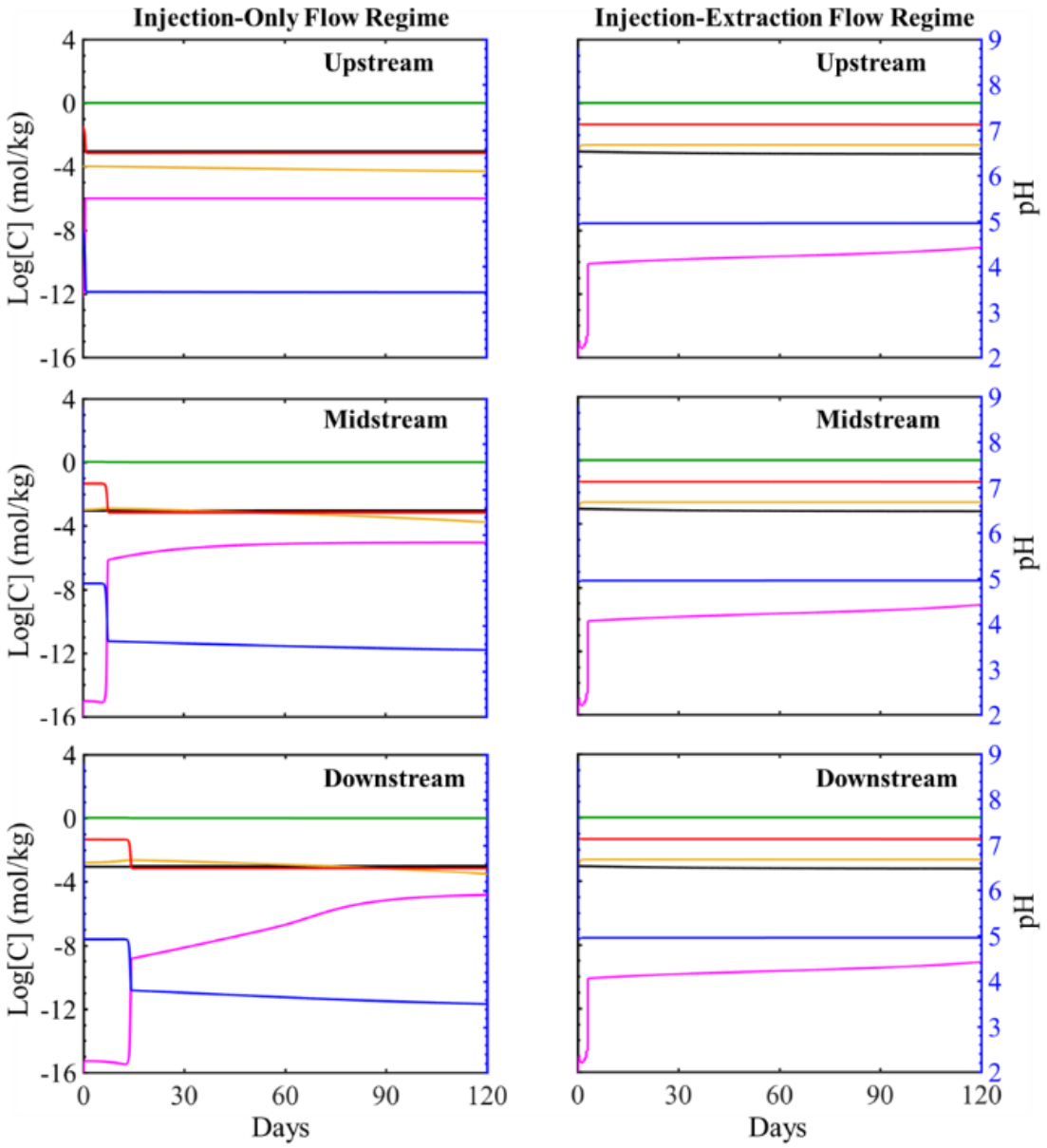

Figure 2.11: Simulated evolution of major ion concentrations and pH over the 120 day study period for the injection-only flow regime (left) and injection-extraction flow regime (right). Upstream is the cell closest to the injection well and downstream is the furthest. The red represents calcium, yellow iron, green total CO_2, magenta magnesium, black silica and blue pH.

2.3.3.1 Injection-Only Flow Regime

The simulated evolution of major ion concentrations in the brine on its individual axis during the injection-only flow regime is shown in Figure 2.9 for the first two days and Figure 2.11 for the 120-day simulation duration. At the start of the

simulation, the introduction of acidified brine results in a sharp increase in calcium, iron, and magnesium and a reduction in pH. The increase in calcium is from the rapid dissolution of calcite which results in an increase of calcium concentration of two orders of magnitude relative to its initial concentration. Calcite dissolution concurrently buffers the pH and results in an increase in pH of the brine from 3.42 (pH of entering brine) to 4.8, 4.9 and 4.9 in the upstream, midstream and downstream locations, respectively. After the initial rapid change, the calcium ion concentration in the upstream location starts to decrease due to the reduction in calcite dissolution with decreasing calcite volume fraction in these cells. This is closely coupled with pH where the pH gradually drops as calcite is depleted and the extent of buffering is reduced. As calcite is depleted, calcium concentrations return to background levels, first in the upstream cell and later in the midstream and downstream locations. The increase in iron and magnesium concentrations reflects dissolution of siderite and smectite where concentrations are lowest in the grid cell closet to the injection well and increase with distance from the well. As siderite is depleted after tens of days, iron concentrations decrease. Magnesium remains at a constant elevated concentration in the upstream location while mid- and downstream concentrations continue to increase, reflecting the constant dissolution of smectite and eventually muscovite following initial muscovite precipitation. No change in aqueous silica or potassium concentrations occur within the first two days.

2.3.3.2 Injection-Extraction Flow regime

The species evolution for the injection-extraction flow regime initially evolves similarly to the injection-only flow regime where increases in iron, calcium, magnesium, and silica are observed as calcite, siderite and smectite dissolve. After 0.5 days, simulations begin to diverge as the near-saturated brine is recycled as the flow reverses and the first extraction cycle begins (Figure 2.9). The returning brine contains relatively high concentrations of the ions from the minerals that dissolved during the

first injection half-cycle. As such, the returning concentrations reflect effluent ion concentrations in the downstream grid cell at the end of the previous injection period. The high concentration of calcium in recycled brine prevents further calcite dissolution. Iron and magnesium concentrations fluctuate but maintain undersaturated conditions with respect to siderite and smectite dissolution, facilitating additional dissolution. No change in SiO_2 concentration occurs. At one day, the second injection cycle begins where CO_2 concentrations are refreshed in the solution, as during each injection cycle. This replenished acidity results in additional increases in iron concentration from more siderite dissolution and further buffering of the system pH while calcium ion concentrations remain stable. SiO_2 concentrations continues to be elevated over the first two days.

Over longer times, calcium concentrations remain constant at elevated levels (Figure 2.11) in each grid cell. Magnesium concentrations continuously increase throughout the simulation domain reflecting continued smectite dissolution throughout the study period. The initially over-saturated silicate concentration begins to decrease after approximately 30 days as quartz begins to precipitate, albeit the variations are overall small. Iron concentrations gradually increase as siderite continuously dissolves.

2.3.4 Porosity Evolution

The simulated evolution of porosity for the injection-extraction flow regime and injection-only flow regimes are shown in Figure 2.12 and figure 2.13 over 15 days and 120 days period. The porosity evolution serves to quantify the total effect of the mineral dissolution and precipitation reactions occurring in the sample following injection of CO_2.

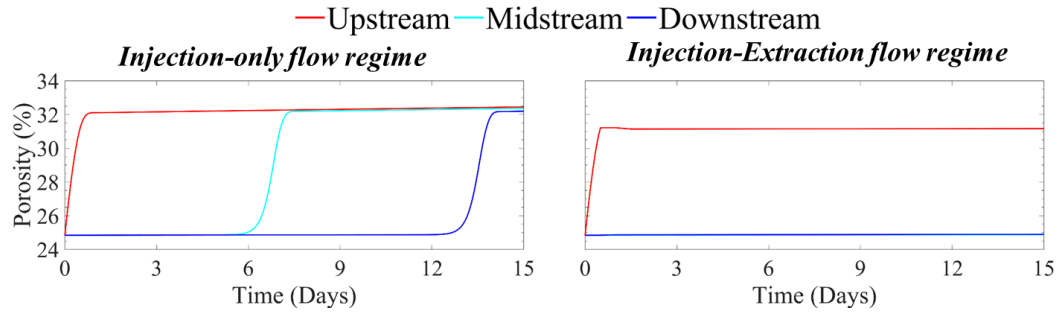

Figure 2.12: The simulated evolution of mineral porosity of the porous formation in three different grid cells over the first fifteen days for the injection-only flow regimes and injection-extraction flow regimes. Upstream is closest to the injection well and downstream is furthest.

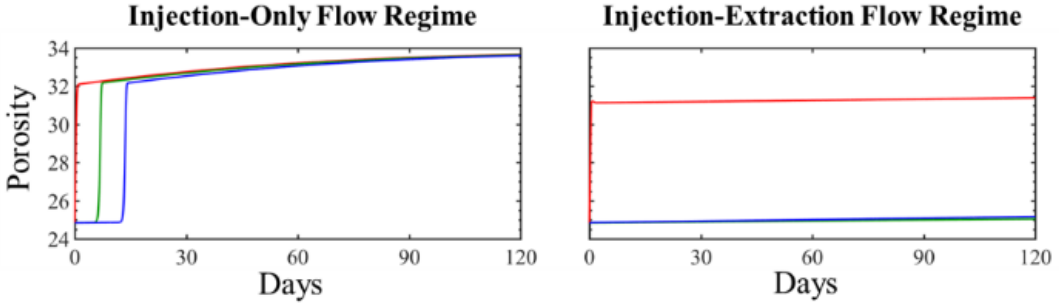

Figure 2.13: The simulated evolution of mineral porosity of the core sample in three different grid cells over the four month study period for the injection only flow regime and injection-extraction flow regime. The upstream location is closest to the injection well and downstream is furthest. The red represents the upstream location, green the midstream location, and blue the downstream location.

In the injection-only simulations, porosity rapidly increases throughout the simulation domain within the first 15 days of CO_2-acidified brine injection and continuously increases throughout the study period (Fig 2.12). This is largely a result of dissolution of calcite and siderite. At the end of the study period, the porosity has increased to 33.6%, from 24.8%, throughout the simulation domain. During the injection-extraction flow regime for the cyclic flow conditions, dissolution of calcite, siderite, smectite and muscovite result in an overall increase in porosity. The porosity increase is highest near the injection well and deceases away from the well, largely due to spatial variations in calcite dissolution where 87.4%, 1.6% and 0.1% of calcite

dissolve in the upstream, midstream and downstream locations at the end of the 120 cycles. This results in final porosities of 31.4%, 25.1% and 25.2% for the three locations at the end of the four months study period. After the initial cycle, there is little additional variation in porosity as little additional dissolution occurs. The overall porosity increase in the cyclic flow conditions is small in comparison with the injection-only flow conditions, with the exception of the location closest to the cushion gas boundary. This is because brine recycling maintains elevated ion concentrations and limits mineral dissolution as injection-extraction cycles progress, even under CO_2-saturated conditions. Both simulation systems result in rapid, large increases in porosity near the injection well. However, it should be noted that this may be dependent on the model domain where reservoir scale simulations have observed much smaller variations in porosity near the injection well due to simulated near-well pH buffering in the larger domains(S. Zhang and DePaolo 2017; Y. Wang et al. 2019).

2.4 System Implications

Geochemical reactions are anticipated in porous aquifers utilized for developing subsurface technologies, such as CO_2 sequestration and subsurface energy storage. The potential rate and extent of these reactions in subsurface energy storage systems and the resulting implications on operational performance, however, have largely not been investigated while numerous works have considered reactions in the context of CO_2 sequestration. Energy storage in porous saline aquifers and geologic CO_2 sequestration systems have many system similarities, including target reservoir formations. However, there is a major difference in the operational flow regime of energy storage systems that may impact the gas dissolution zone initiated during the lifecycle of the project(R. D. Allen 1981; B. P. McGrail et al. 2011). Here, reactive transport simulations are developed and leveraged to compare the reaction pathways during CO_2 sequestration and subsurface energy storage to predict the difference in potential geochemical reactions and implications for operational efficiency.

Geochemical reactions play an important role in these subsurface energy systems, impacting potential associated environmental risks and the operational efficiency of the system. In terms of risk, previous investigations of CO_2 sequestration systems have highlighted the need to evaluate the risk of leakage and land subsidence, two adverse effects that are largely controlled by geochemical reactions. The formation of leakage pathways in caprock formations(Fitts and Peters 2013) following CO_2 injection can result in flow of brine or injected fluids to overlying formations and endanger natural resources and protected entities including drinking water aquifers(Bauer et al. 2013). Land subsidence may jeopardize the integrity of the site of operation and has been observed in pilot CO_2 systems(Onuma and Ohkawa 2009). In terms of operational efficiency, geochemical reactions may also alter the porosity and permeability of the formation and thus the injectivity during the operational life of the energy storage system. In general, dissolution at the plume boundary would increase the storage volume and injectivity but may have adverse effects in terms of migration of the cushion or storage gas further into the formation and a corresponding reduction in pressure and energy recovery. Precipitation at the boundary may limit injectivity but can also serve to limit migration of the plume into the formation and increase efficiency of energy recovery by maintaining pressurization.

The results of this study show that geochemical reactions will occur in energy storage systems when CO_2 is utilized as a cushion gas. Both mineral dissolution and precipitation reactions are anticipated in the single-phase brine-saturated region adjacent to the cushion gas plume. The dissolution potential for the case of CO_2 sequestration, however, supersedes that of the cyclic flow regime of the compressed energy storage system. The cyclic flow pattern of energy storage and recovery results in a high concentration of dissolved ion concentrations as CO_2 saturated brine flows away from and towards the well, reducing the extent of dissolution at the plume boundary in comparison to that occurring in CO_2 sequestration conditions. Similar observations with regards to limited dissolution have been observed experimentally in

studies with low water-rock ratios where high dissolved ion concentrations limited the extent of dissolution(W. L. Huang, Bishop, and Brown 1986). The reduced dissolution extent in the cyclic flow conditions limits porosity variation as reactions predominantly occur during the initial cycle and only impact carbonate minerals after the first injection cycle. This means that the storage volume and injectivity will largely remain constant after the first cycle. As properties are anticipated to be less dynamic, this can potentially reduce the risk and likelihood of over-pressurization of the aquifer during the life cycle of operation by improving the predictability of the system. If conditions continuously favored dissolution, as in the CO_2 sequestration scenario, this would result in a constant increase of porosity and allow migration of the working and/or cushion gas plume further into the formation. This would result in a fluctuation of the pressure of the system as the injected fluid migrates further into the reservoir. This condition would require more frequent monitoring during operation and more frequent injections of additional cushion gas to ensure sufficient pressure for energy recovery. However, the increased dissolution may additionally allow for the mineralization of the injected CO_2 which is a means of secure CO_2 sequestration. This secondary mineral precipitation may decrease porosity and permeability.

While limited reaction rates and extents were observed in the cyclic flow simulations here over the four-month study period, the difficulty in accurately simulating reaction rates and extents in field scale systems should be noted. In part, this is due to uncertainties in the parameters used for modeling(L. Zhang et al. 2020; Bourg, Beckingham, and DePaolo 2015; Black, Carroll, and Haese 2015), namely accurate estimation of reaction rate constants and mineral surface areas. Rate constants vary widely with pH, as much as 8 orders of magnitude between pH 3 and 8(Black, Carroll, and Haese 2015; S. Zhang and DePaolo 2017). However, rate constants are anticipated to vary by only approximately one order of magnitude for the simulated pH values here following CO_2 injection, pH ~3-5(S. Zhang and DePaolo 2017). Estimates of mineral reactive surface areas depend largely on approximation approach where variations in

estimation method yield as much as seven orders of magnitude variation in surface area values(Bourg, Beckingham, and DePaolo 2015; Beckingham et al. 2017; Black, Carroll, and Haese 2015). For the study period considered here, variations in surface area may result in differences in reaction rates and slight differences in porosity, as determined in sensitivity simulations considering the impact of surface area approximation on the rate and extent of reactions for the geologic storage condition in this formation in (Qin and Beckingham, 2020). However, recent work considering reaction rates in porous media found that image obtained accessible surface areas best reflected the surface area of reacting mineral phases and reaction rates were overestimated using other common approaches(Beckingham et al. 2017). As such, mineral accessible surface areas determined using the same multi-scale imaging approach(Qin and Beckingham 2019) are used in the simulations here and are anticipated to reflect reaction rates and extents in porous media.

The impact of mineral dissolution and precipitation reactions on the operation lifecycle of these systems will largely depend on the corresponding evolution of permeability in the formation. While the evolution of porosity can be estimated based on changes in mineral volume fractions with the micro-continuum reactive transport simulations here, changes in permeability depend location of mineral reactions within individual pores and the larger pore network. This, however, is not well understood. Based on the simulated permeability evolution, previous pore network modeling work has shown that permeability will likely range between 1000 - 2200mD, in comparison to the initial permeability of 1555.4 mD, but may be more extreme depending on the spatial distribution of mineral reactions(Bensinger and Beckingham 2020).

In the four-month study period considered here, a significant difference in the simulated geochemical reactions and porosity evolution for the case of CO_2 sequestration and compressed energy storage using CO_2 as the cushion gas is anticipated. It should be noted that this result is for an operational system comprised of constant injection and extraction for 12 hours each. In terms of operational cycles,

injection-extraction periods can vary from hours to months and may include long storage periods(R. D. Allen et al. 1983). In comparison to geologic CO_2 sequestration, the extent, rate, and impact of geochemical reactions are limited in the single-phase zone of energy storage systems utilizing CO_2 as a cushion gas. In the CO_2 sequestration system, reactions progress continuously as under-saturated acidic formation brine flows through the aquifer and porosity increases continuously. The cyclic flow conditions of energy storage systems limit reactions such that a stabilized working system can be attained after only one cycle, making utilization of reactive cushion gases, including CO_2, a viable alternative.

2.5 Acknowledgements

This work supported by Auburn University by the Auburn University Intramural Grants Program and Presidential Awards for Interdisciplinary Research.

2.6 References

Alkattan, M., Oelkers, E.H., Dandurand, J.L. and Schott, J., 1998. An experimental study of calcite and limestone dissolution rates as a function of pH from− 1 to 3 and temperature from 25 to 80 C. *Chemical geology*, *151*(1-4), pp.199-214. https://doi.org/10.1016/S0009-2541(98)00080-1.

Allen, R.D., 1981. *Basis for compressed air energy storage (CAES) field test at Pittsfield, Illinois* (No. PNL-SA-9447; CONF-811066-6). Pacific Northwest Lab., Richland, WA (USA).

Allen, R.D., Doherty, T.J., Erikson, R.L. and Wiles, L.E., 1983. *Factors affecting storage of compressed air in porous-rock reservoirs* (No. PNL-4707). Pacific Northwest Lab., Richland, WA (USA). https://www.osti.gov/servlets/purl/6270908.

Amram, K. and Ganor, J., 2005. The combined effect of pH and temperature on smectite

dissolution rate under acidic conditions. *Geochimica et Cosmochimica Acta*, *69*(10), pp.2535-2546. https://doi.org/10.1016/j.gca.2004.10.001.

Bachu, S., 2000. Sequestration of CO2 in geological media: criteria and approach for site selection in response to climate change. *Energy conversion and management*, *41*(9), pp.953-970. https://doi.org/10.1016/S0196-8904(99)00149-1.

Bary, A., Crotogino, F., Prevedel, B., Berger, H., Brown, K., Frantz, J., Sawyer, W., Henzell, M., Mohmeyer, K., Ren, N. and Stiles, K., 2002. Storing natural gas underground. *Oilfield Review*, *14*(2), pp.2-17.

Bauer, S., Beyer, C., Dethlefsen, F., Dietrich, P., Duttmann, R., Ebert, M., Feeser, V., Görke, U., Köber, R., Kolditz, O. and Rabbel, W., 2013. Impacts of the use of the geological subsurface for energy storage: an investigation concept. *Environmental earth sciences*, *70*(8), pp.3935-3943. https://doi.org/10.1007/s12665-013-2883-0.

Beckingham, L.E. and Winningham, L., 2019. Critical knowledge gaps for understanding water–rock–working phase interactions for compressed energy storage in porous formations. *ACS Sustainable Chemistry & Engineering*, *8*(1), pp.2-11. https://doi.org/10.1021/acssuschemeng.9b05388.

Bensinger, J. and Beckingham, L.E., 2020. CO2 storage in the Paluxy formation at the Kemper County CO2 storage complex: Pore network properties and simulated reactive permeability evolution. *International Journal of Greenhouse Gas Control*, *93*, p.102887. https://doi.org/10.1016/j.ijggc.2019.102887.

Bevan, J. and Savage, D., 1989. The effect of organic acids on the dissolution of K-feldspar under conditions relevant to burial diagenesis. *Mineralogical Magazine*, *53*(372), pp.415-425. https://doi.org/10.1180/minmag.1989.053.372.02.

Black, J.R., Carroll, S.A. and Haese, R.R., 2015. Rates of mineral dissolution under CO2 storage conditions. *Chemical Geology*, *399*, pp.134-144. https://doi.org/10.1016/j.chemgeo.2014.09.020.

Bourg, I.C., Beckingham, L.E. and DePaolo, D.J., 2015. The nanoscale basis of CO2 trapping for geologic storage. *Environmental science & technology*, *49*(17), pp.10265-10284. https://doi.org/10.1021/acs.est.5b03003.

Brady, P.V. and Walther, J.V., 1990. Kinetics of quartz dissolution at low temperatures. *Chemical geology*, *82*, pp.253-264. https://doi.org/10.1016/0009-2541(90)90084-K.

Carden, P.O. and Paterson, L., 1979. Physical, chemical and energy aspects of underground hydrogen storage. *International Journal of Hydrogen Energy*, *4*(6), pp.559-569. https://doi.org/10.1016/0360-3199(79)90083-1.

Carr, S., Premier, G.C., Guwy, A.J., Dinsdale, R.M. and Maddy, J., 2014. Hydrogen storage and demand to increase wind power onto electricity distribution networks. *International journal of hydrogen energy*, *39*(19), pp.10195-10207. https://doi.org/10.1016/j.ijhydene.2014.04.145.

Cavallo, A., 2007. Controllable and affordable utility-scale electricity from intermittent wind resources and compressed air energy storage (CAES). *Energy*, *32*(2), pp.120-127. https://doi.org/10.1016/j.energy.2006.03.018.

Crotogino, F., Donadei, S., Bünger, U. and Landinger, H., 2010, May. Large-scale hydrogen underground storage for securing future energy supplies. In *18th World hydrogen energy conference* (Vol. 78, pp. 37-45). https://doi.org/10.1109/INTMAG.2015.7157557.

Cui, G., Wang, Y., Rui, Z., Chen, B., Ren, S. and Zhang, L., 2018. Assessing the combined influence of fluid-rock interactions on reservoir properties and

injectivity during CO2 storage in saline aquifers. *Energy*, *155*, pp.281-296. https://doi.org/10.1016/j.energy.2018.05.024.

Deng, H., Steefel, C., Molins, S. and DePaolo, D., 2018. Fracture evolution in multimineral systems: The role of mineral composition, flow rate, and fracture aperture heterogeneity. *ACS Earth and Space Chemistry*, *2*(2), pp.112-124. https://doi.org/10.1021/acsearthspacechem.7b00130.

Duan, Z., Sun, R., Zhu, C. and Chou, I.M., 2006. An improved model for the calculation of CO2 solubility in aqueous solutions containing Na+, K+, Ca2+, Mg2+, Cl−, and SO42−. *Marine chemistry*, *98*(2-4), pp.131-139. https://doi.org/10.1016/j.marchem.2005.09.001.

Dussaud, M., 1989. New techniques in underground storage of natural gas in France. In *Underground Storage of Natural Gas* (pp. 371-383). Springer, Dordrecht. https://doi.org/10.1007/978-94-009-0993-9_24.

Ellis, B., Peters, C., Fitts, J., Bromhal, G., McIntyre, D., Warzinski, R. and Rosenbaum, E., 2011. Deterioration of a fractured carbonate caprock exposed to CO2-acidified brine flow. *Greenhouse Gases: Science and Technology*, *1*(3), pp.248-260. https://doi.org/10.1002/ghg.25.

Farquhar, S.M., Dawson, G.K.W., Esterle, J.S. and Golding, S.D., 2013. Mineralogical characterisation of a potential reservoir system for CO2 sequestration in the Surat Basin. *Australian Journal of Earth Sciences*, *60*(1), pp.91-110. https://doi.org/10.1080/08120099.2012.752406.

Fazeli, H., Patel, R.A., Ellis, B.R. and Hellevang, H., 2019. Three-dimensional pore-scale modeling of fracture evolution in heterogeneous carbonate caprock subjected to CO2-enriched brine. *Environmental science & technology*, *53*(8), pp.4630-4639. https://doi.org/10.1021/acs.est.8b05653.

Fitts, J.P. and Peters, C.A., 2013. Caprock fracture dissolution and CO2 leakage. *Rev. Mineral. Geochem*, *77*, pp.459-479. https://doi.org/10.2138/rmg.2013.77.13.

Fleming, M.R., Adams, B.M., Randolph, J.B., Ogland-Hand, J.D., Kuehn, T.H., Buscheck, T.A., Bielicki, J.M. and Saar, M.O., 2018, February. High efficiency and large-scale subsurface energy storage with CO2. In *43rd Workshop on geothermal reservoir engineering, Stanford, CA*.

Gelhar, L.W., Welty, C. and Rehfeldt, K.R., 1992. A critical review of data on field-scale dispersion in aquifers. *Water resources research*, *28*(7), pp.1955-1974. https://doi.org/10.1029/92WR00607.

Gharbi, O., Bijeljic, B., Boek, E. and Blunt, M.J., 2013. Changes in pore structure and connectivity induced by CO2 injection in carbonates: A combined pore-scale approach. *Energy Procedia*, *37*, pp.5367-5378. https://doi.org/10.1016/j.egypro.2013.06.455.

Gharbi, O., 2013. Fluid-rock interactions in carbonates: applications to CO2 storage. https://doi.org/10.5339/qfarf.2012.EEPS21.

Golubev, S.V., Bénézeth, P., Schott, J., Dandurand, J.L. and Castillo, A., 2009. Siderite dissolution kinetics in acidic aqueous solutions from 25 to 100 C and 0 to 50 atm pCO2. *Chemical Geology*, *265*(1-2), pp.13-19. https://doi.org/10.1016/j.chemgeo.2008.12.031.

He, Q., Liu, H., Hao, Y., Liu, Y. and Liu, W., 2018. Thermodynamic analysis of a novel supercritical compressed carbon dioxide energy storage system through advanced exergy analysis. *Renewable energy*, *127*, pp.835-849. https://doi.org/10.1016/j.renene.2018.05.005.

Huang, W.L., Bishop, A.M. and Brown, R.W., 1986. The effect of fluid/rock ratio on feldspar dissolution and illite formation under reservoir conditions. *Clay*

Minerals, *21*(4), pp.585-601. https://doi.org/10.1180/claymin.1986.021.4.10.

Huq, F., Haderlein, S.B., Cirpka, O.A., Nowak, M., Blum, P. and Grathwohl, P., 2015. Flow-through experiments on water–rock interactions in a sandstone caused by CO2 injection at pressures and temperatures mimicking reservoir conditions. *Applied Geochemistry*, *58*, pp.136-146. https://doi.org/10.1016/j.apgeochem.2015.04.006.

Warner, A.J., 1993. *Regional geologic framework of the Cretaceous, offshore Mississippi*. Mississippi Department of Environmental Quality, Office of Geology.

Kabuth, A., Dahmke, A., Beyer, C., Bilke, L., Dethlefsen, F., Dietrich, P., Duttmann, R., Ebert, M., Feeser, V., Görke, U.J. and Köber, R., 2017. Energy storage in the geological subsurface: dimensioning, risk analysis and spatial planning: the ANGUS+ project. *Environmental Earth Sciences*, *76*(1), pp.1-17. https://doi.org/10.1007/s12665-016-6319-5.

Ketzer, J.M., Iglesias, R., Einloft, S., Dullius, J., Ligabue, R. and De Lima, V., 2009. Water–rock–CO2 interactions in saline aquifers aimed for carbon dioxide storage: experimental and numerical modeling studies of the Rio Bonito Formation (Permian), southern Brazil. *Applied geochemistry*, *24*(5), pp.760-767.https://doi.org/10.1016/j.apgeochem.2009.01.001.

Knauss, K.G. and Wolery, T.J., 1988. The dissolution kinetics of quartz as a function of pH and time at 70 C. *Geochimica et Cosmochimica Acta*, *52*(1), pp.43-53. https://doi.org/10.1016/0016-7037(88)90055-5.

Laille, J.P., Molinard, J.E. and Wents, A., 1988, June. Inert gas injection as part of the cushion of the underground storage of Saint-Clair-Sur-Epte, France. In *SPE Gas Technology Symposium*. OnePetro. https://doi.org/10.2523/17740-ms.

Van der Linden, S., 2006. Bulk energy storage potential in the USA, current

developments and future prospects. *Energy*, *31*(15), pp.3446-3457. https://doi.org/10.1016/j.energy.2006.03.016.

Liu, H.H., Zhang, G., Yi, Z. and Wang, Y., 2013. A permeability-change relationship in the dryout zone for CO2 injection into saline aquifers. *International Journal of Greenhouse Gas Control*, *15*, pp.42-47. https://doi.org/10.1016/j.ijggc.2013.01.034.

Luquot, L. and Gouze, P., 2009. Experimental determination of porosity and permeability changes induced by injection of CO2 into carbonate rocks. *Chemical Geology*, *265*(1-2), pp.148-159. https://doi.org/10.1016/j.chemgeo.2009.03.028.

McGrail, B.P., Spane, F.A., Sullivan, E.C., Bacon, D.H. and Hund, G., 2011. The Wallula basalt sequestration pilot project. *Energy Procedia*, *4*, pp.5653-5660. https://doi.org/10.1016/j.egypro.2011.02.557.

Metcalf, G.E., 2020. Designing a carbon tax to reduce US greenhouse gas emissions. *Review of Environmental Economics and Policy*. https://doi.org/10.1093/reep/ren015.

Mouli-Castillo, J., Wilkinson, M., Mignard, D., McDermott, C., Haszeldine, R.S. and Shipton, Z.K., 2019. Inter-seasonal compressed-air energy storage using saline aquifers. *Nature Energy*, *4*(2), pp.131-139. https://doi.org/10.1038/s41560-018-0311-0.

Nathenson, M. and Guffanti, M., 1988. Geothermal gradients in the conterminous United States. *Journal of Geophysical Research: Solid Earth*, *93*(B6), pp.6437-6450. https://doi.org/10.1029/JB093iB06p06437.

Nogues, J.P., Fitts, J.P., Celia, M.A. and Peters, C.A., 2013. Permeability evolution due to dissolution and precipitation of carbonates using reactive transport modeling in pore networks. *Water Resources Research*, *49*(9), pp.6006-6021.

https://doi.org/10.1002/wrcr.20486.

Oelkers, E.H., Schott, J., Gauthier, J.M. and Herrero-Roncal, T., 2008. An experimental study of the dissolution mechanism and rates of muscovite. *Geochimica et Cosmochimica Acta*, *72*(20), pp.4948-4961. https://doi.org/10.1016/j.gca.2008.01.040.

Oldenburg, C.M., Stevens, S.H. and Benson, S.M., 2004. Economic feasibility of carbon sequestration with enhanced gas recovery (CSEGR). *Energy*, *29*(9-10), pp.1413-1422. https://doi.org/10.1016/j.energy.2004.03.075.

Oldenburg, C.M., 2003. Carbon dioxide as cushion gas for natural gas storage. *Energy & Fuels*, *17*(1), pp.240-246. https://doi.org/10.1021/ef020162b.

Oldenburg, C.M. and Pan, L., 2013. Utilization of CO2 as cushion gas for porous media compressed air energy storage. *Greenhouse Gases: Science and Technology*, *3*(2), pp.124-135.https://doi.org/10.1002/ghg.1332.

Onuma, T. and Ohkawa, S., 2009. Detection of surface deformation related with CO2 injection by DInSAR at In Salah, Algeria. *Energy Procedia*, *1*(1), pp.2177-2184. https://doi.org/10.1016/j.egypro.2009.01.283.

Ozarslan, A., 2012. Large-scale hydrogen energy storage in salt caverns. *International journal of hydrogen energy*, *37*(19), pp.14265-14277. https://doi.org/10.1016/j.ijhydene.2012.07.111.

Pfeiffer, W.T. and Bauer, S., 2015. Subsurface porous media hydrogen storage–scenario development and simulation. *Energy Procedia*, *76*, pp.565-572. https://doi.org/10.1016/j.egypro.2015.07.872.

Pfeiffer, W.T., Beyer, C. and Bauer, S., 2017. Hydrogen storage in a heterogeneous sandstone formation: dimensioning and induced hydraulic effects. *Petroleum Geoscience*, *23*(3), pp.315-326. https://doi.org/10.1144/petgeo2016-050.

Qin, F. and Beckingham, L.E., 2019. Impact of image resolution on quantification of mineral abundances and accessible surface areas. *Chemical Geology*, *523*, pp.31-41. https://doi.org/10.1016/j.chemgeo.2019.06.004.

Qin, F. and Beckingham, L.E., 2021. The impact of mineral reactive surface area variation on simulated mineral reactions and reaction rates. *Applied Geochemistry*, *124*, p.104852.

Reysa, Gary. 2012. "Ground Temperature as a Function of Location, Season, and Depth." *Build It Solar*.

Schoenung, Susan M, and William Hassenzahl. 2001. "Characteristics and Technologies for Long-vs. Short-Term Energy Storage A Study by the DOE Energy Storage Systems Program SAND2001-0765." *Sandia National Laboratories U.S. Dept. of Energy*.

Sopher, Daniel, Christopher Juhlin, Tegan Levendal, Mikael Erlström, Karl Nilsson, and José Pedro Da Silva Soares. 2019. "Evaluation of the Subsurface Compressed Air Energy Storage (CAES) Potential on Gotland, Sweden." *Environmental Earth Sciences*. https://doi.org/10.1007/s12665-019-8196-1.

Steefel, C. I., C. A.J. Appelo, B. Arora, D. Jacques, T. Kalbacher, O. Kolditz, V. Lagneau, et al. 2015. "Reactive Transport Codes for Subsurface Environmental Simulation." *Computational Geosciences*. https://doi.org/10.1007/s10596-014-9443-x.

Steefel, Carl I, and Sergi Molins. 2016. *CrunchFlow*. Berkeley: Earth Science Division, Lawrence Berkeley National Laboratory.

Succar, Samir, and Robert H Williams. 2008. "Compressed Air Energy Storage: Theory, Resources, and Applications for Wind Power." *Princeton Environmental Institute Report* *8*.

http://citeseerx.ist.psu.edu/viewdoc/download?doi=10.1.1.374.7597&rep=rep1&type=pdf.

Suekane, Tetsuya, Shingo Soukawa, Satoshi Iwatani, Shoji Tsushima, and Shuichiro Hirai. 2005. “Behavior of Supercritical CO2 Injected into Porous Media Containing Water.” In *Energy*. https://doi.org/10.1016/j.energy.2003.10.026.

Tutolo, Benjamin M., Xiang Zhao Kong, William E. Seyfried, and Martin O. Saar. 2015. “High Performance Reactive Transport Simulations Examining the Effects of Thermal, Hydraulic, and Chemical (THC) Gradients on Fluid Injectivity at Carbonate CCUS Reservoir Scales.” *International Journal of Greenhouse Gas Control*. https://doi.org/10.1016/j.ijggc.2015.05.026.

Wang, Bo, and Sebastian Bauer. 2017. “Compressed Air Energy Storage in Porous Formations: A Feasibility and Deliverability Study.” *Petroleum Geoscience*. https://doi.org/10.1144/petgeo2016-049.

Wang, Yan, Liwei Zhang, Yee Soong, Robert Dilmore, Hejuan Liu, Hongwu Lei, and Xiaochun Li. 2019. “From Core-Scale Experiment to Reservoir-Scale Modeling: A Scale-up Approach to Investigate Reaction-Induced Permeability Evolution of CO 2 Storage Reservoir and Caprock at a U.S. CO 2 Storage Site.” *Computers and Geosciences*. https://doi.org/10.1016/j.cageo.2019.01.006.

Xiong, Wei, Rachel K. Wells, Jake A. Horner, Herbert T. Schaef, Philip A. Skemer, and Daniel E. Giammar. 2018a. “CO2 Mineral Sequestration in Naturally Porous Basalt.” *Environmental Science and Technology Letters*. https://doi.org/10.1021/acs.estlett.8b00047.

Xiong, W., Wells, R.K., Horner, J.A., Schaef, H.T., Skemer, P.A. and Giammar, D.E., 2018. CO2 mineral sequestration in naturally porous basalt. *Environmental Science & Technology Letters*, *5*(3), pp.142-147. https://doi.org/10.1021/acs.estlett.8b00047.

Zhang, Liwei, Argha Namhata, Robert Dilmore, Bin Wang, Yan Wang, Manguang Gan, and Xiaochun Li. 2020. “Application of Arbitrary Polynomial Chaos (APC) Expansion for Global Sensitivity Analysis of Mineral Dissolution and Precipitation Modeling under Geologic Carbon Storage Conditions.” *Computational Geosciences*. https://doi.org/10.1007/s10596-020-09953-6.

Zhang, Shuo, and Donald J. DePaolo. 2017. “Rates of CO2 Mineralization in Geological Carbon Storage.” *Accounts of Chemical Research*. https://doi.org/10.1021/acs.accounts.7b00334.

Zou, Yushi, Sihai Li, Xinfang Ma, Shicheng Zhang, Ning Li, and Ming Chen. 2018a. “Effects of CO2–Brine–Rock Interaction on Porosity/Permeability and Mechanical Properties during Supercritical-CO2 Fracturing in Shale Reservoirs.” *Journal of Natural Gas Science and Engineering*. https://doi.org/10.1016/j.jngse.2017.11.004.

Zou, Y., Li, S., Ma, X., Zhang, S., Li, N. and Chen, M., 2018. Effects of CO2–brine–rock interaction on porosity/permeability and mechanical properties during supercritical-CO2 fracturing in shale reservoirs. *Journal of Natural Gas Science and Engineering*, *49*, pp.157-168. https://doi.org/10.1016/j.jngse.2017.11.004.

Chapter 3: Influence of storage period on the geochemical evolution of brine and cushion gas boundary zone of porous saline aquifers used for compressed energy storage.

Chidera O. Iloejesi; Lauren E. Beckingham*

Department of Civil and Environmental Engineering, Auburn University, Auburn, Alabama, 36849.

Corresponding Author* Tel: 334-844-6260; e-mail: leb0071@auburn.edu

Published in Frontiers in Water, *Front. Water* 3:689404. doi: 10.3389/frwa.2021.689404

Abstract

Subsurface porous aquifers are being considered for use as reservoirs for compressed energy storage of renewable energy. In these systems, a gas is injected during times in which production exceeds demand and extracted for energy generation during periods of peak demand or scarcity in production. Current operational subsurface energy facilities use salt caverns for storage and air as the working gas. CO_2 is potentially a more favorable choice of working gas where under storage conditions CO_2 has high compressibility which can improve operational efficiency. However, the interaction of CO_2 and brine at the boundary of the storage zone can produce a chemically active fluid which can result in mineral dissolution and precipitation reactions and alter the properties of the storage zone. This study seeks to understand the geochemical implications of utilization of CO_2 as a working gas during injection, storage and extraction flow cycles. Here, reactive transport simulations are developed based on 7 hours of injection, 11 hours of withdrawal and 6 hours of reservoir closure, corresponding to the schedule of the Pittsfield field test, for 15 years of operational life span to assess the geochemical evolution of the reservoir. The evolution in the storage system is compared to a continuously cyclic system of 12 hours injection and extraction. The result of the study on operational schedule shows that while some

reactivity might occur at the inlet of the domain, the pore structure of the inner domain is significantly preserved during the cycling of CO_2 acidified brine for both systems.

3.1.0 Introduction

The global renewable energy share in terms of final energy consumption has increased over the past decade to 17.5% in 2016(IEA 2019). Increased utilization of renewables resulted from government policy incentives(Lyon and Yin 2010; Chandler 2009; M. Y. Huang et al. 2007; Jenner et al. 2012), technical advancements(Mensah et al. 2018; Álvarez-Herránz et al. 2017; Lin and Zhu 2019), and environmental benefits that promote social acceptance(Haar and Theyel 2006; Aslani, Naaranoja, and Zakeri 2012; Bing Wang et al. 2018). Moreover, adopting renewable energy has been positively linked to economic development(Sadorsky 2009b; 2009a; Apergis and Payne 2010) and reductions in anthropogenic greenhouse gas emissions while diversifying energy production(Chen, Kim, and Yamaguchi 2014; Chien and Hu 2008; Lund 2007; Marques, Fuinhas, and Manso 2011). However, the intermittency of renewable energy production requires a reliable means of long term, large capacity energy storage to achieve energy security through renewable energy(van der Linden 2006). Efforts to increase and improve energy storage have included fast discharging, low capacity options like lead-acid batteries to slow discharging, high capacity options like pumped hydro and compressed energy storage(Dunn, Kamath, and Tarascon 2011). The high capacity options store bulk energy in megawatts for hours to months, which offers increased reliability in grid-scale applications of renewable energy.

Compressed energy storage is a promising means of long-term, grid-scale energy storage that has the potential to be widely deployed across the globe in subsurface reservoir formations including salt caverns or porous saline aquifers(Aghahosseini and Breyer 2018). In these systems, a working gas is injected into the storage formation during periods of excess energy production and extracted to power a turbine during periods of excess energy demand(Succar and Williams 2008).

Salt caverns, mined hard rock caverns and porous saline aquifers can be utilized as storage reservoirs(K. Allen 1985). Energy storage has only been carried out in salt caverns to date and using air as a working fluid in salt caverns commands a competitive capital cost of installation and the lowest operating cost in comparison to other currently used bulk energy storage options(van der Linden 2006). Salt caverns, however, are geographically limited. Porous saline aquifers, on the other hand, are ubiquitous which makes them a potentially more favorable option(Succar and Williams 2008; Report 2003). The idea of extending the compressed energy storage medium beyond the currently used salt caverns to porous aquifers will facilitate more widespread possible utilization of this technology for municipal energy storage.

To initialize the system in a porous aquifer, a cushion gas may first be permanently injected into the porous formation to raise background pressure to help increase working gas recovery(Carden and Paterson 1979). The cushion gas is injected into the formation to buffer the pressure fluctuation during the cycling of a working gas during energy storage. Hence, the compressibility of the cushion gas is thus an important consideration in helping to improve the economics and efficiency of compressed energy storage. The injection of these storage gases stratifies the porous saline aquifer into zones with varying compositions of gas to brine ratio(Cui et al. 2018). Although, these zones may not be distinctly classified and there could be mixing of working gas and cushion gas at the interface of the two gases(Kim, Choi, and Park 2015). Furthest from the injection well is the zone where the cushion gas and the brine interface. At this zone, gas dissolution into the brine is controlled by mutual solubilities(Beckingham and Winningham 2019).

For over eight decades that subsurface storage has been prevalent(K. Allen 1985; Carden and Paterson 1979), a variety of gases have been considered as cushion and working gases including nitrogen(Pfeiffer and Bauer 2015a; Bauer et al. 2015), native methane(Curtis M. Oldenburg 2003), and air(Succar and Williams 2008) have all been considered as potential cushion gases. It was in the wake of geologic CO_2

sequestration that studies began to investigate the potential of using CO_2 as cushion gas. At the typical depth of saline aquifers, CO_2 becomes a supercritical fluid with a high density and compressibility, making it a particularly favorable choice of cushion gas where its high compressibility may improve available storage capacity, recovery and efficiency (Curtis M. Oldenburg 2003). Further consideration of the compressibility of CO_2 shows that using CO_2 as cushion gas can help reduce significant pressure variation during working gas cycling(Curtis M. Oldenburg and Pan 2013a). An additional positive benefit of using CO_2, a major greenhouse gas, is that it can remain permanently sequestered in the storage formation once injected. Hence, utilizing CO_2 for this purpose would provide potential environmental benefits and economic benefits in the form of tax credits(Mai et al. 2016). However, careful system design needs to be considered to not produce CO_2 during the extraction of the working gas(Curtis M. Oldenburg and Pan 2013a). This can lead to pressure losses in the formation to affect working gas recovery(Ma et al. 2019). Also, failure to sequester CO_2 while being used as cushion gas could offset potential tax credits gained by using CO_2 as a cushion gas(Rul 2009). It should also be noted that CO_2 can also be used as the working gas but this would require using a closed-loop system to exploit the beneficial physical properties of CO_2 for energy production while ensuring that none escapes to the atmosphere(Alami et al. 2019).

Injecting CO_2 in porous Saline aquifers, however, introduce additional technical complexities that need to be considered before adoption. This includes a need to understand possible geochemical limitations that can result from interactions between the injected gas, formation brine, and formation minerals. One of the key geochemical considerations is the interaction of the aquifer formation with the cushion gas which occupies one-third of the total storage volume(Walters, n.d.). While CO_2 is a favorable choice of cushion gas from its physical property point of view, there could be potential geochemical implications of reactions between CO_2, formation brine, and formation minerals that could pose to be a challenge to system operation(Z. Zhang and Huisingh

2017). These reactions, however, have not largely been considered and less reactive gases have been previously used as cushion gasses(Laille, Molinard, and Wents 1988; Misra et al. 1999). Injecting reactive fluids like CO_2 in the subsurface can acidify the formation brine and result in complex mineral dissolution and precipitation reactions within the formation rock matrix, as has been observed in the context of geologic CO_2 sequestration(DePaolo and Cole 2013; Kharaka and Cole 2011; Gunter, Perkins, and McCann 1993; Fischer, Liebscher, and Wandrey 2010). However, flow conditions in geologic CO_2 sequestration systems are distinctly different than those in energy storage systems. In geologic CO_2 sequestration systems, flow is predominately unidirectional away from the injection well while energy storage systems utilize cyclic, bi-directional flow conditions as a result of the injection and extraction of the working gas and may contain intermittent storage periods. Previous reactive transport simulations have considered the impact of cyclic flow conditions on geochemical reactions in energy storage systems in a porous saline aquifer. These simulations have shown that the rate and extent of potential dissolution and precipitation reactions in the formation are significantly reduced in the energy storage system in comparison to what is anticipated in geologic CO_2 sequestration system(Chidera O. Iloejesi; Lauren E. Beckingham 2559). While this result is promising in showing the geochemical challenges of using CO_2 in a porous saline aquifer for energy storage systems could be abated, the study only considered a flow condition where there is constant injection and extraction flow condition in a porous saline aquifer for which can be referred to as continuous operational schedule. Specifically, the study investigated geochemical evolution for flow conditions consisting of a 24-hour cycle evenly split between 12 hours duration of injection flow cycle and 12 hours duration of extraction flow cycle for a four-month operational period. However, operational schedules in most subsurface storage aquifers integrate duration of storage or shut-in which is when the injected gas is allowed to sit in the aquifer with little to no flow in the storage reservoir before it is extracted to meet demand. This operational schedule that includes duration of storage between the

injection and extraction flow cycles can be referred to as the periodic schedule. The resulting geochemical reactions and implications for these types of operating conditions have not been considered.

This study aims to enhance understanding of the rate and extent of potential geochemical reactions in porous saline aquifer utilized for energy storage which operates using a periodic schedule. This is done by comparing the difference between the already understood geochemical evolution of porous aquifer – compressed energy storage system operating with continuous schedule with the geochemical evolution when the system operates using the periodic operational schedule. Here, reactive transport simulations are developed considering daily cyclic interactions between CO_2 utilized as a cushion gas, formation brine, and formation minerals over a 15 years study period. The evolution of major ions in the formation brine, formation minerals, and porosity for each system is tracked and compared to aid in the understanding of the use of CO_2 as a cushion gas for compressed energy storage systems in porous saline aquifers operating with periodic schedule.

3.2.0 Method

3.2.1 Sample

The Paluxy formation is considered here as a potential storage reservoir. This formation has been considered for CO_2 enhanced oil recovery(Robinson and Davis 2012) and geologic CO_2 storage projects(Petrusak et al. 2010). Previous investigation of this formation has found it as high porosity, high permeability sandstone(Jack C Pashin et al. 2018; Bensinger and Beckingham 2020). This formation is predominantly quartz (76.45%) with 9.64% calcite, 8.23% smectite, and the remainder minor phases (<5%), as determined from SEM imaging analysis in Qin and Beckingham (2019), where the mineral abundances are given in Table 3.1. The porosity of the sample obtained from image segmentation is 24.84% and the simulated permeability, as

estimated using pore network modeling in Bensinger and Beckingham (2020), is 1555.5 mD(Bensinger and Beckingham 2020).

Table 3.1: Properties of the Paluxy formation obtained from multi-scale imaging of the sample(Qin and Beckingham 2019) and rate constants for the respective mineral phases as obtained from the literature (superscripts) (Brady and Walther 1990; Knauss and Wolery 1988; Alkattan et al. 1998; Bevan and Savage 1989; Amram and Ganor 2005; Oelkers et al. 2008; Golubev et al. 2009).

Mineral	Ideal Chemical Formula	Abundance (%)(Qin and Beckingham 2019)	Volume Fraction(Qin and Beckingham 2019)	Surface Area (m^2g^{-1})(Qin and Beckingham 2019)	Log Rate Constant (mol s^{-1} m^{-2})
Quartz(Brady and Walther 1990; Knauss and Wolery 1988)	SiO_2	76.45	0.5740	2.59E-2	-11.60
Calcite(Alkattan et al. 1998)	$CaCO_3$	9.63	0.0724	1.42E-3	-4.21
K-Feldspar(Bevan and Savage 1989)	$KAlSi_3O_8$	3.50	0.0263	1.15E-3	-11.65
Smectite(Amram and Ganor 2005)	$(Na,Ca)_{0.33}(Al,Mg)_2(Si_4O_{10})$	8.23	0.0619	1.63E+1	-13.35
Muscovite(Oelkers et al. 2008)	$KAl_2(Si_3AlO_{10})(OH)_2$	0.31	0.0023	1.10E+0	-12.67
Siderite(Golubev et al. 2009)	$FeCO_3$	1.98	0.0141	6.49E-4	-5.69

3.2.2 Reactive Transport Simulations

Reactive transport simulations to understand the geochemical evolution of the reservoir in the brine-saturated region surrounding the gas plume were developed here for energy storage systems using CO_2 as a cushion gas for two storage operational schedules for 15 years. Simulations were developed in CrunchFlow, a multi-species

reactive transport simulation code(Carl I Steefel and Molins 2016) that has been used extensively used to understand subsurface geochemical reactions(Dávila et al. 2016; L. Zhang et al. 2015).

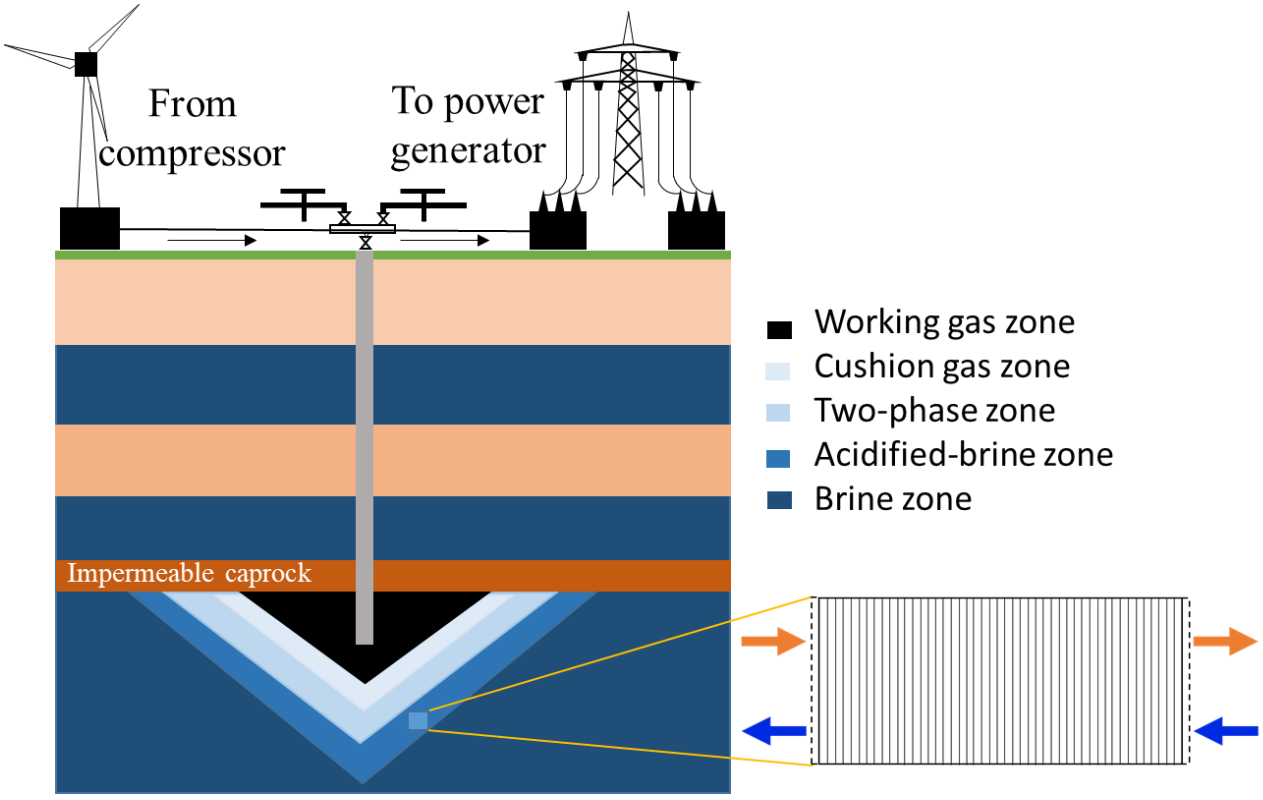

Figure 3.1: Schematic of the energy storage system and model domain for the reactive transport simulations.

To consider the most reactive zone in the storage system, the brine-saturated region adjacent to the cushion gas plume was considered here (Figure 3.1). In this region, CO_2 will dissolve into the brine phase, creating a region of acidified-brine favorable for geochemical reactions in the system(Huq et al. 2015). Here, a fifteen-centimeter domain in the acidified-brine zone was selected for simulations. The model domain was discretized into forty-five equally spaced grid cells. For ease of comparison of the concentration of major ion species, mineral volume fractions, and porosity evolutions, the model system is monitored at three locations called the upstream, midstream and downstream locations. The upstream is in the first internal grid cell, the midstream in the central internal grid cell, and the downstream location is the furthest

mineral grid cell from the injection well. The model domain was bounded by two 'ghost' cells that serve as the boundary condition in the one-dimensional flow through simulation.

Two daily operational schedules are used in this study, one consisting of a periodic storage schedule that includes a shut-in or storage period and the other a continuous storage schedule without the shut-in or storage period. In this study, we referred to the subsurface flow condition generated during continuous schedule as the injection-extraction flow regime because it comprises of the injection cycle and extraction cycle. The flow condition for the periodic schedule is referred to as the injection-storage-extraction flow regime as it includes the duration of storage or storage cycle. The continuous schedule consists of 12 hours of injection cycle followed by 12 hours of extraction cycle. The periodic schedule incorporates a 6 hours shut-in or storage cycle between 7 hours of injection cycle and 11 hours of extraction cycle. The periodic storage schedule is similar to the schedule used during the Pittsburg, Illinois field test(R. D. Allen 1981; R. D. Allen et al. 1983). In both simulations, the injection cycle corresponds to flow of CO_2 saturated brine away from the injection well from the 'ghost' boundary cell adjacent to the upstream cell location. During the extraction cycle, the effluent brine from the injection cycle is captured in the downstream boundary or 'ghost' cell. Then it will serve as a source cell for the brine to be recycled through the system by making the first contact with the downstream location. Also, the upstream boundary or 'ghost' cell serves as a catchment for the effluent injected into the system during the extraction cycle. Therefore, the composition of the influent brine for each cycle is based on the effluent of the preceding flow cycle. However, the difference is that the brine for each injection cycle is equilibrated with CO_2 to demonstrate the constant dissolution of CO_2 into the acidified-brine zone as expected at the brine-cushion gas boundary. For the flow regime that incorporates the duration of storage, flow ceases during storage cycle and the system effectively becomes a batch system. Both simulations undergo a complete cycle in 24-hour which corresponds to a

CES system used daily for power generation(Fleming et al. 2018; Pfeiffer, Beyer, and Bauer 2017; R. D. Allen et al. 1983) and the cycles were studied for over a fifteen years study period.

The model system was assumed as a homogenous and isotropic domain and initialized based on the mineral compositions, surface areas, and porosity from Qin and Beckingham(Qin and Beckingham 2019). The initial brine composition was calculated based on a 1M NaCl brine in equilibrium with formation minerals for ten thousand years at reservoir temperature and pressure(Qin and Beckingham 2021a; Xu et al. 2007). The corresponding reservoir temperature and pressures were 50^{o}C and 100 bar based on the geothermal gradient at Kemper, Mississippi and a typical pressure gradient(Reysa 2012; Nathenson and Guffanti 1988; Bachu 2000). The pH of the brine was determined via charge balance. The CO_2 saturated brine composition was determined by equilibrating brine with a constant partial pressure of CO_2 at the depth of storage in the Paluxy formation. The Duan CO_2 solubility model, which factors for high pressure and temperature conditions, was used to calculate the CO_2 solubility in brine(Duan et al. 2006). A brine flowrate of 0.489 m/day was used for the continuous schedule. The flowrate is extrapolated for the Paluxy reservoir conditions from field-scale simulations of brine fluid velocities adjacent to injected CO_2 plumes in a similar reservoir condition(S. Zhang and DePaolo 2017). Flowrates of 0.838 m/day and 0.533m/day are used for injection cycles and extraction cycles, respectively. Two different flow rates were used for the periodic operational schedule to maintain equal pore volumes as to the continuous operational system during each 24-hour cycle.

Mineral reactions in CrunchFlow are simulated using a rate law based on transition state theory. The corresponding parallel rate laws are given by,

$$r_s = -A\left(\sum_{a=1}^{N} K_a \left(\prod_{i=1}^{N_c+N_x} a_i^{p_{ia}}\right)\right)\left(1-\left(\frac{Q_s}{K_s}\right)^{M}\right)^{n} \qquad (1)$$

where r_s is the reaction rate, A is the reactive surface area of a constituting mineral in the rock sample, K_a is the equilibrium dissolution rate constant for the 'a'th parallel reaction, N is number of parallel reactions, p_{ia} is an exponent that gives the dependence

of a species i on the 'a'th parallel reaction, $\prod_{i=1}^{N_c+N_x} a_i^{p_{ia}}$ explains the degree of equilibrium effect of ions in solution, n and M are exponents which are experimentally determined to explain nonlinear dependence of the affinity term, K_s is the equilibrium constant, and Q_s is the ion activity product for the rock-water interaction. Here, reaction rate constants from previously published experimental works were extrapolated to formation conditions, following the method in Beckingham et al. 2017. Mineral accessible surface areas determined from a multi-scale imaging analysis in Qin and Beckingham 2020 on a sample from the Paluxy formation were used here as reactive surface areas. These surface areas reflect the mineral surfaces accessible to reactive fluids in the formation. The aqueous activity coefficients of the brine solution were calculated using the extended Debye-Huckle model.

Table 3.2: Simulation Parameters for the periodic and continuous simulation model.

Simulation Parameters		Periodic Schedule	Continuous Schedule
Flow rate (m/day)	Injection	0.838	0.489
	Shut-in	0	-
	Extraction	0.533	0.489
Operation schedule (hours)	Injection duration	7	12
	Shut-in duration	6	-
	Extraction duration	11	12
Reservoir Permeability		1555.5 mD	
Reservoir porosity		24.84 %	

3.3.0 Result and Discussion

3.3.1 Continuous Operation Schedule

The simulated evolution of mineral volume fractions for the continuous operational schedule (cyclic injection and extraction) are shown in Figure 3.2. During the first cycle, the flow of acidified brine into the domain during injection results in rapid dissolution of calcite close to the injection point. This increases the calcium ion concentration (Fig. 3.3) and buffers the pH (Fig. 3.4) such that no additional calcite dissolution occurs downstream (Fig. 3.2). Siderite also dissolves, resulting in an

increase in iron concentrations and further buffering of the pH. Dissolution of siderite occurs throughout the domain with greater extents of dissolution closer to the injection well where the brine is the most undersaturated with respect to siderite. Smectite dissolves equally across the simulation domain, resulting in the production of aluminum ions. The produced aluminum results in early supersaturation of muscovite followed by slight dissolution of muscovite throughout the domain. Quartz and K-feldspar remain stable across the domain throughout the first injection period.

After twelve hours, the flow reverses as the first extraction cycle begins and continues until 24 hours. During this period, a constant composition brine, corresponding to the brine composition at the end of the proceeding injection cycle, enters the domain at the location furthest from the injection well and flows towards the injection well. The recycled brine has a pH of 4.93 (Fig. 3.4) and results in dissolution of siderite (Fig. 3.6), producing iron ions (Fig 3.4). The dissolution rate of siderite is the greatest furthest from the injection well, where the distance from equilibrium is greatest and reduces closer to the injection well as iron concentrations in solution increase. Smectite dissolves across the simulation domain at a relatively constant dissolution rate. No additional calcite dissolution occurs during this period due to elevated calcium ion concentrations in the solution from dissolution during the proceeding injection cycle. Quartz and K-feldspar remain stable.

The second injection period begins after 24 hours. During this period, a constant composition brine saturated with CO_2 enters the simulation domain. As the brine is recycled, the ion concentrations from the proceeding extraction period are maintained with additional acid added from equilibrium with the adjacent CO_2 plume. This results in conditions favorable for additional mineral dissolution, most notably siderite and smectite which are still undersaturated in solution. While the pH of the brine is 4.93, no additional calcite dissolution occurs because of the high concentration of calcium in the brine.

This continuous cycling of injection and extraction continues over the 15-year study period and the resulting simulated evolution of mineral volume fractions are shown in Figure 3.2. Calcite dissolution predominantly occurs at the edges of the simulation domain and calcite is relatively stable in the middle of the domain for the duration of the simulation. Muscovite continuously dissolves and is completely consumed within the first 1.5 years. The dissolution of muscovite results in an increase in the concentration of aluminum and silicate ions used by precipitating minerals in the system. The precipitating mineral favored as a result includes albite, kaolinite and gibbsite which are minerals dependent on the aluminum and silicate ion which was released into the brine by the muscovite dissolution. After 1.5 years, the siderite mineral which dissolved throughout the domain started precipitating throughout the domain. This behavior of siderite stems from the fact that before the precipitation of siderite began, there was high iron ions (Fig 3.5) released from siderite dissolution was used to promote chlorite precipitation. Hence, the consumption of released iron ions favors continued siderite dissolution (Fig 3.6). However, after 1.5 years, when the muscovite mineral is completely consumed to reduce the concentration of other ions that creates the conditions that are favorable for chlorite precipitation. The solution becomes supersaturated with respect to siderite ion to favor siderite precipitation (Fig. 3.7). To compensate for the depleted aluminum ion due to muscovite complete dissolution, the system triggered an increase in smectite dissolution. However, the low reactivity of the smectite meant that it cannot reverse the saturation condition of the brine to favor siderite dissolution. On the other hand, the increase in smectite dissolution resulted in the sufficient increase in magnesium ion concentration. The availability of calcium and magnesium ions in the brine result in dolomite precipitation. As calcium is consumed with dolomite precipitation after 1.5 years, calcite dissolution is again favored. After 5.5 years, calcite is completely depleted near the injection well. Calcite dissolution mostly occurs at the inlets of the domain because this is where the mineral is in contact with the most acidified brine and the brine is mainly buffered within the domain. The

addition of silicate based on the dissolution of muscovite and smectite results in precipitation of quartz and conditions favorable for chalcedony precipitation. K-feldspar remains stable throughout the simulation.

Ions released from dissolving minerals create conditions favorable for formation of secondary mineral phases. Figure 3.8 shows the simulated evolution of saturation indices for potential secondary mineral precipitates at three locations in the simulation domain. Dissolution of calcite, siderite, and smectite during the cycle create conditions favorable for precipitation of chlorite, gibbsite, chalcedony, kaolinite, dolomite, and albite minerals.

3.3.2 Operational Schedule Comparison

The simulated evolution of mineral volume fractions for the operational schedule that includes the storage period is shown in Figure 3.2. As evident in Figure 3.2, injection, storage, and extraction result in the dissolution of calcite at the simulation domain boundaries and siderite, smectite, and muscovite throughout the simulation domain. Quartz precipitation occurs throughout the simulation domain.

The variations in the evolution of calcite and siderite at closest and furthest from the injection well makes it easy to compare the continuous operational schedule with the periodic operational schedule, especially within the plots of the first two cycles (fig. 3.6). The two operational schedule has equal pore volume of acidified brine flowing into the system during injection resulting in a rapid dissolution of calcite and siderite during injection flow of acidified brine. The flow duration for the injection period of the continuous schedule is 12 hours while the periodic schedule operates with 7 hours injection period. The prolong period of injection of the acidified brine resulted in more dissolution of calcite and siderite near the injection well in the continuous schedule. In the storage schedule, there is less dissolution close to the injection well regardless of the higher flowrate during injection period of the periodic schedule. After the 7 hours of injection, the periodic schedule undergoes a 6 hours of storage. During storage,

calcite dissolution slows as the transport component of the reaction is eliminated. The calcite mineral undergo a halt in reaction progress while the siderite resulted in decrease in dissolution rate. There was no storage period in the continuous schedule.

During the first extraction period, calcite mineral stayed stable. As the brine is already close to saturation with the calcite, this does not result in enhanced dissolution during extraction. However, the dissolution rate again increases in siderite. The dissolution rate of siderite is highest at the downstream location which is closest to the source of brine during the extraction period. The observed dissolution extent during extraction period of the injection-storage-extraction cycle is because there was less dissolution during storage which result in a lower saturation of the brine relative to siderite. This created conditions that are more favorable for further siderite dissolution during extraction unlike calcite. Conversely, more siderite dissolves in the continuous schedule during the injection period, resulting in a relatively higher saturation of the brine with siderite to limit the extent of downstream siderite dissolution during extraction period.

During the first 1.5 years, there was more upstream dissolution in the continuous flow regime during the siderite dissolution phase. During the siderite precipitation phase after 1.5 year, the periodic schedule shows a more upstream precipitation extent than the continuous schedule but the continuous schedule shows more precipitation extent at the downstream location. As for calcite, there was less calcite dissolution close to the injection well in the periodic schedule because the injection period is shorter. However, the relatively long period of extraction period in the periodic schedule allowed for more calcite dissolution at the downstream location notwithstanding that equal pore volume flow through the domain during the injection and extraction period of each cycle. For the simulation timeline, however, there was incomplete calcite dissolution in the upstream location of the periodic flow regime while the upstream calcite completely dissolves in the continuous flow regime. The periodic schedule has

greater extents of dissolution furthest from the injection well and less calcite dissolution occurs in the continuous schedule at the downstream location.

Generally, there is a significant similarity in the evolution during the two operational schedules. The reaction progresses initially with the ongoing calcite and siderite dissolution to buffer the system. And eventually, siderite dissolves to buffer the reaction condition for duration of the first 1.5 years. However, the complete dissolution of muscovite in the periodic system within the first 1.5 years of simulation causes the readjustment of saturation condition of the brine which kicks in the long-term reaction pathways in the system which is similar to the periodic and continuous schedule system. Calcite dissolution rate increased in the system to singly act as the only buffer mineral as siderite begins to precipitate in the system. Also, in both systems, the precipitation rate of siderite decreased with the decreasing rate of calcite dissolution in both operational schedules which was more obvious in the periodic flow regime when the downstream calcite is approaching complete dissolution. Also, both schedules show the tendency to support similar mineral precipitate in the system.

Irrespective of whether the ongoing simulation cycle is an injection cycle or extraction flow cycle, the midstream location in each operational schedule is expected to mainly encounter the buffered acidified-brine solution. As a result, the mineral system under the two flow regimes evolves similarly within the domain. Muscovite and smectite minerals exhibited a continuous dissolution reaction within the domain. Muscovite mineral is the only mineral to completely dissolve within the domain while the smectite volume fraction within the domain continuously decreased. Within the domain, the quartz mineral initially stayed stable but reversed its reaction pathway to start undergoing precipitation reaction. However, K-feldspar stayed approximately stable in the formation throughout the simulation timeline. Generally, the least dissolution and the most stability occur within the domain during the two operational schedules.

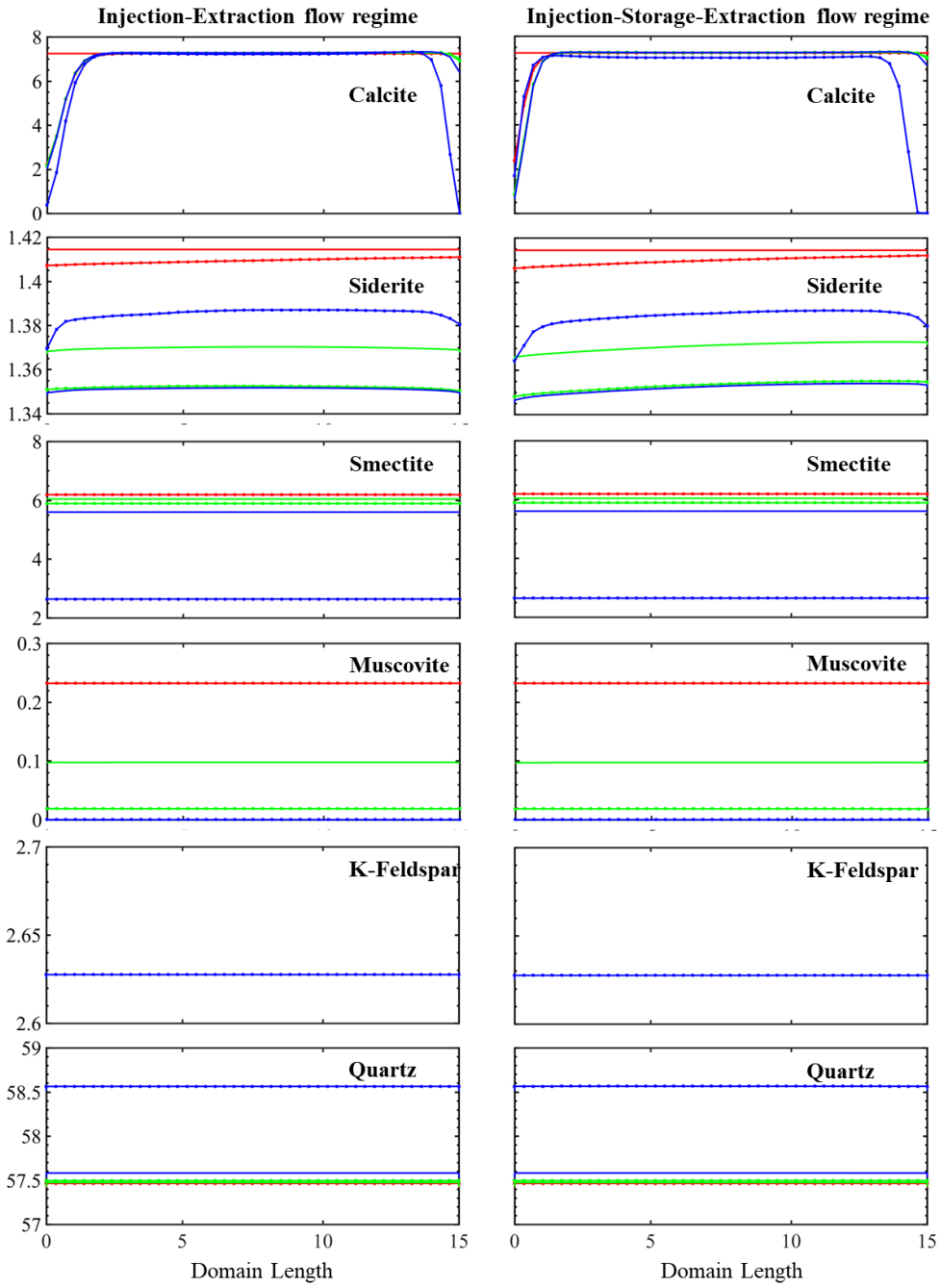

Figure 3.2: The simulated evolution of relative mineral volume fractions at three locations across the simulation domain over 15 years for the injection-storage-extraction flow regimes (left) and injection-extraction flow regimes (right). 0 cycle is the initial condition, and 5475 cycles PV is the last pore volume to flow through the porous media. red reflects 0 cycles, dotted red 1 cycle, green 180 cycles, dotted green 365 cycles, blue 730 cycles, and dotted blue 5475 cycles. One cycle is completed in 24 hours.

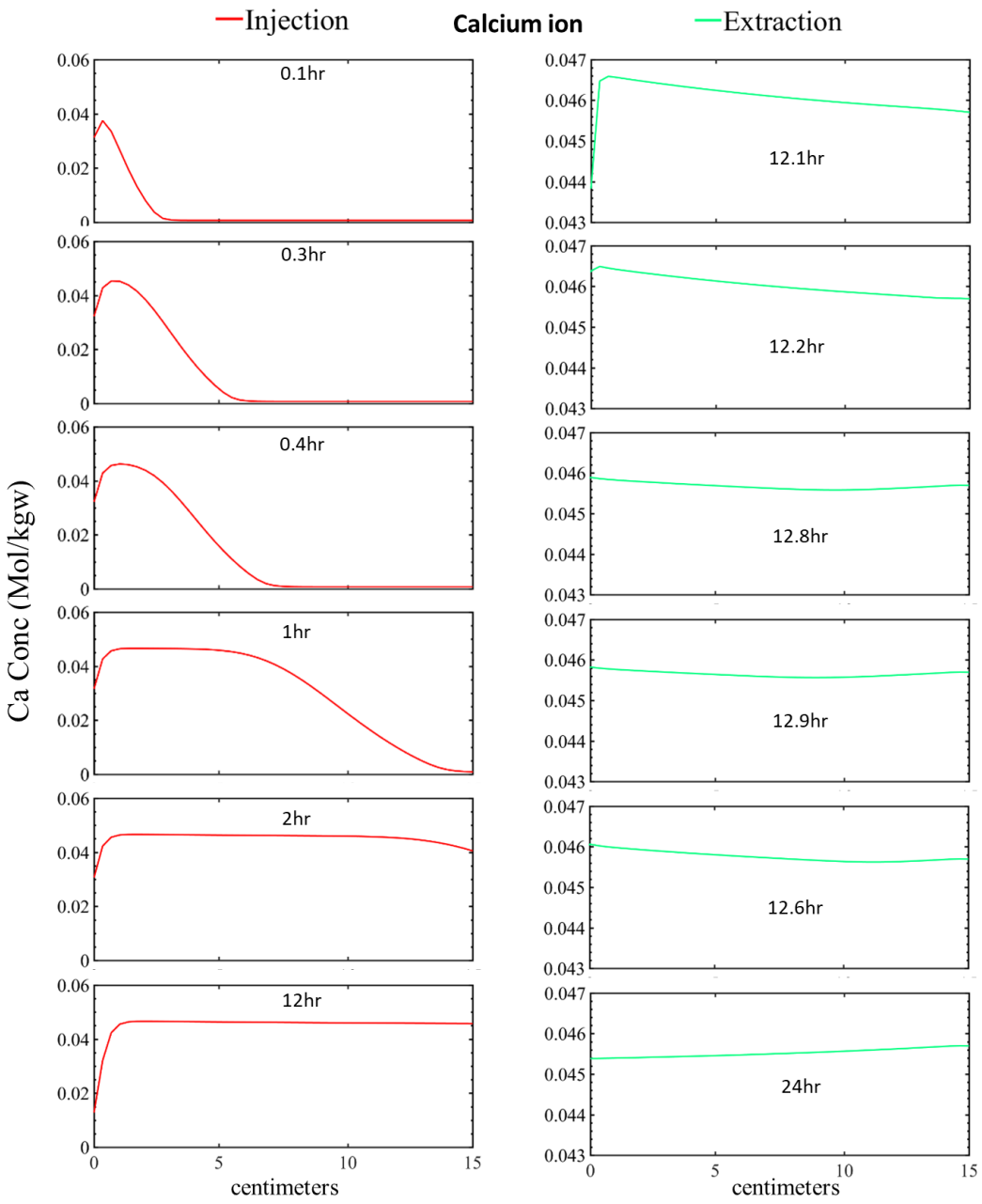

Figure 3.3: The simulated evolution of calcium ion concentrations of the porous formation at specific times during the first cycle of injection and extraction. The red represents the evolution during the injection cycle, and green the evolution during the extraction cycle.

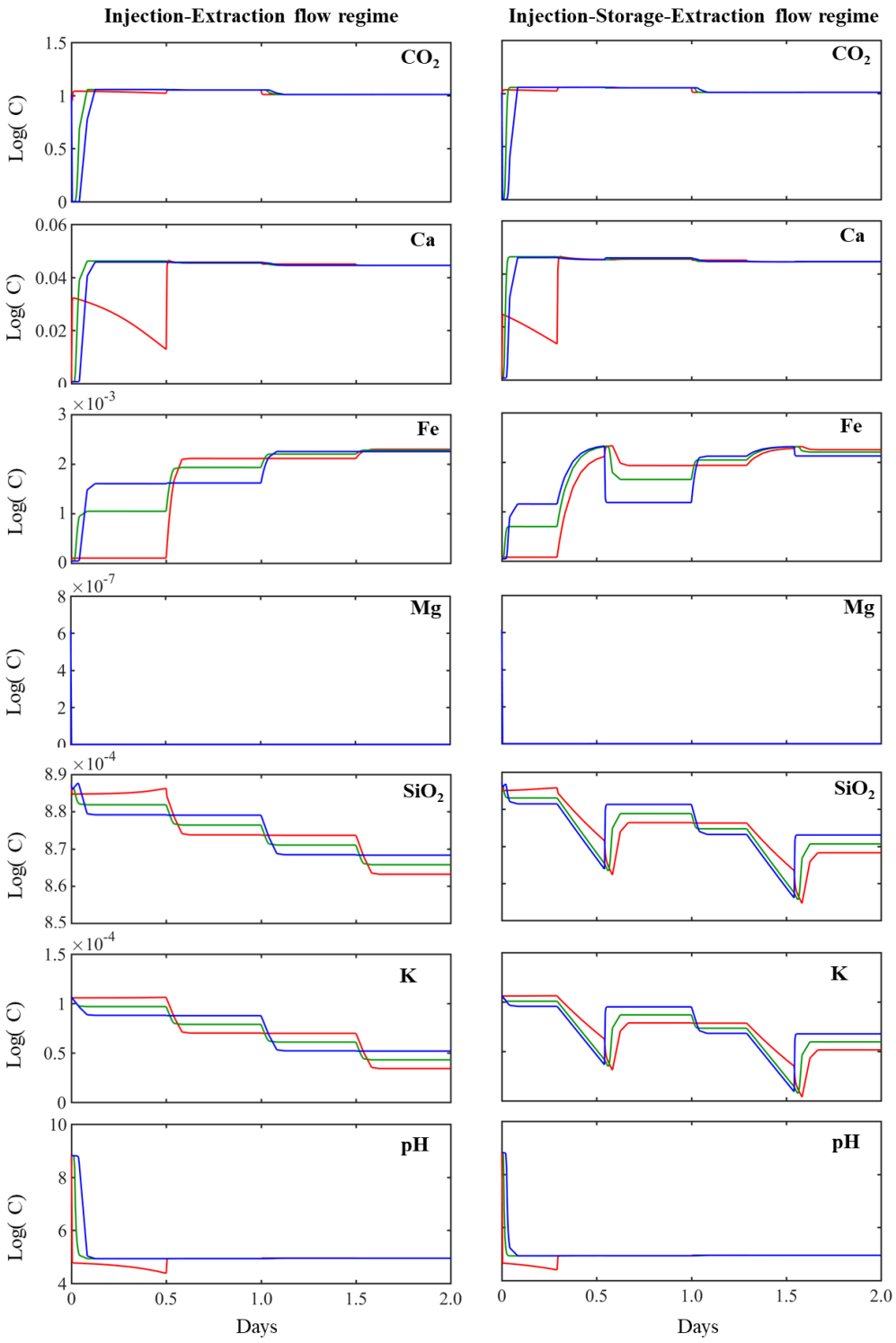

Figure 3.4: The simulated evolution of major ion concentrations and pH of the porous formation in three different grid cells over the first two cycles for the injection-storage-extraction flow regimes (left) and injection-extraction flow regimes (right). Upstream is closest to the source of CO_2 injection and downstream is furthest. The red represents the upstream location, green the midstream location, and blue the downstream location.

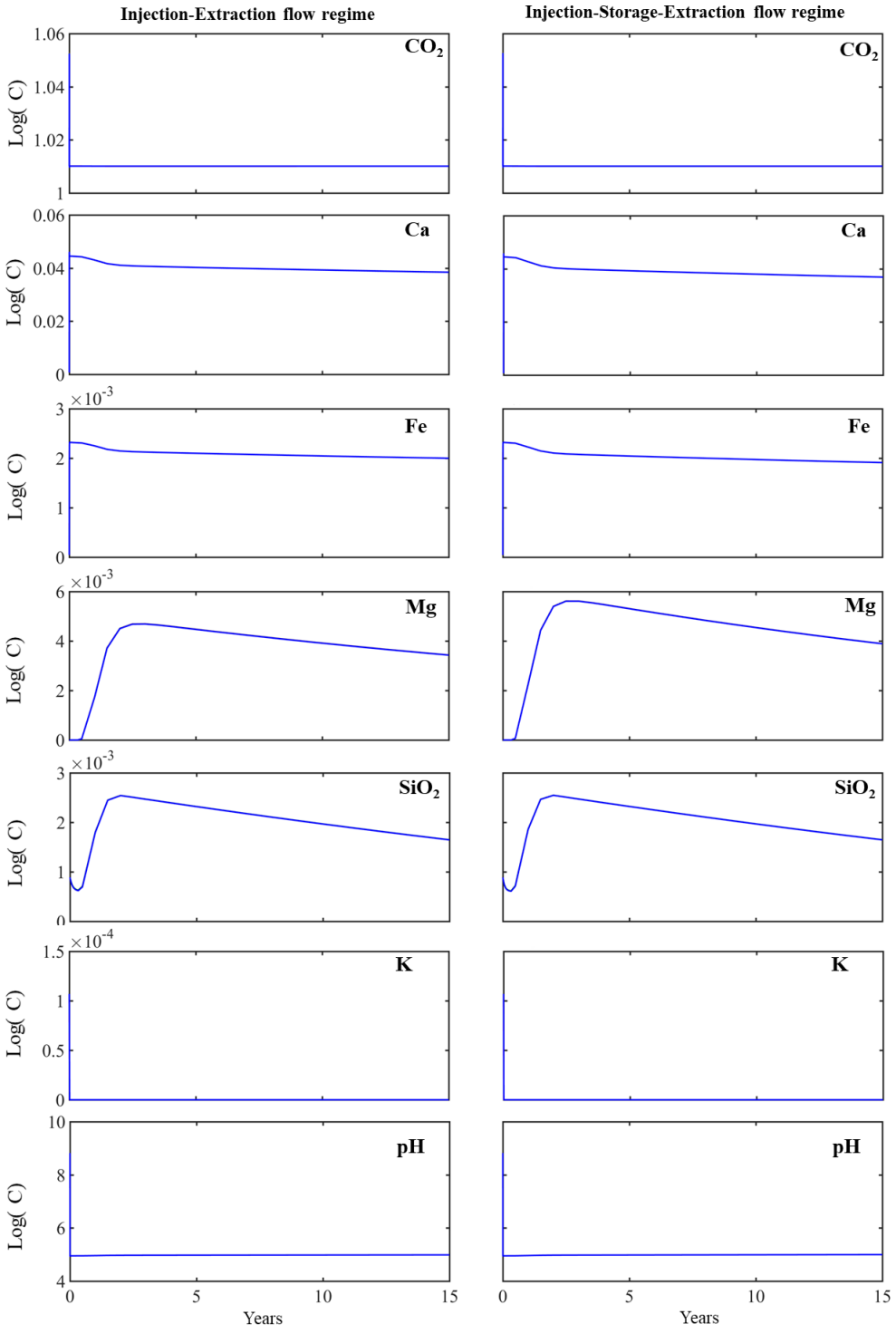

Figure 3.5: The simulated evolution of major ion concentrations and pH in three different grid cells over the 15 years study period for the injection-storage-extraction flow regimes (left) and injection-extraction flow regime (right). Upstream is closest to the source of CO_2 injection and downstream is furthest. The red represents the upstream location, green the midstream location, and blue the downstream location.

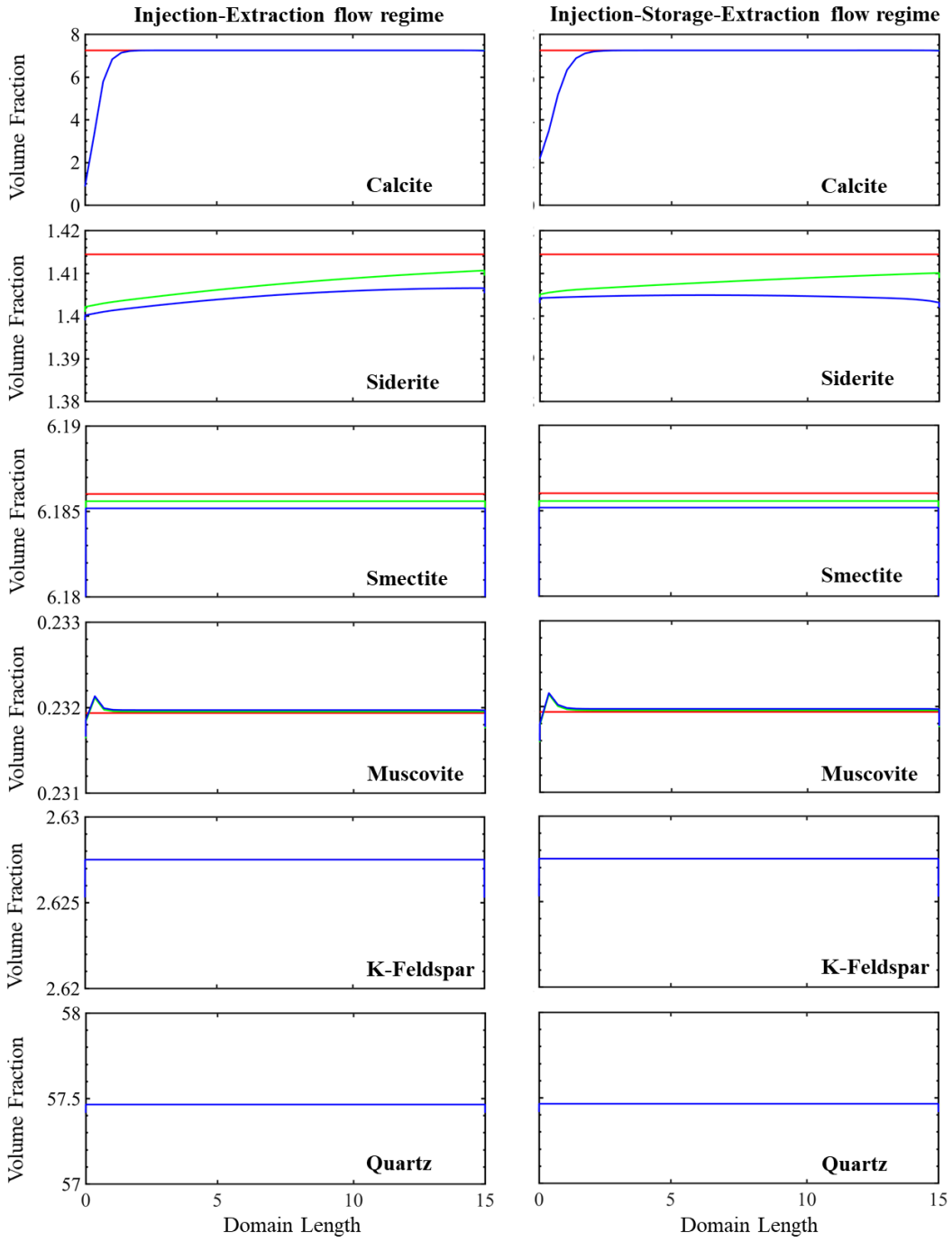

Figure 3.6: The simulated evolution of mineral volume fraction across the domain length at 0hr (red line), 12 hrs (green line), 24 hrs (blue line) for the injection-storage-extraction flow regimes (left) and injection-extraction flow regimes (right).

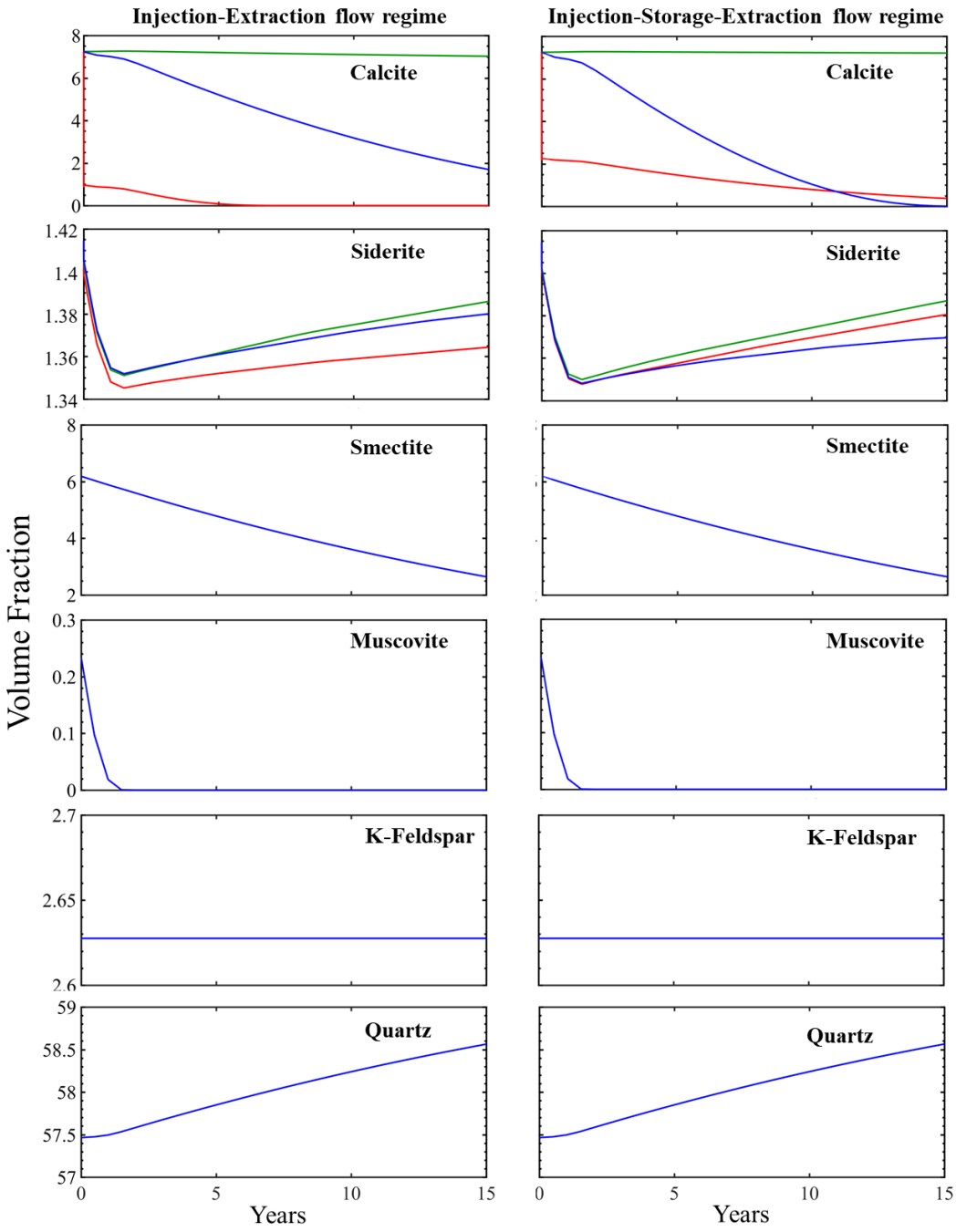

Figure 3.7: The simulated evolution of mineral volume fraction in three different grid cells over the 15 years study period for the injection-storage-extraction flow regimes (left) and injection-extraction flow regime (right). Upstream is closest to the source of CO_2 injection and downstream is furthest. The red represents the upstream location, green the midstream location, and blue the downstream location.

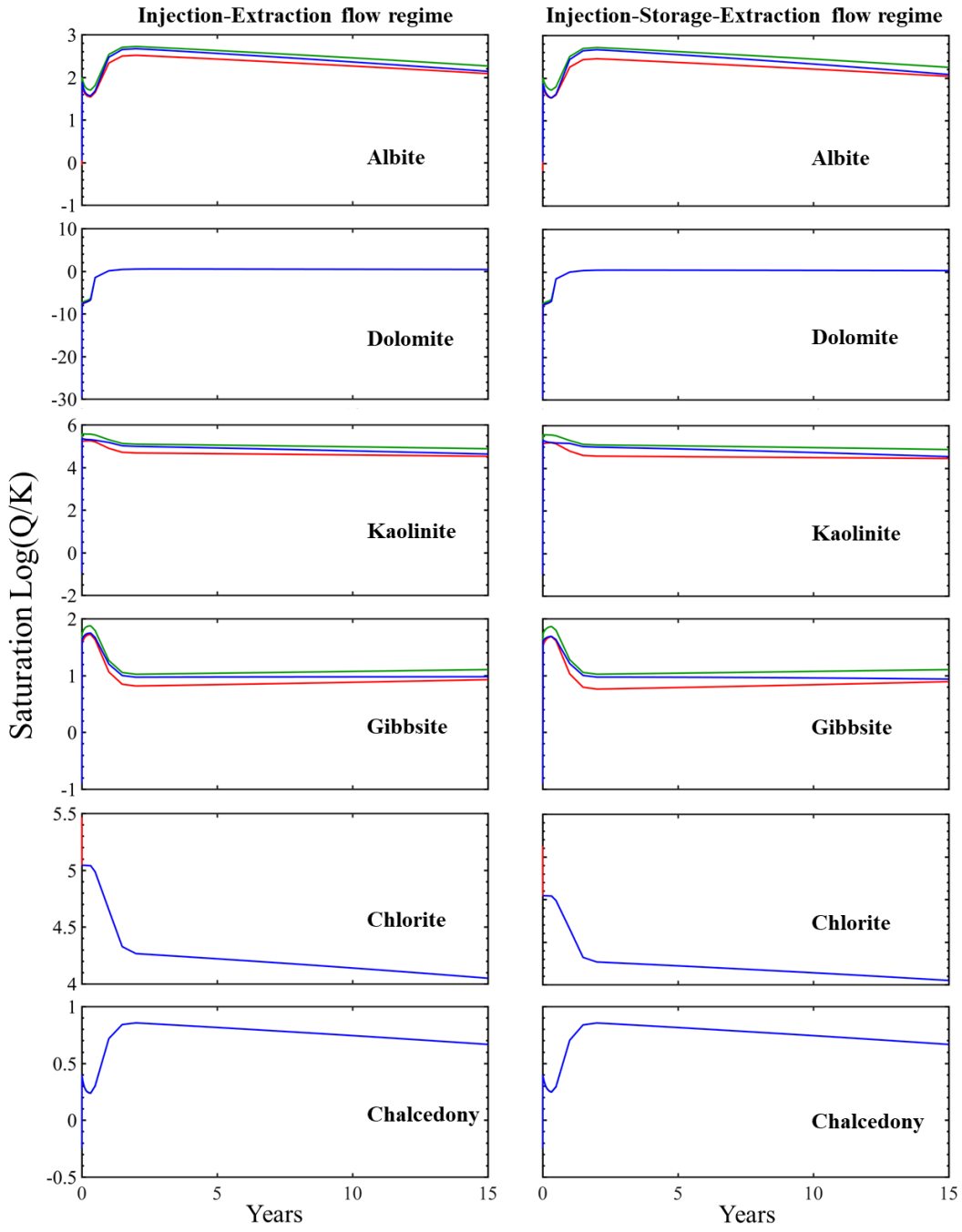

Figure 3.8: The simulated evolution of mineral saturation in three different grid cells locations over the 15 years study period for the injection-storage-extraction flow regimes (left) and injection-extraction flow regime (right). Upstream location is closest to the source of CO_2 injection and downstream location is furthest. The red represents the upstream location, green the midstream location, and blue the downstream location.

3.3.3 Porosity

The simulated evolution of porosity for the continuous and periodic schedules are shown in Figure 3.9 and Figure 3.10. These plots give the overall picture of the mineral evolution relative to pore spaces in the system.

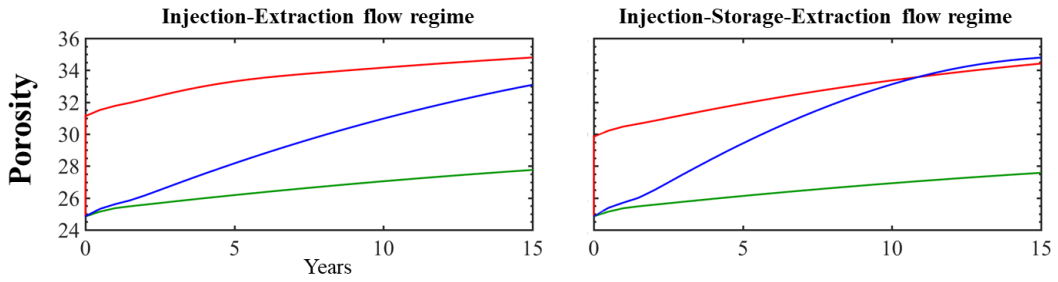

Figure 3.9: The simulated evolution of mineral porosity of the core sample in three different grid cells location over the fifteen years study period for the injection-storage-extraction flow regime (left) and injection-extraction flow regime (right). The upstream location is closest to the injection well and the downstream is furthest. The upstream location is closest to the injection well and downstream is furthest. The red represents the upstream location, green the midstream location, and blue the downstream location.

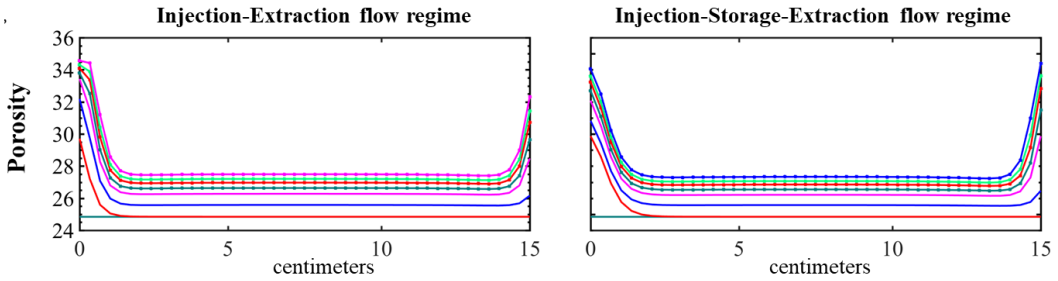

Figure 3.10: The simulated evolution of porosity with increasing number of pore volumes (PV) of CO_2 acidified brine flowing through the simulation domain over 15 years for the injection-storage-extraction flow regime (left) and injection-extraction flow regime (right). 0 cycle is the initial condition and 5475 cycles PV is the last pore volume to flow through the porous media. Dark green represents 0cycle, red 1cycles, light green 730cycles, blue 1460cycles, magenta 2005cycles, dotted dark green 2735cycles, dotted red 3465cycles, dotted light green 4015cycles, dotted blue 4745cycles, and dotted magenta 5475cycles. One cycle is completed in 24 hours.

The downstream porosity evolution is the main difference in the porosity of the two flow regimes. Both flow regimes have a similar evolution for the midstream

location. The upstream location has a similar final porosity evolution despite the initial 1.33% difference in porosity after two cycles. The upstream porosity evolution increased in the periodic flow regime to reduce the final porosity difference to 0.38% difference in upstream porosity. It is important to note that there is moderate evolution of porosity within the domain in the system shown by the porosity evolution across the domain length (Figure 3.10) even after 15 years of cycling acidified brine in the single-phase zone of the reservoir adjacent to CO_2 cushion gas. This signifies that regardless of the operational schedule, there is potential for flow cycling to preserve a mineral pore structure of a mineral system when a geochemical reaction is solely considered in a compressed energy storage system. The porosity evolution is dependent on the extent and rate of dissolving minerals. In this simulation, calcite, siderite, smectite, and muscovite are the dissolving mineral. However, given the small volume fraction (0.23%) of the muscovite that completely dissolved and about 3.54% of smectite that dissolves, it can be said that calcite dissolution primarily controlled the overall porosity evolution. Hence, explaining why the temporal porosity plot mirrored the calcite dissolution plot. The other controlling factor to porosity evolution is tied to mineral ion saturation. From the simulation result, elevated ion concentrations are maintained in the recycling brine. This limits mineral dissolution rate for both the periodic and continuous schedules, regardless of the acidification of the brine by the adjacent CO_2 cushion gas. Overall, the system attained 86% and 91% of its final porosity with the first year of cycling the acidified brine in the formation. This can serve as a guideline to know that using CO_2 as a cushion gas will require adequate monitoring during the early stages of the project.

3.4 Conclusion

Energy generation through renewable energy production can help reduce the concentration of anthropogenic emissions. The challenge of developing sufficient

storage to ensure energy security during the intermittency of renewable energy production could be solved through porous media compressed energy storage (PM – CES) system. When a certain condition is met, CO_2 could be securely stored in the subsurface as its favorable properties are exploited for energy to increase the efficiency of PM-CES system(Curtis M. Oldenburg and Pan 2013a). Also, the prospect of utilizing CO_2 as a cushion gas and sequestrating the gas in the process for clean energy production could be done using operational schedules that can be broadly categorized as the continuous operational schedule and periodic operational schedule. Where the major difference between the operational models is the presence of storage duration in the periodic operational schedule.

Storage duration became a geochemical concern after it was understood from the previous study that there is relatively mild geochemical evolution in porous media used for energy storage under continuous operational schedule in comparison to using the same formation for CO_2 sequestration(Chidera O. Iloejesi; Lauren E. Beckingham 2021). The concern with the storage duration is that the evolution of rock minerals and their major ions in solution is expected to behave differently during the storage period, and the cumulative effect of the distinctive storage geochemical evolution could result in developing a unique reaction pathway for the geochemical reaction occurring in a formation used for compressed energy storage that incorporates a shut-in or storage duration. Hence, this study used reactive transport simulation to evaluate the difference between the periodic and continuous flow schedules by comparing mineral volume fraction, ion concentration, and porosity.

The injection-storage-extraction operational schedule and injection-extraction operational schedule induces two acidified brine flow patterns referred to in this study as the periodic or continuous flow regime, respectively. The difference in the mineral volume fraction of the two flow regimes is in the carbonate mineral evolution. The downstream carbonate dissolution is greater in the periodic flow regime. Similar to the volume fraction evolution, the downstream porosity evolution is greater for the periodic

flow regime in comparison to the continuous flow regime. The major ion concentration shows that the storage duration encourages a slower rate of reaction. The slow storage period explains the overall reason for increased downstream dissolution. This is because the slow reaction period makes the saturation condition of the injected brine in a condition that allows for more downstream dissolution during the recycling of the brine as the storage cycle progresses. However, the overall difference in the downstream carbonate and porosity evolution is not statistically significant. Hence the operational schedule does not have any effect on the geochemical evolution of formation used for compressed energy storage.

This means that there will be an unexpected geochemical condition in a closed-boundary, single-phase region of a PM-CES system based on the operational schedule used in running the plant. A mild evolution pattern of the system shows that adequate monitoring of the system, especially at the early stage of the simulation, can be helpful to avoid unexpected operational hazards. Furthermore, the evolution pattern predicts the relative preservation of pore structure especially in the midstream location despite the geochemical reaction occurring in the system due to the use of a reactive gas as cushion gas. As a result, concerns about the injectivity and working gas production rate during the operation of the storage plant could be manageable. If the reaction in the single-phase zone is excessive, there will be a high increase in porosity across the mineral location that would allow the CO_2 cushion gas to migrate. The migration will reduce the pressure buildup in the storage zone and this will affect the efficiency of storage. The fifteen years of simulation as shown in this study show that the overall impact of geochemical reactions in the single-phase zone of PM-CES utilizing CO_2 as a working gas promises a limited geochemical reactivity.

3.5 Acknowledgment

This work supported by Auburn University by the Auburn University Intramural Grants Program and Presidential Awards for Interdisciplinary Research.

3.6 References

Aghahosseini, A., & Breyer, C. (2018). "Assessment of geological resource potential for compressed air energy storage in global electricity supply." *Energy conversion and management* 169, 161-173. DOI: 10.1016/j.enconman.2018.05.058.

Alami, A. H., Hawili, A. A., Hassan, R., Al-Hemyari, M., & Aokal, K. (2019). "Experimental study of carbon dioxide as working fluid in a closed-loop compressed gas energy storage system." *Renewable Energy* 134, 603-611. DOI: 10.1016/j.renene.2018.11.046.

Alkattan, M., Oelkers, E. H., Dandurand, J. L., & Schott, J. (1998). "An experimental study of calcite and limestone dissolution rates as a function of pH from− 1 to 3 and temperature from 25 to 80 C." *Chemical geology* 151(1-4), 199-214. DOI: 10.1016/S0009-2541(98)00080-1.

Allen, K. (1985). "CAES: the underground portion." *IEEE Transactions on Power Apparatus and Systems* 4, 809-812. DOI: 10.1109/TPAS.1985.319078.

Allen, R. D. (1981) *Basis for compressed air energy storage (CAES) field test at Pittsfield, Illinois*. No. PNL-SA-9447; CONF-811066-6. Pacific Northwest Lab., Richland, WA (USA).

Allen, R. D., T. J. Doherty, R. L. Erikson, & L. E. Wiles. (1983). *Factors affecting storage of compressed air in porous-rock reservoirs*. No. PNL-4707. Pacific Northwest Lab., Richland, WA (USA).

Álvarez-Herránz, A., Balsalobre, D., Cantos, J. M., & Shahbaz, M. (2017). "Energy innovations-GHG emissions nexus: fresh empirical evidence from OECD countries." *Energy Policy* 101, 90-100.DOI: 10.1016/j.enpol.2016.11.030.

Amram, K., & Ganor, J. (2005). "The combined effect of pH and temperature on smectite dissolution rate under acidic conditions." *Geochimica et Cosmochimica Acta* 69(10), 2535-2546. DOI: 10.1016/j.gca.2004.10.001.

Apergis, N., & Payne, J. (2010). "Renewable energy consumption and economic

growth: evidence from a panel of OECD countries." *Energy policy* 38(1), 656-660. DOI: 10.1016/j.enpol.2009.09.002.

Aslani, A., Naaranoja, M., & Zakeri, B. (2012). "The prime criteria for private sector participation in renewable energy investment in the Middle East (case study: Iran)." *Renewable and Sustainable Energy Reviews* 16(4), 1977-1987. DOI: 10.1016/j.rser.2011.12.015.

Bachu, S. (2000). "Sequestration of CO2 in geological media: criteria and approach for site selection in response to climate change." *Energy conversion and management* 41(9), 953-970. DOI: 10.1016/S0196-8904(99)00149-1.

Bauer, S., Pfeiffer, T., Boockmeyer, A., Dahmke, A., & Beyer, C. (2015). "Quantifying induced effects of subsurface renewable energy storage." *Energy Procedia* 76, 633-641. DOI: 10.1016/j.egypro.2015.07.885.

Beckingham, L. E., & Winningham, L. (2019). "Critical Knowledge Gaps for Understanding Water–Rock–Working Phase Interactions for Compressed Energy Storage in Porous Formations." *ACS Sustainable Chemistry & Engineering* 8(1), 2-11. DOI: 10.1021/acssuschemeng.9b05388.

Bensinger, J., & Beckingham, L. E. (2020). "CO2 storage in the Paluxy formation at the Kemper County CO2 storage complex: Pore network properties and simulated reactive permeability evolution." *International Journal of Greenhouse Gas Control* 93, 102887. DOI: 10.1016/j.ijggc.2019.102887.

Bevan, J., & Savage, D (1989). "The effect of organic acids on the dissolution of K-feldspar under conditions relevant to burial diagenesis." *Mineralogical Magazine* 53(372), 415-425. DOI: 10.1180/minmag.1989.053.372.02.

Bourg, I. C., Beckingham, L. E., & DePaolo, D. J. (2015). "The nanoscale basis of CO2 trapping for geologic storage." *Environmental science & technology* 49(17), 10265-10284. DOI: 10.1021/acs.est.5b03003

Brady, P. V., & Walther, J. V. (1990). "Kinetics of quartz dissolution at low temperatures." *Chemical geology* 82, 253-264. DOI: 10.1016/0009-

2541(90)90084-K.

Carden, P. O., & Paterson, L. (1979). "Physical, chemical and energy aspects of underground hydrogen storage." *International Journal of Hydrogen Energy* 4(6), 559-569. DOI: 10.1016/0360-3199(79)90083-1.

Carman, P. C. (1997). "Fluid flow through granular beds." *Chemical Engineering Research and Design* 75, S32-S48. DOI: 10.1016/S0263-8762(97)80003-2

Chandler, J. (2009). "Trendy solutions: Why do states adopt sustainable energy portfolio standards?." *Energy Policy* 37(8), 3274-3281. DOI: 10.1016/j.enpol.2009.04.032.

Chen, W. M., Kim, H., & Yamaguchi, H. (2014). "Renewable energy in eastern Asia: Renewable energy policy review and comparative SWOT analysis for promoting renewable energy in Japan, South Korea, and Taiwan." *Energy Policy* 74, 319-329. DOI: 10.1016/j.enpol.2014.08.019.

Chien, T., & Hu, J. L. (2008). "Renewable energy: An efficient mechanism to improve GDP." *Energy policy* 36(8), 3045-3052. DOI: 10.1016/j.enpol.2008.04.012.

Cui, G., Wang, Y., Rui, Z., Chen, B., Ren, S., & Zhang, L. (2018). "Assessing the combined influence of fluid-rock interactions on reservoir properties and injectivity during CO2 storage in saline aquifers." *Energy* 155, 281-296. DOI: 10.1016/j.energy.2018.05.024.

Dávila, G., Cama, J., Gali, S., Luquot, L., & Soler, J. M. (2016). "Efficiency of magnesium hydroxide as engineering seal in the geological sequestration of CO2." *International Journal of Greenhouse Gas Control* 48, 171-185. DOI: 10.1016/j.ijggc.2016.01.031.

DePaolo, D. J., & Cole, D. R. (2013). "Geochemistry of geologic carbon sequestration: an overview." *Reviews in Mineralogy and Geochemistry* 77(1), 1-14. DOI: 10.2138/rmg.2013.77.1.

Duan, Z., Sun, R., Zhu, C., & Chou, I. M. (2006). "An improved model for the calculation of CO2 solubility in aqueous solutions containing Na+, K+, Ca2+,

Mg2+, Cl−, and SO42−." *Marine Chemistry* 98(2-4), 131-139. DOI: 10.1016/j.marchem.2005.09.001.

Dunn, B., Kamath, H., & Tarascon, J. M. (2011). "Electrical energy storage for the grid: a battery of choices." *Science* 334(6058), 928-935. DOI: 10.1126/science.1212741.

Fischer, S., Liebscher, A., Wandrey, M., & CO2SINK Group. (2010). "CO2–brine–rock interaction—First results of long-term exposure experiments at in situ P–T conditions of the Ketzin CO2 reservoir." *Geochemistry* 70, 155-164. DOI: 10.1016/j.chemer.2010.06.001.

Fleming, M. R., Adams, B. M., Randolph, J. B., Ogland-Hand, J. D., Kuehn, T. H., Buscheck, T. A., & Saar, M. O. (2018). "High efficiency and large-scale subsurface energy storage with CO2." In *43rd Workshop on geothermal reservoir engineering, Stanford, CA*.

Golubev, S. V., Bénézeth, P., Schott, J., Dandurand, J. L., & Castillo, A. (2009). "Siderite dissolution kinetics in acidic aqueous solutions from 25 to 100 C and 0 to 50 atm pCO2." *Chemical Geology* 265(1-2), 13-19. DOI: 10.1016/j.chemgeo.2008.12.031.

Gunter, W. D., Perkins, E. H., & McCann, T. J. (1993). "Aquifer disposal of CO2-rich gases: reaction design for added capacity." *Energy Conversion and management* 34(9-11), 941-948. DOI: 10.1016/0196-8904(93)90040-H.

Haar, N., & Theyel, G. (2006). "US electric utilities and renewable energy: Drivers for adoption." *International journal of green energy* 3(3), 271-281. DOI: 10.1080/01971520600704043.

Helgeson, H. C., & Kirkham, D. H. (1974). "Theoretical prediction of the thermodynamic behavior of aqueous electrolytes at high pressures and temperatures; II, Debye-Huckel parameters for activity coefficients and relative partial molal properties." *American Journal of Science* 274(10), 1199-1261. DOI:10.2475/ajs.274.10.1199

Huang, M. Y., Alavalapati, J. R., Carter, D. R., & Langholtz, M. H. (2007). "Is the choice of renewable portfolio standards random?." *Energy Policy* 35(11), 5571-5575. DOI: 10.1016/j.enpol.2007.06.010.

Huq, F., Haderlein, S. B., Cirpka, O. A., Nowak, M., Blum, P., & Grathwohl, P. (2015). "Flow-through experiments on water–rock interactions in a sandstone caused by CO2 injection at pressures and temperatures mimicking reservoir conditions." *Applied Geochemistry* 58, 136-146. DOI: 10.1016/j.apgeochem.2015.04.006.

IEA. (2019). "SDG7: Data and Projections." *SDG7: Data and Projections*. https://www.iea.org/data-and-statistics/?country=WORLD&fuel=Renewables%20and%20waste&indicator=SDG72 [accessed August 15, 2020]

Iloejesi, C. O., & Beckingham, L. E. (2021). "Assessment of Geochemical Limitations to Utilizing CO2 as a Cushion Gas in Compressed Energy Storage Systems." *Environmental Engineering Science*. DOI: 10.1089/ees.2020.0345.

Jenner, S., Chan, G., Frankenberger, R., & Gabel, M. (2012). "What drives states to support renewable energy?." *The Energy Journal* 33(2), DOI: 10.5547/01956574.33.2.1.

Kanakiya, S., Adam, L., Esteban, L., Rowe, M. C., & Shane, P. (2017). "Dissolution and secondary mineral precipitation in basalts due to reactions with carbonic acid." *Journal of Geophysical Research: Solid Earth* 122(6), 4312-4327. DOI:10.1002/2017JB014019

Kharaka, Y. K., & Cole, D. R. (2011). "Geochemistry of geologic sequestration of carbon dioxide." *Frontiers in Geochemistry: Contribution of Geochemistry to the Study of the Earth*, 133-174. DOI: 10.1002/9781444329957.ch8.

Kim, J., Choi, J., & Park, K. (2015). "Comparison of nitrogen and carbon dioxide as cushion gas for underground gas storage reservoir." *Geosystem Engineering* 18(3), 163-167. DOI: 10.1080/12269328.2015.1031916.

Knauss, K. G., & Wolery, T. J. (1988). "The dissolution kinetics of quartz as a function of pH and time at 70 C." *Geochimica et Cosmochimica Acta* 52(1), 43-53. DOI: 10.1016/0016-7037(88)90055-5.

Lin, B., & Zhu, J. (2019) "The role of renewable energy technological innovation on climate change: empirical evidence from China." *Science of the Total Environment* 659, 1505-1512. DOI: 10.1016/j.scitotenv.2018.12.449.

Van der Linden, S. (2006). "Bulk energy storage potential in the USA, current developments and future prospects." *Energy* 31(15), 3446-3457. DOI: 10.1016/j.energy.2006.03.016.

Lund, P. D. (2007). "Effectiveness of policy measures in transforming the energy system." *Energy policy* 35(1), 627-639. DOI: 10.1016/j.enpol.2006.01.008.

Lyon, T. P., & Yin, H. (2010). "Why do states adopt renewable portfolio standards?: An empirical investigation." *The Energy Journal* 31(3), DOI: 10.5547/ISSN0195-6574-EJ-Vol31-No3-7.

Ma, J., Li, Q., Kempka, T., & Kühn, M. (2019). "Hydromechanical response and impact of gas mixing behavior in subsurface CH4 storage with CO2-based cushion gas." *Energy & Fuels* 33(7), 6527-6541. DOI: 10.1021/acs.energyfuels.9b00518.

Mai, T., Cole, W., Lantz, E., Marcy, C., & Sigrin, B. (2016). *Impacts of federal tax credit extensions on renewable deployment and power sector emissions*. No. NREL/TP-6A20-65571. National Renewable Energy Lab.(NREL), Golden, CO (United States).

Marques, A. C., Fuinhas, J. A., & Manso, J. P. (2011). "A quantile approach to identify factors promoting renewable energy in European countries." *Environmental and Resource Economics* 49(3), 351-366. DOI: 10.1007/s10640-010-9436-8.

Mensah, C. N., Long, X., Boamah, K. B., Bediako, I. A., Dauda, L., & Salman, M. (2018). "The effect of innovation on CO 2 emissions of OCED countries from 1990 to 2014." *Environmental Science and Pollution Research* 25(29), 29678-29698. DOI: 10.1007/s11356-018-2968-0.

Nathenson, M., & Guffanti, M. (1988). "Geothermal gradients in the conterminous United States." *Journal of Geophysical Research: Solid Earth* 93(B6), 6437-6450. DOI: 10.1029/JB093iB06p06437.

Oelkers, E. H., Schott, J., Gauthier, J. M., & Herrero-Roncal, T. (2008). "An experimental study of the dissolution mechanism and rates of muscovite." *Geochimica et Cosmochimica Acta* 72(20), 4948-4961. DOI: 10.1016/j.gca.2008.01.040.

Oldenburg, C. M. (2003). "Carbon dioxide as cushion gas for natural gas storage." *Energy & Fuels* 17(1), 240-246. DOI: 10.1021/ef020162b.

Oldenburg, C. M., & Pan, L. (2013). "Porous media compressed-air energy storage (PM-CAES): Theory and simulation of the coupled wellbore–reservoir system." Oldenburg, C. M. *Transport in porous media* 97(2), 201-221. DOI: 10.1007/s11242-012-0118-6.

Pashin, J. C., Achang, M., Chandra, A., Folaranmi, A., Martin, S., Meng, J., & Esposito, R. (2018). "The Paluxy Formation in the East-Central Gulf of Mexico Basin: Geology of an Ultra-Giant Anthropogenic CO2 Sink." In *AAPG ACE 2018*.

Petrusak, R., Cyphers, S., Bumgardner, S., Hills, D., Pashin, J., & Esposito, R. (2010) "Saline reservoir storage in an active oil field: extracting maximum value from existing data for initial site characterization; Southeast Regional Carbon Sequestration Partnership (SECARB) phase III." In *SPE international conference on CO2 capture, storage, and utilization*. Society of Petroleum Engineers.

Pfeiffer, W. T., & Bauer, S. (2015). "Subsurface porous media hydrogen storage–scenario development and simulation." *Energy Procedia* 76, 565-572. DOI: 10.1016/j.egypro.2015.07.872.

Pfeiffer, W. T., Beyer, C., & Bauer, S. (2017). "Hydrogen storage in a heterogeneous sandstone formation: dimensioning and induced hydraulic effects." *Petroleum Geoscience* 23(3), 315-326. DOI: 10.1144/petgeo2016-050.

Qin, F., & Beckingham, L. E. (2019). "Impact of image resolution on quantification of

mineral abundances and accessible surface areas." *Chemical Geology* 523, 31-41. DOI: 10.1016/j.chemgeo.2019.06.004.

Qin, F., & Beckingham, L. E. (2021). "The impact of mineral reactive surface area variation on simulated mineral reactions and reaction rates." *Applied Geochemistry* 124, 104852. DOI: 10.1016/j.apgeochem.2020.104852

Eckroad, S., & Gyuk, I. (2003). "EPRI-DOE handbook of energy storage for transmission & distribution applications." *Electric Power Research Institute, Inc*, 3-35. DOI: 1001834.

Reysa, G. (2005). "Ground Temperatures as a Function of Location, Season, and Depth." *Build It Solar.[Online]. Available: https://www. builditsolar. com/Projects/Cooling/EarthTemperatures. htm.[Accessed: 01-May-2019]*.

Robinson, H., & Davis, T. (2012). "Seismic reservoir characterization of distributary channel sandstones in the Lower Cretaceous Paluxy reservoir, Delhi Field, Louisiana." In *SEG Technical Program Expanded Abstracts 2012*, pp. 1-6. Society of Exploration Geophysicists. DOI: 10.1190/segam2012-0164.1.

Rul, Internal Revenue Service. (2009). Credit for Carbon Dioxide Sequestration Under Section 45Q. https://www.irs.gov/irb/2009-44_IRB#NOT-2009-83 [accessed September 10, 2020]

Sadorsky, P. (2009). "Renewable energy consumption, CO2 emissions and oil prices in the G7 countries." *Energy Economics* 31(3), 456-462. DOI: 10.1016/j.eneco.2008.12.010.

Sadorsky, P. (2009). "Renewable energy consumption and income in emerging economies." *Energy policy* 37(10), 4021-4028. DOI: 10.1016/j.enpol.2009.05.003.

Steefel, C. I. "CrunchFlow." (2009). *Software for modeling multicomponent reactive flow and transport. User's manual. Lawrence Berkeley National Laboratory, Berkeley*.

Xu, T., E. Sonnenthal, N. Spycher, and L. Zheng. (2017). "TOUGHREACT V3. 32

Reference Manual: a Parallel Simulation Program for Non-isothermal Multiphase Geochemical Reactive Transport." *Lawrence Berkeley National Laboratory, Report LBNL-Draft, Berkeley, Calif* , doi:10.11578/dc.20190130.1.

Succar, S., & Williams, R. H. (2008). "Compressed air energy storage: theory, resources, and applications for wind power." *Princeton environmental institute report* 8, 81. DOI: 10.1.1.374.7597&rep=rep1&type=pdf.

Walters, A. B. "Technical and environmental aspects of underground hydrogen storage." In *1st World Hydrogen Energy Conference, Volume 2*, vol. 2, pp. 2B_65-2B_79. 1976.

Wang, B., Wang, Q., Wei, Y. M., & Li, Z. P. (2018). "Role of renewable energy in China's energy security and climate change mitigation: An index decomposition analysis." *Renewable and sustainable energy reviews* 90, 187-194. DOI: 10.1016/j.rser.2018.03.012.

Xu, T., Apps, J. A., Pruess, K., & Yamamoto, H. (2007). "Numerical modeling of injection and mineral trapping of CO2 with H2S and SO2 in a sandstone formation." *Chemical Geology* 242(3-4), 319-346. DOI: 10.1016/j.chemgeo.2007.03.022.

Zhang, L., Soong, Y., Dilmore, R., & Lopano, C. (2015). "Numerical simulation of porosity and permeability evolution of Mount Simon sandstone under geological carbon sequestration conditions." *Chemical Geology* 403, 1-12. DOI: 10.1016/j.chemgeo.2015.03.014.

Zhang, S., & DePaolo, D. J. (2017). "Rates of CO2 mineralization in geological carbon storage." *Accounts of chemical research* 50(9), 2075-2084. DOI: 10.1021/acs.accounts.7b00334.

Zhang, Z., & Huisingh, D." (2017). Carbon dioxide storage schemes: technology, assessment and deployment." *Journal of Cleaner Production* 142, 1055-1064. DOI: 10.1016/j.jclepro.2016.06.199.

Chapter 4: Field Scale Insight Towards Understanding Impact of Aquifer Properties on Extent and Timeline of CO_2 Trapping.

Chidera O. Iloejesi[1]; Shuo Zhang[2]; Lauren E. Beckingham[1*]

[1]Department of Civil and Environmental Engineering, Auburn University, Auburn, Alabama, 36849.

[2]State Key Laboratory of Hydroscience and Engineering, Department of Hydraulic Engineering, Tsinghua University, Beijing, China, 100084.

Corresponding Author* Tel: 334-844-6260; e-mail: leb0071@auburn.edu

Submitted to International Journal of Greenhouse Gas Control

Abstract

Geologic CO_2 sequestration in porous saline aquifers is a promising approach to reducing atmospheric concentrations of CO_2. Once injected, CO_2 will dissolve into the brine to create an acidic environment, resulting in dissolution of primary formation minerals. Released ions can reprecipitate as secondary minerals, including carbonate minerals which securely trap injected CO_2. This mineral trapping is highly desirable as it is the most secure CO_2 trapping mechanism. Reactive transport simulations provide the opportunity to analyze which factors influence geochemical reactivity in the reservoir and understand those most important for promoting mineral trapping. Here, reactive transport simulations are leveraged to enhance understanding of aquifer properties (porosity, permeability, depth, and carbonate mineralogy) on the overall CO_2 trapping potential. A controlled set of field scale simulations is carried out successively varying aquifer properties to understand the impact of each unique property on CO_2 sequestration. For each simulation, the amount of gaseous, aqueous, and mineralized CO_2 is tracked and compared. Simulations reveal that the considered aquifer properties impact the sequestration efficiency, defined as the rate at which the CO_2 injected into the aquifer is converted to aqueous or mineralized CO_2. Based on the studied properties, the impact of aquifer properties on CO_2 evolution depends on the stage of the

sequestration project. During injection, understanding the amount of carbonate mineralogy of an aquifer has the most significant impact on predicting the evolution of injected CO_2. Post injection, the depth of the storage reservoir has the largest impact on the evolution of CO_2.

4.1 Introduction

Adopting CO_2 sequestration technology is necessary to tackle the emission of greenhouse gases due to fossil fuel energy generation. Geologic CO_2 sequestration is one such promising technology for reducing point-source CO_2 emissions. A key component of developing this technology is determining the subsurface storage aquifers where the captured CO_2 gases would be safely injected. Potential deep storage geological sites include coal seams, aquifers, and oil and gas fields. The enormous capacity and ubiquity of subsurface storage aquifers make the prospect of subsurface CO_2 sequestration in saline formations appealing (Goodman et al. 2011). In the United States alone, 75% of saline geological formations favor underground storage (K. Allen 1985).

Sequestration projects typically use CO_2 for enhanced oil recovery, like in Weyburn project (Whittakera et al. 2011), or inject CO_2 into porous saline aquifers for stroage, such as in Sleipner project (Baklid, Korbol, and Owren 1996). These CO_2 sequestration projects have been carried out at the pilot and commercial scale in geological media (NETL 2015). However, optimizing the CO_2 sequestration technology in subsurface formations requires an adequate understanding of all aspects of injection and its implications for efficient CO_2 trapping. Once injected into the subsurface, CO_2 evolves through four different trapping mechanisms including structural/stratigraphic trapping, residual trapping, dissolution trapping, and mineral trapping (De Coninck and Benson 2014b). Initial trapping results from CO_2 being structurally trapped in the target storage aquifer below a low or impermeable barrier in the supercritical phase (Espinoza and Santamarina 2017). The trapped CO_2 then

dissolves into the brine in a process called dissolution trapping (Duan et al. 2006). As most sedimentary storage aquifers are water-wet, imbibition of the brine results in residual trapping of CO_2 (Hunt, Sitar, and Udell 1988; Juanes et al. 2006). Finally, the acidified brine geochemically reacts with the subsurface rock minerals, dissolving primary minerals and forming new carbonate phases that permanently trap injected CO_2 through mineral trapping, the most secure form of trapping (J. Matter, Geoscience, and 2009 2008). The geochemical timeline for attaining mineralization of injected CO_2, however, is not well understood. Hence, understanding the factors that influence the injected CO_2 evolution will be the focus of this work and will ultimately be helpful towards understanding CO_2 mineralization.

Several factors have been identified in previous studies that affect the efficiency and rate of mineralization in a storage site. This includes the vertical permeability of caprocks, the residual CO_2 saturation in aquifer rocks, abundance of potential cations, and the reactive surface area of silicate rocks (Bourg, Beckingham, and DePaolo 2015). Core scale evaluation of potential target formations has identified the importance of abundant iron, magnesium, and calcium cations in silicate and oxide minerals which can neutralize acidified brine and eventually mineralize into new carbonates (S. Zhang and DePaolo 2017). It is shown that the ease with which these species can be released by the potential host rock can facilitate further reaction and hence increase storage efficiency (Kelemen et al. 2011; J. M. Matter et al. 2016; B. Peter McGrail et al. 2017). Mineral reactive surface area has a noted impact on geochemical reactions where higher reactive surface areas increase the rate of mineral reactions (Qin and Beckingham 2021b).

While these nano- and microscale properties have shown to contribute significantly to understanding the storage efficiency, it is also important to understand how field-scale properties correlate to potential geochemical reactivity necessary for CO_2 trapping. Typically, field-scale subsurface characterization is conducted before CO_2 injection to determine aquifer suitability for storage. Most storage site

investigations produce data on the porosity, permeability, mineralogy, stratigraphy, and depth and thickness of the storage formation(s). These are used to predict the stress-, and flow state of the subsurface and as indicators for the feasibility of subsurface CO_2 sequestration in the targeted formation. For instance, porosity and permeability are typically used to evaluate the ease of injection. Core samples extracted during borehole drilling can be used to help determine the mineral composition. The stratigraphy evaluation of the borehole log confirms the presence or absence of a caprock formation. The depth of storage is a critical factor to consider in most subsurface storage processes because of its impact in achieving a supercritical state of injected CO_2. Furthermore, depth influences aquifer deliverability (Pfeiffer and Bauer 2015b). Petrologically, the depth is critical in characterizing the texture and compactness of the formation grains. This implies that depth would have an impact on the permeability and porosity of the formation (X. Wang and Economides 2013). The trend typically shows that some deeper formations are less porous or permeable than shallower formations. The disparity in grain size distribution can be accentuated with increasing thickness of the formation. Despite this direct information gained during site investigation, the nano and core scale are typically used to infer the magnitude of potential geochemical reactions and CO_2 mineralization potential of a storage site.

This study conducts a field-scale simulation study of CO_2 sequestration to gain insight into how different aquifer properties could affect CO_2 trapping and the timeline of storage processes. Here, the evaluated aquifer properties include the depth of storage, aquifer thickness, volume fraction of carbonate minerals, porosity, and permeability. The study approach simulates small to large variations of each aquifer property as compared to a base case model to evaluate the impact of each aquifer property on CO_2 trapping. By no means could the properties considered in the study be an exhaustive list. Moreover, the paucity of data currently available for most aquifer properties presents the challenge of using the actual deviation of field investigation data of each

aquifer property from the mean value. However, this study will provide a metric to understand the relationship between aquifer properties and CO_2 trapping potential.

The geochemical predictive capacity of numerical reactive transport simulations are used in this study. Reactive transport simulations have successfully been used to predict and analyze geochemical reactions in subsurface aquifers (Audigane et al. 2007). Generally, numerical modeling of geochemical processes is an important tool in understanding the slow-reacting alumino-silicates minerals that influence sequestration. Specific site evaluations require that the numerical model uses site-specific parameters to uniquely identify the physical and geochemical conditions of a storage site. Also, kinetic parameters will influence simulations of geochemical reactivity and should be adequately evaluated. Since this study is not entirely tailored to a particular site in terms of kinetic and hydraulic properties of the model, our study will not be emphasizing the quantitative values of CO_2 trapping produced for a specific geologic sequestration system.

4.2 Model Description and Setup

Field scale reactive transport simulations were used here to evaluate CO_2 trapping efficiency in a porous saline aquifer, evaluating solubility trapping through mineral trapping to understand how changes in aquifer properties impact trapping. The TOUGHREACT reactive transport simulator was used for modeling the coupled subsurface multiphase transport and reaction system in this study (Tianfu Xu, Eric Sonnenthal, Nicolas Spycher 2017). The isothermal simulation setup for the spatial and temporal reactive chemistry evolution in this study used the ECO2N fluid property module (Pruess 2005). This module package of TOUGHREACT helps to handle the CO_2 and water thermophysical properties under the typical range of temperature and pressure conditions of a potential storage aquifer. The computational coupling of the reactive chemistry and transport in the hundreds of grid blocks developed to discretize the system was done using iterative techniques due to the expensive time and space

complexity of the direct solver. For this simulation, changes in porosity and permeability were allowed to influence the flow. A 2-dimensional radially symmetric model used in this study was developed using the TOUGHREACT MeshMaker module.

Five sets of simulations were carried out, systematically varying the porosity, permeability, carbonate mineralogy, and depth of storage. For each simulation set, only the examined aquifer property, like porosity, was changed while others were assigned to a base-case value. The base-case properties here are from the Paluxy formation located in the southern region of the United States which is being considered as a potential CO_2 storage formation (Jalali et al. 2021; Qin and Beckingham 2019; Kuuskraa, V., Koperna, G., & Riestenberg 2020). Table 1 shows the simulation approach adopted to successively change each aquifer property of the model to understand how that aquifer property affects CO_2 trapping.

Table 4.1: Simulation parameter values for each considered aquifer property. Aquifer formation properties for acting and proposed CO_2 reservoir formations were collected from the literature and the low, mid and high values reported here. The values are representative of the range of aquifer properties in these target formation and do not necessarily correspond to the exact minimum or maximum values. The literature values are rounded up or down so that the chosen base case aquifer value could be numerically approximate to the average of the low and high value. [1](Balashov et al. 2013), [2](Ahmmed et al. 2016b), [3](Lu et al. 2012), [4](Climate and 2006 2006), [5](Audigane et al. 2007), [6](Delshad et al. 2013), [7](Ayobami Timothy Folaranmi 2015), [8](Michael et al. 2009).

	Porosity	Permeability	Carbonate mineralogy	Aquifer thickness	Depth
Low Values	10%[1]	50mD[2]	2%[1]	20m[3]	800m[4]
Base Case	25%	500mD	11.5%	100m	1500m
High Value	40%[5]	1000mD[6]	21%[7]	180m[4]	2200m[8]

The fixed aquifer properties used to define the model were also based on the Paluxy formation in the southeastern region of the United States as obtained from the literature and given in Table 2 (Qin and Beckingham 2019). The model was initialized based on a homogeneous mineral composition given in Table 2 including a dominant

quartz mineral phase of 76.45% abundance, calcite at 9.63%, siderite at1.98%, and a few other minerals including smectite, K-feldspar, and muscovite with mineral abundance of 8.23%, 3.50% and 0.31% respectively. The pressure and temperature at the simulated depths were calculated based on the hydrostatic pressure gradient of 0.43 psi/ft (J. C. Pashin et al. 2008), surface temperature of 20^{o}C and temperature gradient of 20^{o}C/km at the location (John Warner 1993; Nathenson and Guffanti 1988). For each simulated aquifer thickness, the aquifer was discretized into 20 layers. The radial boundary of the aquifer was assigned at 100km from the point of injection and reflected constant temperature, concentration, and pressure conditions. The radial discretization was uniform at the proximity of the injection well and increased logarithmically with distance away from the point of injection.

It should be noted that there are additional considerations for defining the mineralogical composition of the formation. For simulations with varied carbonate mineral fraction, the change in calcite fraction was compensated by adjusting the quartz volume fraction as quartz has been shown to minimally affect geochemical reactions because of its slow kinetics (Tullis and Yund 2015). The vertical permeability of the model is assigned a value that is one order of magnitude less than the horizontal permeability while the values of the horizontal permeability used to study the impact of permeability are shown in Table 3.

Table 4.2: Base case mineral composition, mineral abundance, volume fraction, and reactive surface area of primary minerals(Qin and Beckingham 2019), and reactive surface areas of secondary minerals (Xu, Apps, and Pruess 2004b).

Mineral	Mineral Reaction	Mineral Abundance (v%)	Surface Area (m^2g^{-1})
Quartz	Quartz = $SiO_{2(aq)}$	76.45	2.59E-2
Calcite	$CaCO_3 + H^+ = Ca^{2+} + HCO_3^-$	9.63	1.42E-3
K-Feldspar	K-Feldspar + $4H^+ = K^+ + Al^{3+} + SiO_{2(aq)} + 2H_2O$	3.50	1.15E-3
Smectite	Smectite + $7.8H^+ = 0.2K^+ + 1.25Al^{3+} + 3.5SiO_{2(aq)} + 4.9H_2O + 0.7Fe^{2+} + 0.1Na^+ + 0.025Ca^{2+} + 1.15Mg^{2+} + 0.05O_{2(aq)}$	8.23	1.63E+1
Muscovite	Muscovite + $10H^+ = 3SiO_{2(aq)} + 6H_2O + 3Al^{3+} + K^+$	0.31	1.10E+0
Siderite	Siderite + $H^+ = HCO_3^- + Fe^{2+}$	1.98	6.49E-4
Kaolinite	Kaolinite + $6H^+ = 5H_2O + 2Al^{3+} + 2SiO_{2(aq)}$)		9.8
Gibbsite	Gibbsite + $3H^+ = 3H_2O + Al^{3+}$		9.8
Albite	Albite + $4H^+ = 2H_2O + Al^{3+} + Na^+ + 3SiO_{2(aq)}$		9.8
Ankerite	Ankerite + $2H^+ = Ca^{2+} + Mg^{2+} + 2HCO_3^-$		9.8
Chlorite	Chlorite + $10H^+ = 2Fe^{2+} + SiO_{2(aq)} + 2Al^{3+} + 7H_2O$		9.8
Chalcedony	Chalcedony = SiO2(aq)		9.8
Dolomite			9.8

Table 4.3: Fixed aquifer properties of the formation obtained from the literature. Geothermal gradient(John Warner 1993; Nathenson and Guffanti 1988). Hydrostatic gradient(J. C. Pashin et al. 2008), liquid relative permeability and capillary pressure(Van Genuchten 1980), gaseous relative permeability(COREY and T. 1954).

Parameter	Value/description
Geothermal gradient	20°C/km
Hydrostatic gradient	0.43 psi/ft
Salinity (mass fraction)	0.06
CO_2 injection rate	20kg/s
Relative permeability	Liquid $K_{rl} = \sqrt{S^*}\left\{1 - \left(1 - [S^*]^{\frac{1}{m}}\right)^m\right\}^2$ $S^* = (S_l - S_{lr})/(1 - S_{lr})$ Irreducible water saturation, S_l = 0.30 Exponent, m = 0.457
	Gas $K_{rg} = (1 - S)^2 (1 - S^2)$ $S = \frac{(S_l - S_{lr})}{(S_l - S_{lr} - S_{gr})}$ Irreducible gas saturation, S_{gr} = 0.05
Capillary Pressure	$P_{cap} = -P_o([S^*]^{-\frac{1}{m}} - 1)^{1-m}$ $S^* = (S_l - S_{lr})/(1 - S_{lr})$ Irreducible water saturation, S_l = 0.30 Exponent, m = 0.457 Strength coefficient, P_o = 19.61kPa

This study used a single well for injection of CO_2 into the formation that was initially saturated with a brine solution. The injection of CO_2 was simulated using an 8 m injection screen thickness. Two-dimensional simulations of the injected CO_2 gas bubble used the van Genuchten function for capillary pressure and van Genuchtem-Mualem model for water relative permeability, respectively (Mualem 1976; Van Genuchten 1980). The gas relative permeability for the two-phase system was modeled with Corey's curve (COREY and T. 1954). For this simulation, the activity of aqueous species is modeled using the extended Debye-Huckle equation (Helgeson and Kirkham 1974; Helgeson 1981).

TOUGREACT has the ability to treat mineral dissolution and precipitation using either kinetic or equilibrium thermodynamics. Here, calcite was considered under

local equilibrium conditions due to the fast reaction rate of calcite under the associated storage conditions while the remaining mineral phases were considered kinetically. The transition state theory (equation 1) rate expression was used for kinetic mineral reactions as given by,

$$kinetic\ rate, r = kA\left[1 - \left(\frac{Q}{K}\right)^{\theta}\right]^{\eta} \quad (1)$$

where k is the rate constant, A is the specific surface area, K is the equilibrium constant for the mineral-water reaction, Q is the reaction quotient, θ and η are experimentally determined parameters. The kinetic rate constant, k, is a combination of neutral, acidic, and basic conditions. For this simulation, the kinetic parameters for most of the the mineral assemblage were obtained from the literature (Xu et al. 2007). The muscovite kinetic parameter was obtained from literature and the units were converted to a similar format as other inputs (Gérard et al. 1998). Amorphous silica kinetic parameters obtained from (Palandri and Kharaka 2004) were used as a proxy for chalcedony which is the preferred silica polymorph that is expected to precipitate in this system (Audigane et al. 2007; C. Iloejesi 2021). The precipitation rate constant for minerals in this study is equivalent to the dissolution rate constant under the neutral mechanism.

The simulation steps included the equilibration of the formation mineral with brine, then the constant injection of CO_2 for 10 years and CO_2 monitoring simulation for 40 years. The initial brine composition was determined via a two-component simulation of water-rock equilibration using a 1 molal solution of sodium chloride until the brine-rock system attained equilibrium (Xu, Apps, and Pruess 2004b). After equilibrium was attained, the simulation considered CO_2 injection into the aquifer for 10 years. The simulated injection rate was 20 kg/s to attain an annual injection of 6.308×10^6 metric tons of CO_2. The simulated 10 year CO_2 injection period was followed by a 40 year simulated monitoring period.

As simulations progressed, the relative quantity of the aqueous, supercritical, and mineralized CO_2 in the system was tracked. For a given aquifer volume and porosity, the aqueous CO_2 mass is a function of water saturation, water density and CO_2

mass fraction in water. The amount of supercritical CO_2 in the system is directly proportional to gas saturation and gas density for a given volume of porous formation. The mass per unit volume of the carbonate precipitation over time is used to calculate the total CO_2 sequestered in the mineral phase. This result of the total sequestered CO_2 in mineral phase is multiplied by the aquifer volume to obtain the cumulative mass of the mineralized CO_2.

4.3 Result and Discussion

The simulation results presented here will use the base case scenario to discuss the anticipated geochemical evolution of the system following injection of CO_2 in the porous aquifer. Then the analysis will consider how variations in aquifer properties impact the sequestration efficiency.

4.3.1 Base Case

The simulated gas saturation of CO_2 is shown in Figure 4.1 after 5, 10, 20, 30, 40, and 50 years. The figure shows the right sectional view of a radially discretized model vertically bisected at the injection well. The gas saturation at 5 years, which corresponds to a time that is during injection, shows a high gas saturation within the vicinity of the injection well. The high CO_2 gas saturation around the injection well persists until the end of injection period at 10 years. As injection stops, the CO_2 concentration around the well decreases and buoyancy effects result in an increase in the CO_2 gas phase in the upper region of domain, limited by the applied no flow boundary (Fig. 4.1). At this same time, the CO_2 plume migrates laterally away from the injection well from 1400m (10 years) to 2100m (50 years).

CO_2 dissolution into the brine increases the CO_2 mass fraction in the brine to a maximum value of 0.0405 during the injection period which occurs at 60m from the injection well. At the end of the injection simulation, the maximum dissolved CO_2 mass fraction is 0.0401 which occurs at 110 m away from the injection well (Fig. 4.2). This

phase partitioning process as a result of the CO_2 dissolution into the brine increases the density of the brine close to the injection well. Variations in brine density result in convective mixing. In a permeable formation, this flow condition may facilitate acidification of regions in the porous aquifer that otherwise might not have been in contact with the injected CO_2. Since the aquifer boundary is an infinitely long distance from the injection well, the CO_2 mass fraction remains at a value of $10x10^{-12}$ in regions far from the well where we do not expect the acidified CO_2 to be in contact with the brine.

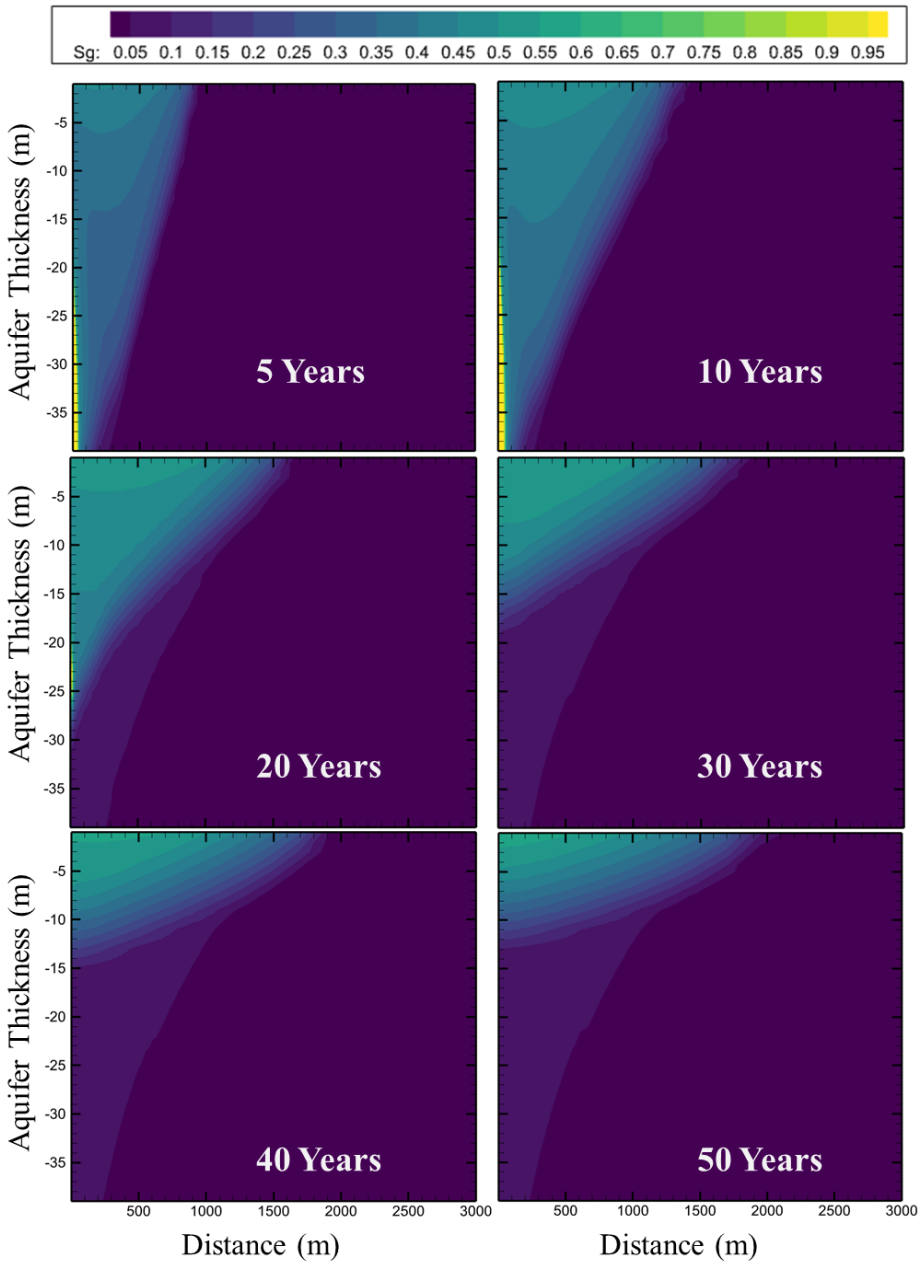

Figure 4.1: Sectional view of CO_2 gas saturation, *Sg*, for the radially discretized model vertically bisected at the injection well.

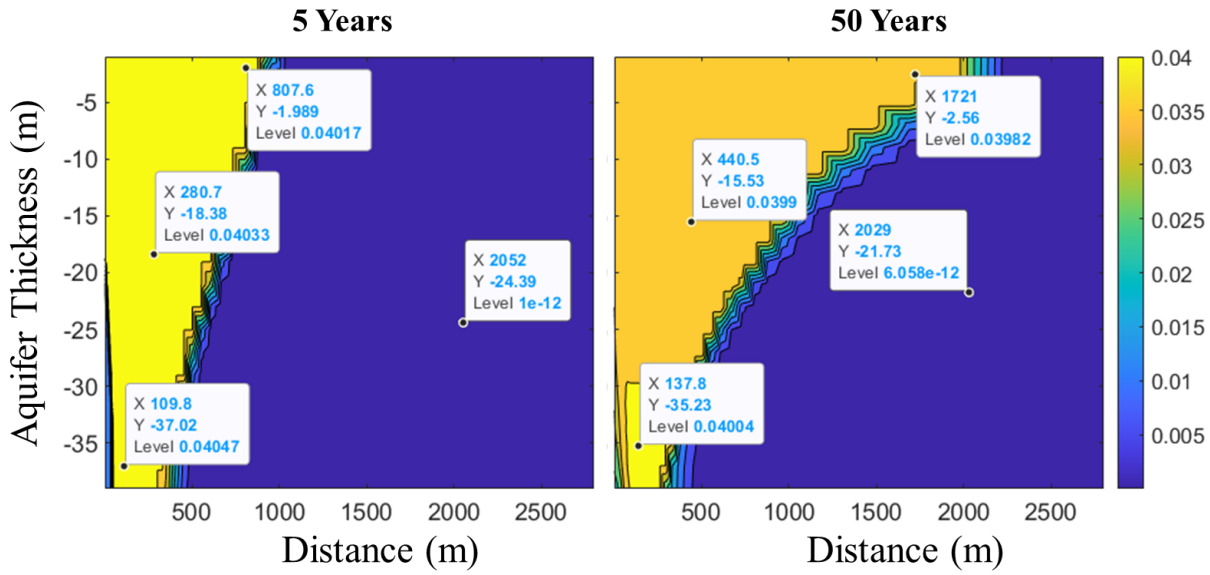

Figure 4.2: Variation in the mass fraction of CO_2 (XCO_2) in the brine at the start of injection and end of CO_2 injection. The Data tip information shows the variation of CO_2 in different regions of the aquifer.

Dissolution of the CO_2 into the brine increases the brine acidity and lowers pH where the resulting brine pH are shown in Figure 4.3. As a result of dissolution of CO_2 into the brine, pH drops from the initial pH of 7.52 to a minimum pH value of 4.86 after five years of CO_2 injection. This pH reflects buffering by dissolution of carbonate minerals, calcite here. Calcite dissolution increases calcium ion concentrations (Fig 4.3c and 4.3d).

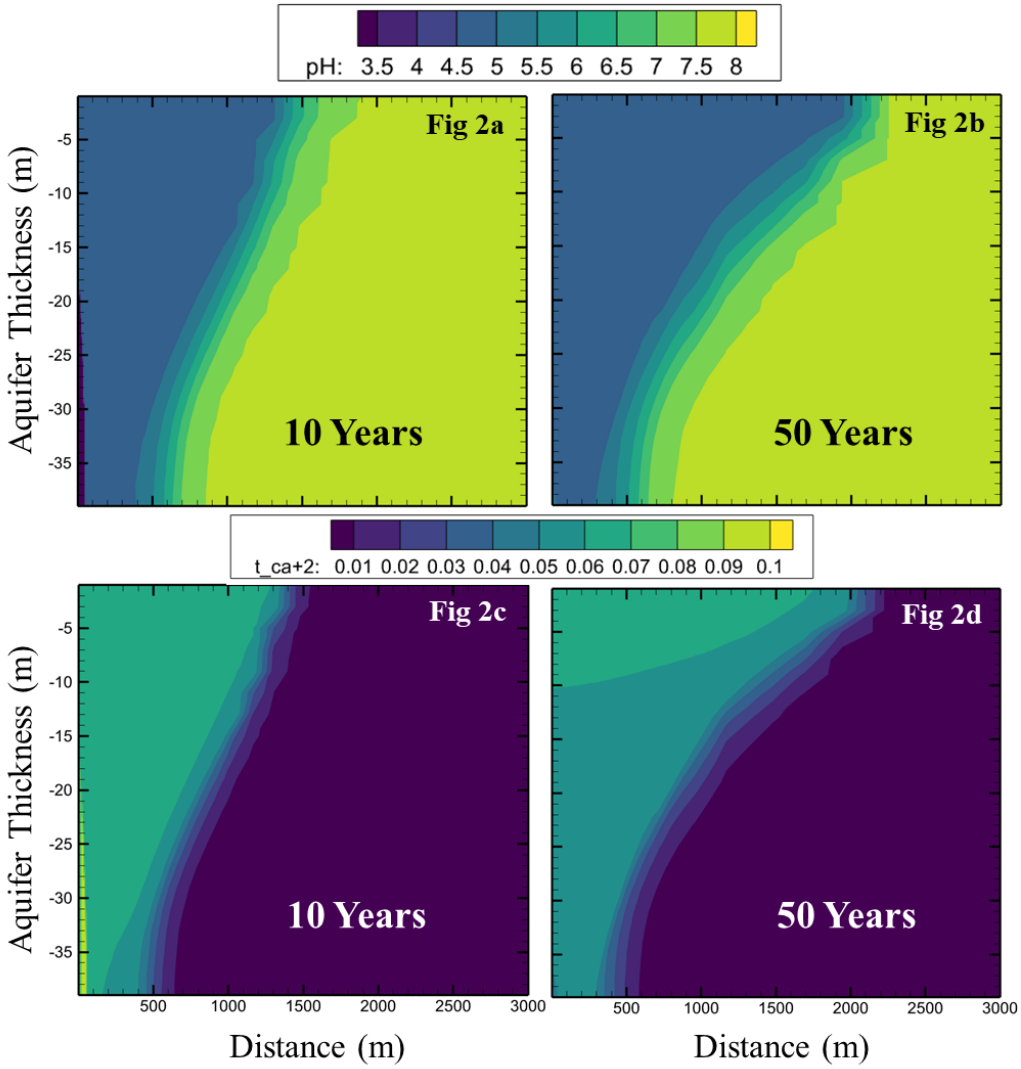

Figure 4.3: Contour maps of brine pH (a, b) and the concentration of total calcium (mol/kg H_2O) (c, d) at the end of CO_2 injection (10 years) and at the end of the simulation timeline (50 years).

Generally, acidification of the brine results in conditions that are favorable for the dissolution of minerals. Dissolving primary minerals increase concentrations of ions in solution (Fig. 4.4). This can create conditions that favor precipitation of secondary minerals. The simulated resulting conditions are favorable for the precipitation of albite, kaolinite, chlorite, dawsonite, illite, hematite, and chalcedony minerals in the system. Some of the primary ions that control mineral reaction can be seen in Fig. 4.4.

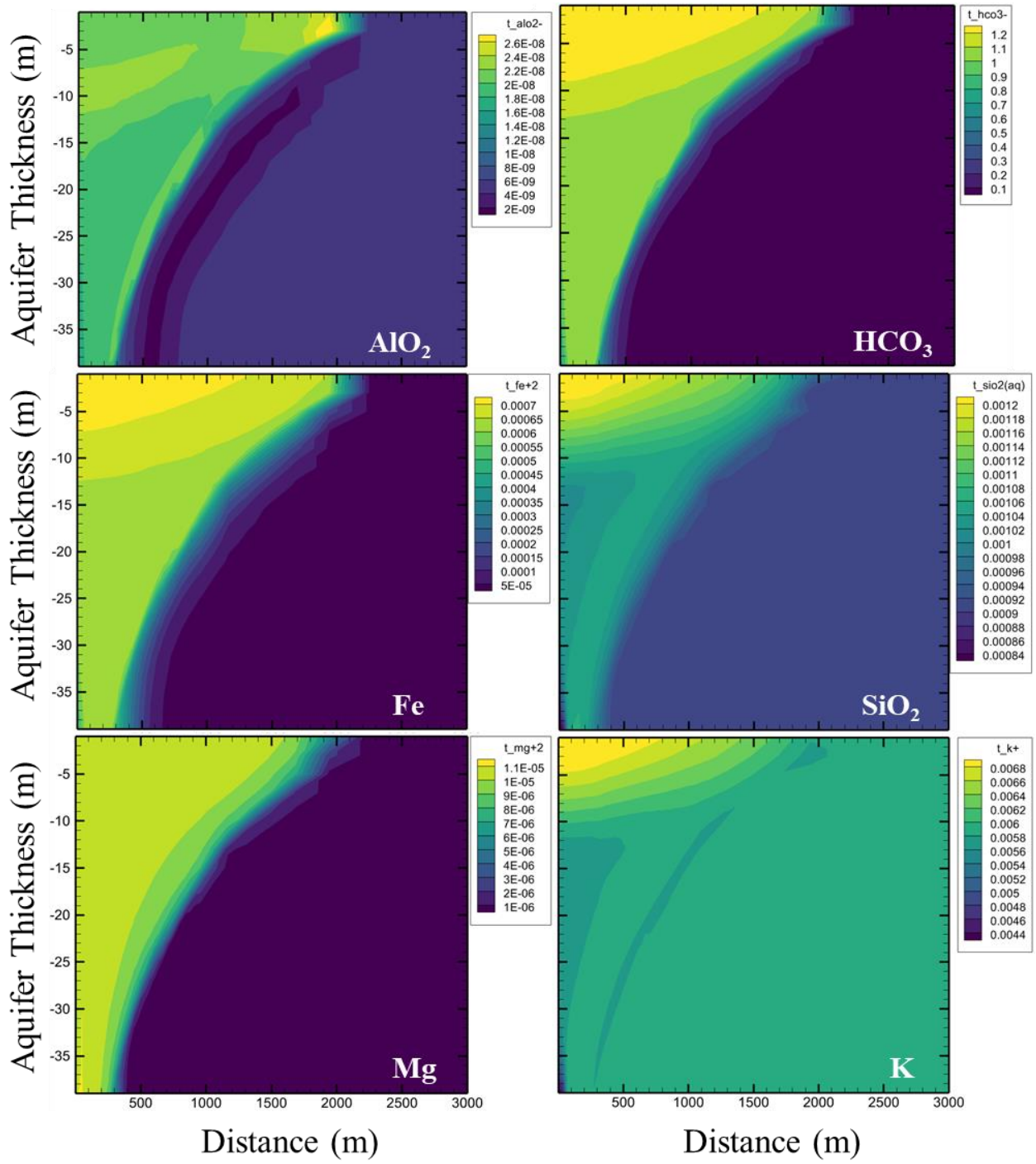

Figure 4.4: Selected simulated concentrations of primary species concentration (mol/kg H_2O) after 50 years.

Typically, the precipitation of carbonate minerals is linked to the mineralization of CO_2. In this system, the saturation index of the carbonate minerals (Fig. 4.5) are used to show the region of carbonate dissolution and precipitation in the system. The region of carbonate precipitation aligns with the regions with positive saturation index values

while a negative saturation index signifies carbonate dissolution (Fig. 4.5). The plot shows that some part of system undergoes calcite dissolution. This calcite dissolution helps buffer the system and influences the simulated positive saturation index for siderite and other precipitating minerals. Siderite precipitation is observed to go on in the system for the mineralization of the injected CO_2

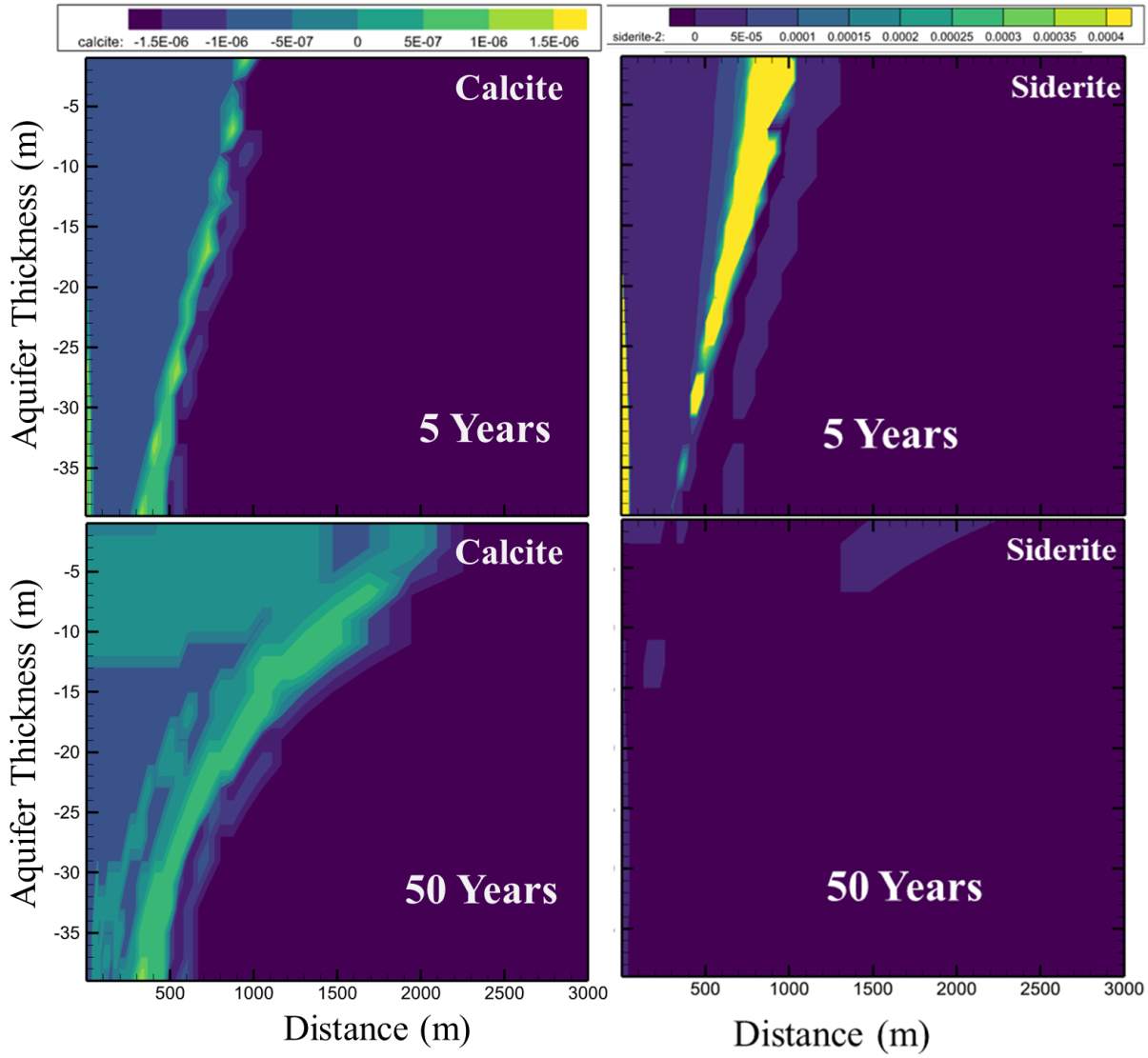

Figure 4.5: Simulated saturation indices of calcite and siderite, the two carbonate minerals in the rock matrix, during the simulated CO_2 injection and monitoring period.

The simulated evolution of CO_2 trapping over time is shown in Figure 4.6. The total amount of trapping includes contributions from aqueous trapping (dissolution of some

of the CO_2 into the brine), mineralization (from precipitation of carbonate minerals), and stratigraphic trapping (where gaseous CO_2 is physically trapped by the overlying caprock). The figure shows that majority of the injected CO_2 is predominantly held stratigraphically as supercritical CO_2 during the simulation timeline which emphasize the importance of low-peremeability caprock feature over the storage aquifer. Over time, the drop in the mass of superciritical CO_2 is reflected by the increase in the amount of aqueous and mineralized CO_2. The slow mineralization process result in lower rate of increase in mineralized CO_2 relative to the increase in the amount of aqeous CO_2.

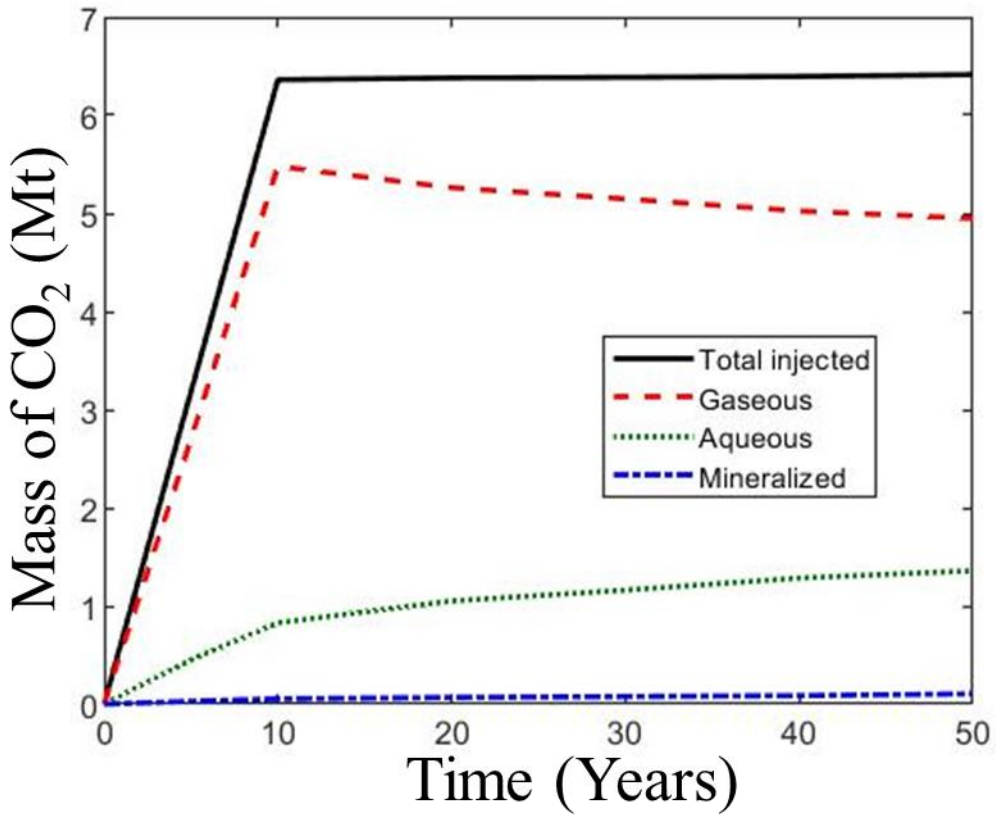

Figure 4.6: Simulated CO_2 trapping mechanisms over the 50 year simulation period in million tons. The simulated injection period ends at 10 years.

4.3.2 Understanding the Impact of Aquifer Properties on CO_2 Trapping

The geochemical evolution of the base case scenario discussed above will serve as a benchmark for the remaining comparisons. Here, impacts of varying aquifer

properties on the evolution of injected CO_2 including the amount of the injected CO_2 sequestered in form of gas, aqueous or mineralized are considered. Simulations consider low and high values (Table 2) of each property and discussion of results focuses on the impact of the aquifer property on the partitioning of the injected CO_2. We will discuss the mass partitioning of the injected CO_2 into aqueous phase and gaseous forms as well as the amount mineralized and the total CO_2 trapped. The term trapped reflects the summation of the mineralized CO_2 and that dissolved in the aqueous phase.

4.3.2.1 Effect of Carbonate Mineralogy

The simulated mass change in the amount of aqueous, mineralized, gaseous, and trapped CO_2 for systems with low and high fractions of carbonate minerals are shown in Fig. 4.7. Here, the amount of CO_2 dissolved in the aqueous phase is the same in each simulation, regardless of the fraction of carbonate minerals in the aquifer. However, the amount of mineralized CO_2 differs significantly. During the simulated injection period, the change in mineralization with time in high carbonate systems is seven times more that the amounts of low carbonate minerals. Post injection of CO_2, the simulated rate of mineralization becomes similar for the two cases. It should be noted that CO_2 mineralization marginally contributes to overall CO_2 trapping, as shown for the base case in Fig. 4.6. As a result, this marginal effect of a higher rate of CO_2 mineralization appears to have no discernable impact based on the scale used to represent the simulated mass of gaseous CO_2 remaining in the system after the 50 years of simulation (Fig. 4.7). However, discernable differences in the simulated mas of trapped CO_2 highlight the advantage of a system with a larger fraction of carbonate minerals in the target aquifer.

These simulation results show that the superior advantage an aquifer with a high fraction of carbonate minerals has over one with a low fraction of carbonate minerals in liberating positive divalent cations like calcium, magnesium, and iron which aid CO_2

mineralization. These reactions are predominately triggered during the early phase of CO_2 sequestration. Early mineralization was also observed in the Carbfix project where the rapid release of divalent ions from the relatively fast dissolving basaltic formation improved mineralization rate (J. M. Matter et al. 2016). The early mineralization that was observed was such that over 60 percent of the injected CO_2 mineralized within four months of continuous injection over a three-half year duration (Clark et al. 2020).

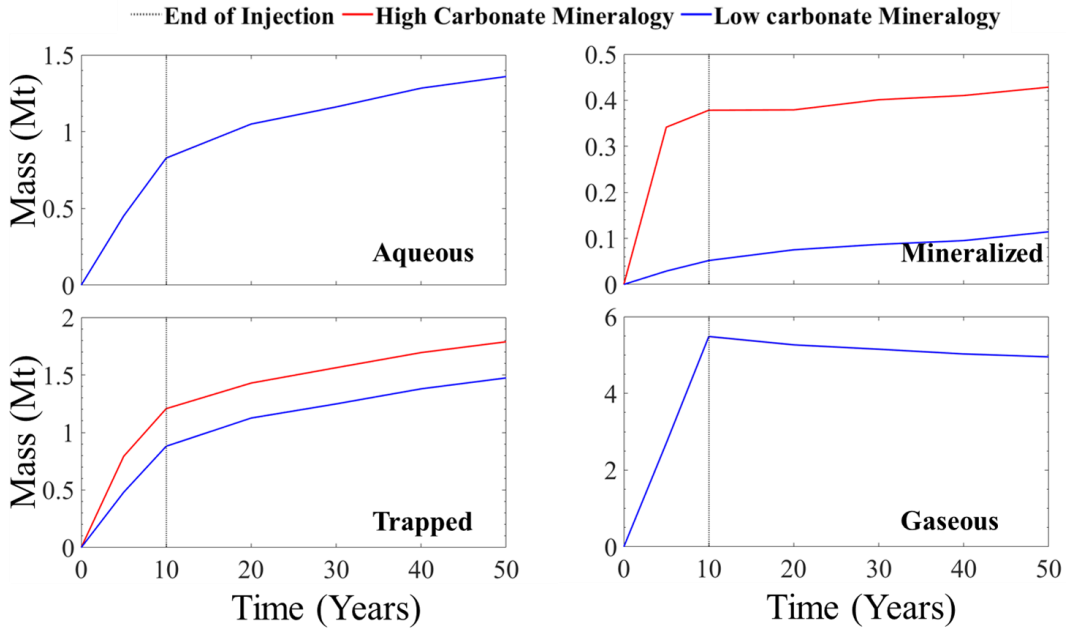

Figure 4.7: Comparison of the simulated aqueous, mineralized, trapped, and gaseous CO_2 in millions of metric tons over 50 years for simulations with varying carbonate mineral fraction. The red line represents the high carbonate scenario, and the blue represents the low carbonate composition scenario.

4.3.2.2 Effect of Depth:

Subsurface temperatures and pressures increase with formation depth (Shafeen et al. 2004). Typically, storage depths greater than 800m are desired such that CO_2 will exist in the supercritical state in the formation (Hitchon and Alberta Research Council. 1996). In this simulation set, the effect of varying injection and storage depth is implemented by changing the simulation temperature and pressure to reflect typical temperatures and pressures at depths of 800 to 2200 m.

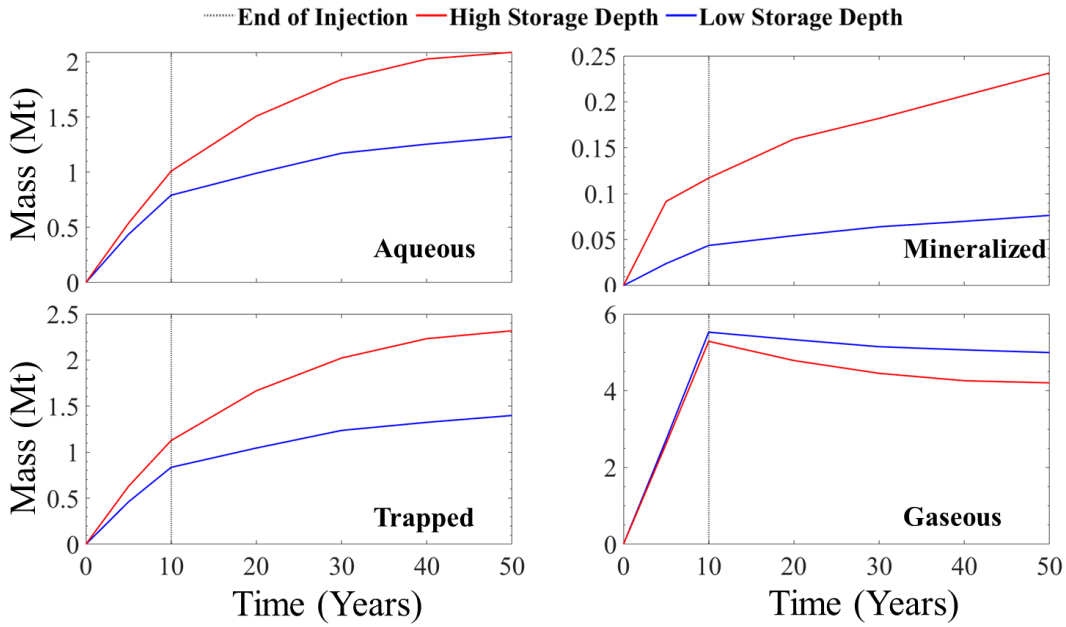

Figure 4.8: Simulated aqueous, mineralized, trapped, and gaseous CO_2 in millions of metric tons in a porous saline aquifer over 50 years due for varied storage depths. The red line represents the high depth of storage scenario (2200 m), and the blue represents the low depth scenario (800 m).

The simulated CO_2 phase partition for depths of 800 m (low) and 2200 m (high) are shown in Fig. 4.8. The figure shows that there is an increase in the mass composition of aqueous CO_2 as depth increases. During the injection phase, this rate of increase in dissolved CO_2 at the higher depth is over 20% greater than the rate at the lower depth. Post injection, the simulated rate of increase in the aqueous CO_2 composition for the greater depth system is more than 2 times the rate aqueous CO_2 increases for the lower depth system. The plot of the mass comparison of mineralized CO_2 shows that the rate of mineralization is significantly higher in the system with greater depth. Hence, the amount of trapped CO_2 is also higher for the deeper storage depth. This implies that the remaining gaseous CO_2 is lower in the greater depth system than in the lower depth system.

The key parameters that control gas dissolution in a solution include salinity, pressure, and temperature (Spycher, Pruess, and Ennis-King 2003; Lagneau, Pipart, and Catalette 2005). Since the salinity for the simulation performed for the low and high

case is the same, the temperature and pressure are the notable parameters impacting CO_2 solubility in this case. The increase in CO_2 concentration is thus a function of pressure and temperature (Benson and Cole 2008). The result in Fig. 4.8 shows that the mass aqueous composition of CO_2 increases significantly during the injection phase in both systems. Injection creates higher pressure conditions in both the deeper and shallower aquifers such that conditions are more comparable in the two formations during this time. However, the rate of dissolution changes post injection when the injection pressure has dissipated to create pressure and temperature difference which dominates the CO_2-brine reaction. Hence, a higher rate of solubility trapping is evident at deeper depths. The increased solubility results in increased mineralization in the deeper formation. The change of mineralization rate here can also be due to increased reaction rate with increasing temperature. This reflects that conditions liberating more Ca^{2+}, Fe^{2+}, and Mg^{2+} can accentuate the rate of mineralization during the injection and monitoring periods.

4.3.2.3 Effect of Porosity

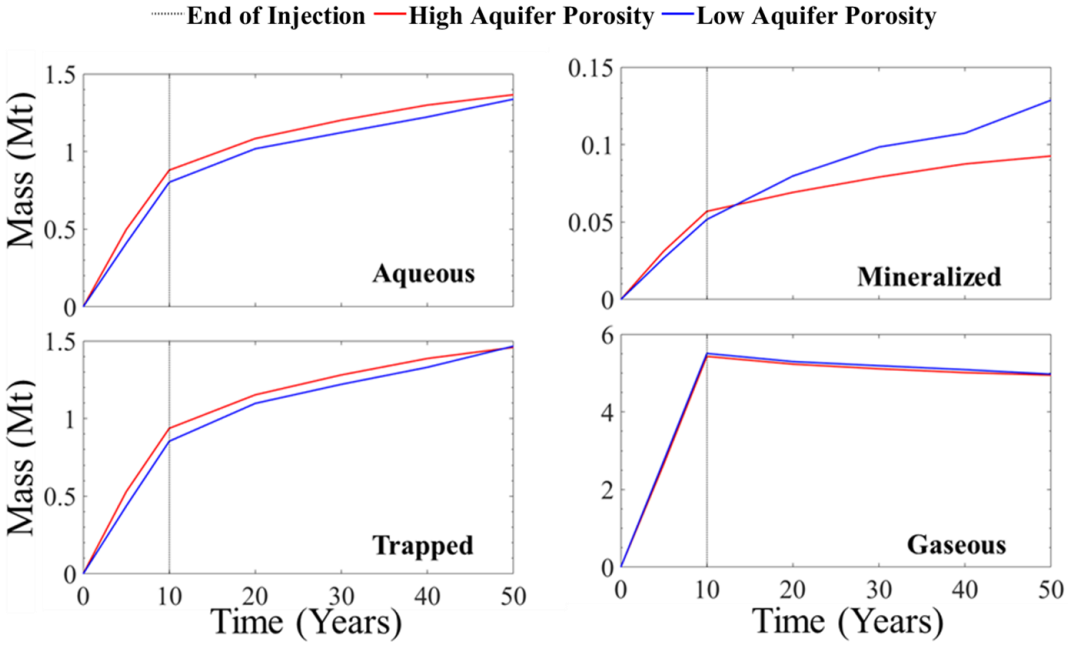

Figure 4.9: The mass comparison in simulated millions of metric tons of the aqueous, mineralized, trapped, and gaseous CO_2 in porous saline aquifer over 50 years due in formations with varying porosity. The red line represents the high formation porosity scenario, and the blue represents the low formation porosity scenario.

Fig. 4.9 shows that the mass of aqueous CO_2 is higher in more porous formations. This indicates that a more porous formation promotes higher CO_2 dissolution in the brine. In this study, we see that the trend in evolution of aqueous dissolution of CO_2 into the brine maintains a similar divergence throughout the simulation timeline. During this timeline, the maximum aqeous mass difference observed due to the thirty percent difference in porosity is 0.09 million tons of CO_2. Given the higher aqueous composition in the higher porosity case, a higher mineralization rate also occurs during the injection period. However, the mineralization rate for less porous aquifers becomes higher over time and surpasses that for the higher porosity formation. This increasing mineralization rate results in overall similarity in the mass quantity of trapped CO_2 at the end of the simulation period. The remaining gaseous CO_2 at the end of the 50 year simulation is also similar.

The results from this simulation show that the larger brine volume associated with higher porosity allows for increased dissolution of CO_2 into the aqueous phase. Hence, the smaller brine volume in the aquifer with lower porosity limits CO_2 dissolution. Porosity also influences the evolution of ion concentrations in the brine and thus the rate of attainment of saturation conditions for mineral precipitation. The result shows that lower system porosity results in faster attainment of saturation conditions which favor mineralization (Fig 4.10). The key mechanism is that with high porosity, you have more water, and less rock, hence increased aqueous CO_2 and less mineralized CO_2. CO_2 mineralization requires dissolution of primary minerals which have smaller volume fractions in a rock with higher porosity.

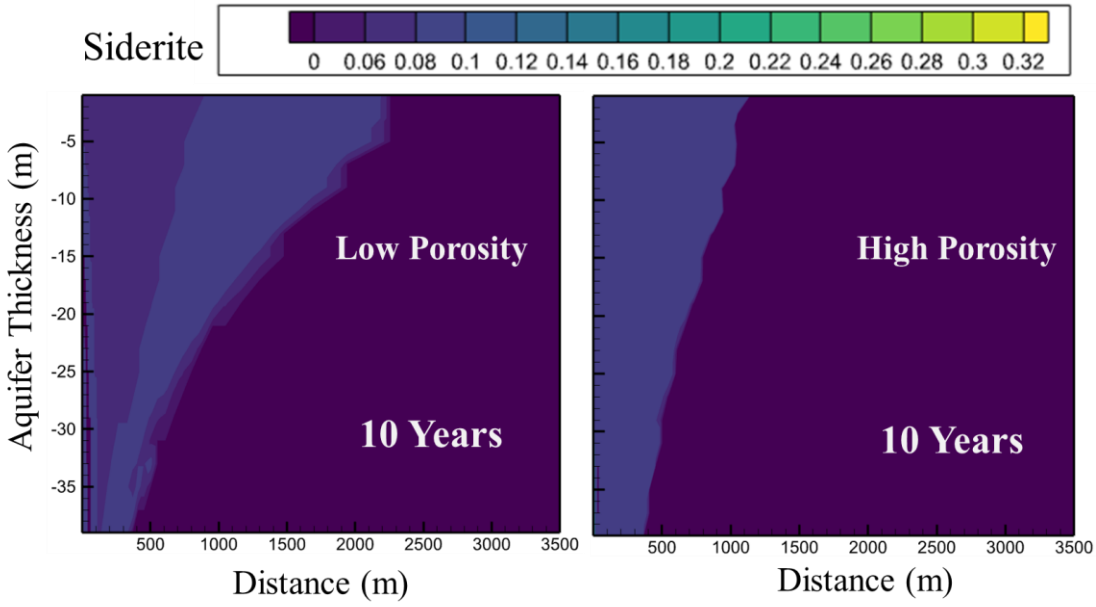

Figure 4.10: Saturation index of Siderite mineral after 10 years period. The position saturation index shows that siderite is precipitating in the system. The low porosity model has more precipitating region.

4.3.2.4 Effect of Permeability

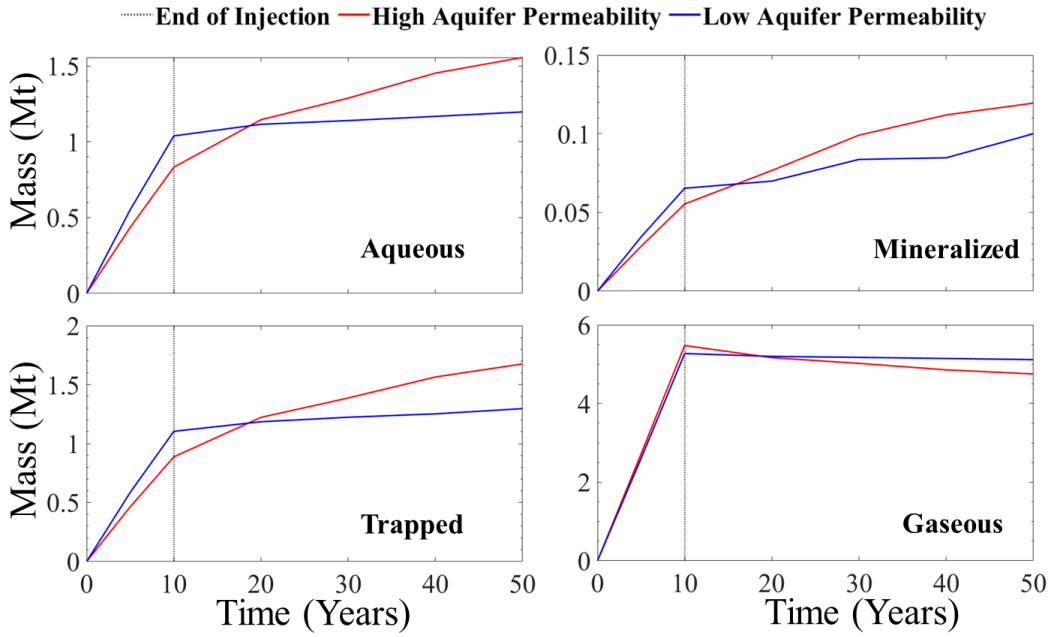

Figure 4.11: Simulated mass comparison in millions of metric tons of the aqueous, mineralized, trapped, and gaseous CO_2 in porous saline aquifer over 50 years due to the impact of permeability. The red line represents the high aquifer permeability scenario, and the blue represents the low aquifer permeability scenario.

The simulated influence of aquifer permeability on CO_2 sequestration efficiency is shown in Fig. 4.11. The figure shows that the aqueous mass of CO_2 dissolving into the brine is higher during the first 10 years of injection in the case of low permeability. However, the rate of CO_2 dissolution in the low permeability model became smaller than the rate of CO_2 dissolution in the high permeability model after injection stops. As such, the total aqueous composition in the high permeability simulation became higher than the low permeability model after 20 years. The mineralized CO_2 plot shows that the rate of mineralization is directly proportional to the rate of CO_2 dissolution into the brine. More interestingly, the amount of CO_2 mineralization plateaus in the low permeability scenario at certain intervals.

This phenomenon of the plateauing amount of mineralization highlights the key mechanism controlling the geochemical reaction in a permeability-controlled system. When temperature, salinity, and pressure conditions are kept constant, the rate of CO_2

dissolution into the brine is controlled by the surface area of CO_2 in contact with the brine (Hendriks and Blok 1993). When the permeability is high, the injected CO_2 attains high mobility as it migrates away from the point of injection. The injected CO_2 interacts with more brine during migration which allows for more CO_2 dissolution. Therefore, a highly permeable formation has a high contact area between CO_2 and brine.

However, Fig. 4.12 shows that the mobility of the injected CO_2 under the elevated pressure conditions associated with injection result in a higher aqueous CO_2 composition in the low permeability system. This is because the high-pressure condition of injection improves the lateral extent of the relatively uniform migration front of CO_2 acidified brine in the low permeability model. This condition increased the volume of brine in contact with the injected CO_2 to establish high CO_2 dissolution into the brine during the early phase of injection. The absence of the injection pressure post injection causes a reduction in the mobility of the injected CO_2. Hence, this results in less CO_2 dissolution as majority of the injected brine remain in the aquifer region where the brine is saturated with CO_2. As a result, the gas saturation in the injection region at 50 years in the low permeability model remains high while the high permeability model shows sighificant reduction in the gas saturation condition.

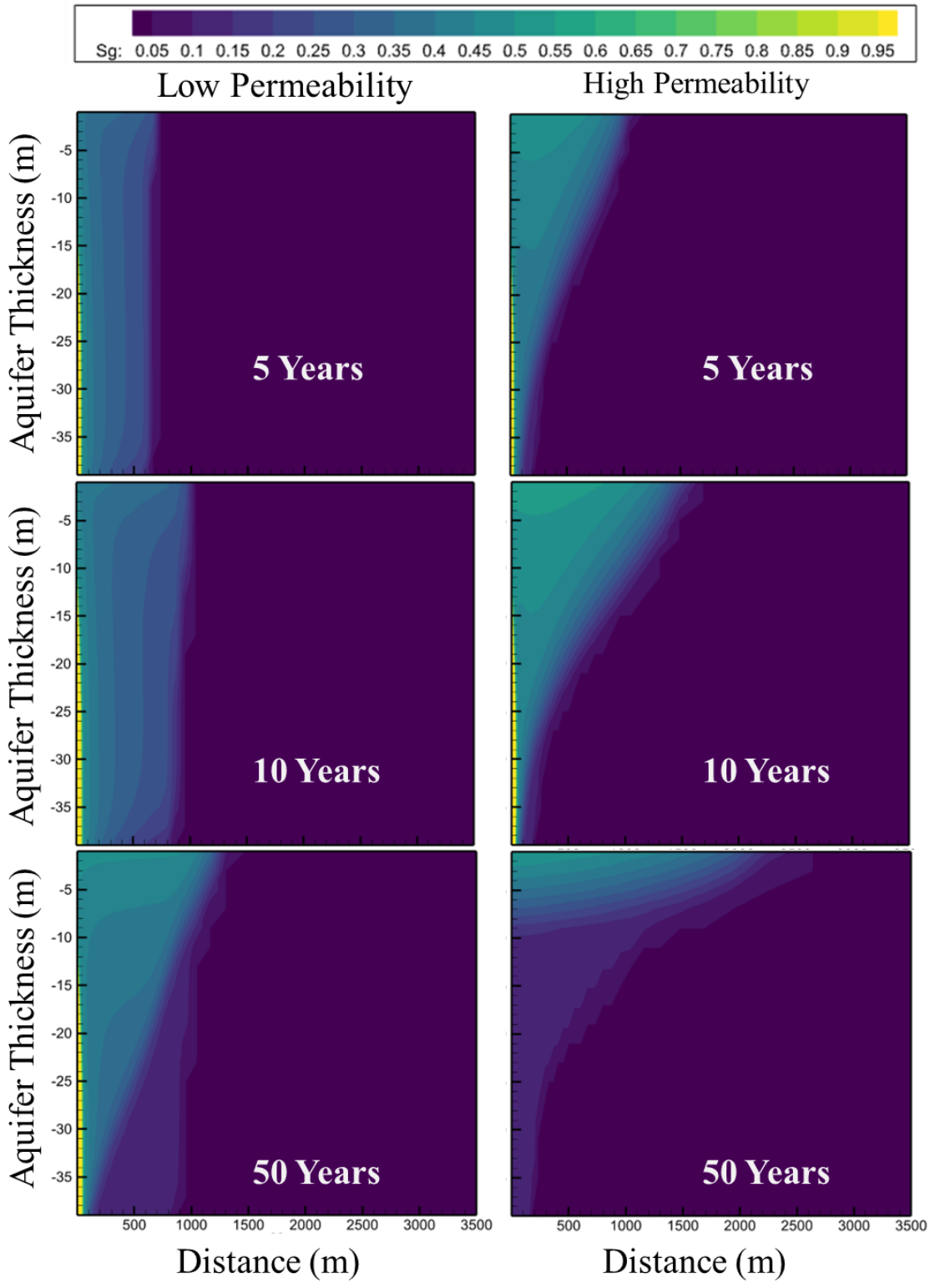

Figure 4.12: The migration pattern of CO_2 acidified brine in the Low and high permeability system during the injection period (5 years, 10 years) and at the end of the study period (50 years).

4.3.2.5 Compiled Effects of Reservoir Properties on CO_2 Trapping

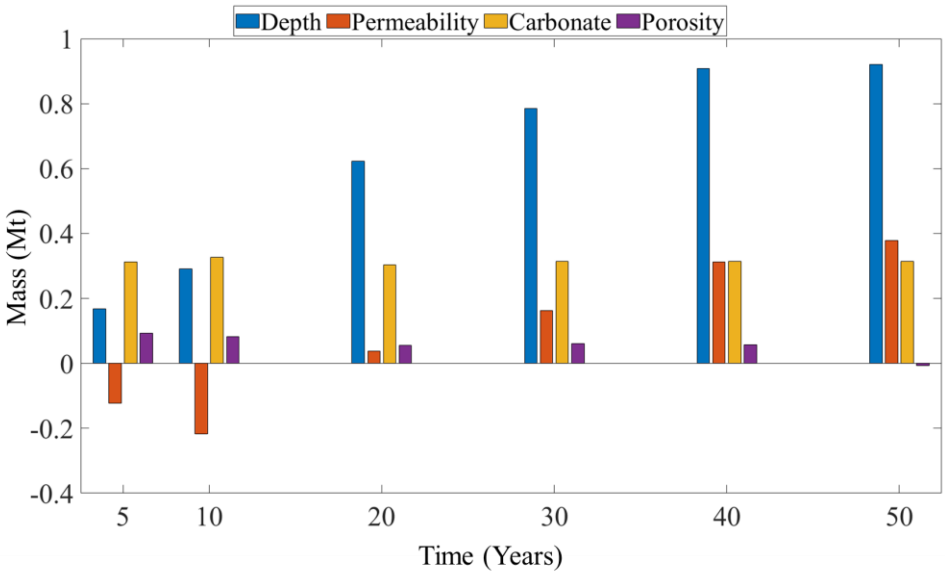

Figure 4.13: Simulated mass comparison in millions of metric tons of the difference between the trapped CO2 in the high and low case scenario of the aquifer properties. The blue, orange, yellow, and purple bar represents the depth, permeability, carbonate, and porosity, respectively. A bar with a value of 2Mt means that the difference in trapped CO_2 for the high scenario and low scenario is 2Mt.

Figure 4.13 shows that during the injection stage of the project, understanding the amount of carbonate mineralogy of an aquifer will have the most significant impact on predicting the evolution of injected CO_2. This study shows that the early phase of injection is critical when an aquifer has a higher chance of liberating divalent ions that mineralize CO_2. To optimize the potential to mineralize more CO_2 during the early phase of the CO_2 sequestration project in a high carbonate formation, it would be necessary to design an injection routine to exploit the mineralization potential.

Post-injection of CO_2, the depth of storing the CO_2 has the most impact on the evolution of CO_2. Generally, the depth of storage can be influenced by a confluence of factors like exploration cost, or availability of suitable caprock . However, this study based on the geochemical perspective presents that the depth of storage has a substantial impact on the evolution of CO_2 throughout the project lifespan, especially after injection. In this study, the impact observed here can be attributed to the temperature and pressure conditions associated with deeper formations. Temperature relates to

reaction rate constant in Arrhenius equation and reaction rate constant relates to the kinetic rate law for mineral dissolution and precipitation (Lasaga 1984; C. I. Steefel and Lasaga 1994). Ultimately, increasing temperature increases the geochemical reaction rate. These geochemical reactions of acidified brine and rock minerals start by CO_2 solubility in the brine. Therefore, ensuring more CO_2 solubility into the brine can aid the reaction.

Porosity and permeability are the two key hydrogeological properties studied here. Fig 4.13 shows that porosity can be considered to marginally impact the evolution of stored CO_2 in the porous aquifer as it has the least impact on the difference between the amount of gaseous CO_2 that evolved in the high and low case scenarios. On the other hand, permeability can be ascribed to have an impact on CO_2 evolution. During the injection stage, CO_2 evolution favors a low permeability scenario, hence the negative net effect on CO_2 trapping. Higher permeability is favored post-injection. These two stages of response due to the effect of permeability could be explained by how the CO_2 flow in brine is controlled. For sufficient CO_2-brine interaction to occur during the advection-driven flow of CO_2 in brine, the aquifer needs flow conditions that create a balance between residence time for CO_2-brine interaction and migration for CO_2 to interact with less saturated brine. During the high-pressure condition of injection that ensures migration, CO_2-brine interaction in less permeable formation becomes optimal. Conversely, the high permeable formation is favored when injection stops.

4.4 Conclusion

This study evaluates the extent of the impact of aquifer properties on the evolution of CO_2 securely sequestered in the storage aquifer. The aquifer properties that were evaluated include the porosity, depth of storage, permeability, and fraction of carbonate minerals. The aquifer properties of the Paluxy formation are used to parameterize a base model for this analysis. This base model demonstrates the overall geochemical evolution for CO_2 trapping in the aquifer. The aquifer properties of the

base model are successively changed with high and low aquifer property values to understand how the change in property affects the trapping potential of the aquifer.

This analysis takes advantage of the ability of numerical simulations to predict the evolution in the formation. Several studies have previously tried to explain the relationship between CO_2 sequestration and various factors that can affect the process. These explanations have looked at all the scales of the processes involved. This study takes a field-scale approach by developing a simulation that monitors the evolution of CO_2 mineralization, solubility trapping, and gaseous CO_2 as a result of changing aquifer properties. We have observed that the impact the aquifer properties have on CO_2 evolution depends on both the stage of the sequestration project and the aquifer properties.

4.5 Acknowledgments

Authors Iloejesi and Beckingham acknowledge support from the Southeast Regional CO_2 Utilization and Storage Acceleration Partnership (SECARB-USA) project funded by the U.S. Department of Energy and cost-sharing partners under grant number FE0031830, managed by the Southern States Energy Board.

4.6 References

Ahmmed, B., Appold, M.S., Fan, T., McPherson, B.J., Grigg, R.B. and White, M.D., 2016. Chemical effects of carbon dioxide sequestration in the Upper Morrow Sandstone in the Farnsworth, Texas, hydrocarbon unit. *Environmental Geosciences*, *23*(2), pp.81-93. https://doi.org/10.1306/EG.09031515006.

Allen, K., 1985. CAES: the underground portion. *IEEE Transactions on Power Apparatus and Systems*, (4), pp.809-812.https://doi.org/10.1109/TPAS.1985.319078.

Audigane, P., Gaus, I., Czernichowski-Lauriol, I., Pruess, K. and Xu, T., 2007. Two-

dimensional reactive transport modeling of CO2 injection in a saline aquifer at the Sleipner site, North Sea. *American journal of science*, *307*(7), pp.974-1008. https://doi.org/10.2475/07.2007.02.

Folaranmi, A.T., 2015. *Geologic characterization of a saline reservoir for carbon sequestration: The Paluxy Formation, Citronelle Dome, Gulf of Mexico Basin, Alabama* (Doctoral dissertation, Oklahoma State University).

Baklid, A., Korbol, R. and Owren, G., 1996, October. Sleipner Vest CO2 disposal, CO2 injection into a shallow underground aquifer. In *SPE Annual Technical Conference and Exhibition*. OnePetro. https://doi.org/10.2118/36600-MS.

Balashov, V.N., Guthrie, G.D., Hakala, J.A., Lopano, C.L., Rimstidt, J.D. and Brantley, S.L., 2013. Predictive modeling of CO2 sequestration in deep saline sandstone reservoirs: Impacts of geochemical kinetics. *Applied Geochemistry*, *30*, pp.41-56. https://doi.org/10.1016/J.APGEOCHEM.2012.08.016.

Benson, S.M. and Cole, D.R., 2008. CO2 sequestration in deep sedimentary formations. *Elements*, *4*(5), pp.325-331. https://doi.org/10.2113/gselements.4.5.325.

Bourg, I.C., Beckingham, L.E. and DePaolo, D.J., 2015. The nanoscale basis of CO2 trapping for geologic storage. *Environmental science & technology*, *49*(17), pp.10265-10284. https://doi.org/10.1021/acs.est.5b03003.

Clark, D.E., Oelkers, E.H., Gunnarsson, I., Sigfússon, B., Snæbjörnsdóttir, S.Ó., Aradottir, E.S. and Gíslason, S.R., 2020. CarbFix2: CO2 and H2S mineralization during 3.5 years of continuous injection into basaltic rocks at more than 250° C. *Geochimica et Cosmochimica Acta*, *279*, pp.45-66. https://doi.org/10.1016/J.GCA.2020.03.039.

Bentham, M., 2006. An assessment of carbon sequestration potential in the UK–Southern North Sea case study. *Nottingham: Tyndall Centre for Climate Change*

Research.

Corey, A.T., 1954. The interrelation between gas and oil relative permeabilities. *Producers monthly*, pp.38-41.

de Coninck, H. and Benson, S.M., 2014. Carbon dioxide capture and storage: issues and prospects. *Annual review of environment and resources*, *39*, pp.243-270. https://doi.org/10.1146/ANNUREV-ENVIRON-032112-095222.

Delshad, M., Kong, X., Tavakoli, R., Hosseini, S.A. and Wheeler, M.F., 2013. Modeling and simulation of carbon sequestration at Cranfield incorporating new physical models. *International Journal of Greenhouse Gas Control*, *18*, pp.463-473.

Duan, Z., Sun, R., Zhu, C. and Chou, I.M., 2006. An improved model for the calculation of CO2 solubility in aqueous solutions containing Na+, K+, Ca2+, Mg2+, Cl−, and SO42−. *Marine chemistry*, *98*(2-4), pp.131-139. https://doi.org/10.1016/j.marchem.2005.09.001.

Espinoza, D.N. and Santamarina, J.C., 2017. CO2 breakthrough—Caprock sealing efficiency and integrity for carbon geological storage. *International Journal of Greenhouse Gas Control*, *66*, pp.218-229. https://doi.org/10.1016/j.ijggc.2017.09.019.

Van Genuchten, M.T., 1980. A closed-form equation for predicting the hydraulic conductivity of unsaturated soils. *Soil science society of America journal*, *44*(5), pp.892-898. https://doi.org/10.2136/sssaj1980.03615995004400050002x.

Gérard, F., Fritz, B., Clément, A. and Crovisier, J.L., 1998. General implications of aluminium speciation-dependent kinetic dissolution rate law in water–rock modelling. *Chemical Geology*, *151*(1-4), pp.247-258. https://doi.org/10.1016/S0009-2541(98)00083-7.

Goodman, A., Hakala, A., Bromhal, G., Deel, D., Rodosta, T., Frailey, S., Small, M.,

Allen, D., Romanov, V., Fazio, J. and Huerta, N., 2011. US DOE methodology for the development of geologic storage potential for carbon dioxide at the national and regional scale. *International Journal of Greenhouse Gas Control*, *5*(4), pp.952-965. https://doi.org/10.1016/j.ijggc.2011.03.010.

Helgeson, H.C., 1981. Prediction of the thermodynamic properties of electrolytes at high pressures and temperatures. *Physics and Chemistry of the Earth*, *13*, pp.133-177. https://doi.org/10.1016/0079-1946(81)90009-4.

Helgeson, H.C. and Kirkham, D.H., 1974. Theoretical prediction of the thermodynamic behavior of aqueous electrolytes at high pressures and temperatures; II, Debye-Huckel parameters for activity coefficients and relative partial molal properties. *American Journal of Science*, *274*(10), pp.1199-1261. https://doi.org/10.2475/ajs.274.10.1199.

Hendriks, C.A. and Blok, K., 1993. Underground storage of carbon dioxide. *Energy Conversion and Management*, *34*(9-11), pp.949-957. https://doi.org/10.1016/0196-8904(93)90041-8.

Hitchon, B., 1996. Aquifer disposal of carbon dioxide: hydrodynamic and mineral trapping-proof of concept.

Hunt, J.R., Sitar, N. and Udell, K.S., 1988. Nonaqueous phase liquid transport and cleanup: 1. Analysis of mechanisms. *Water resources research*, *24*(8), pp.1247-1258. https://doi.org/10.1029/WR024I008P01247/FORMAT/PDF.

Iloejesi, C.O. and Beckingham, L.E., 2021. Influence of storage period on the geochemical evolution of a compressed energy storage system. *Frontiers in Water*, p.100. https://doi.org/10.3389/frwa.2021.689404.

Jalali, J., Koperna, G.J., Cyphers, S., Riestenberg, D. and Esposito, R., 2021, March. Large Volume CO2 Storage and Plume Management in the Southeastern US; Reservoir Characterization and Simulation. In *Proceedings of the 15th Greenhouse Gas Control Technologies Conference* (pp. 15-18).

https://doi.org/10.2139/SSRN.3867756.

Warner, A.J., 1993. *Regional geologic framework of the Cretaceous, offshore Mississippi*. Mississippi Department of Environmental Quality, Office of Geology.

Juanes, R., Spiteri, E.J., Orr Jr, F.M. and Blunt, M.J., 2006. Impact of relative permeability hysteresis on geological CO2 storage. *Water resources research*, *42*(12). https://doi.org/10.1029/2005WR004806/FORMAT/PDF.

Kelemen, P.B., Matter, J., Streit, E.E., Rudge, J.F., Curry, W.B. and Blusztajn, J., 2011. Rates and mechanisms of mineral carbonation in peridotite: natural processes and recipes for enhanced, in situ CO2 capture and storage. *Annual Review of Earth and Planetary Sciences*, *39*, pp.545-576. https://doi.org/10.1146/ANNUREV-EARTH-092010-152509.

Kuuskraa, V., Koperna, G. and Riestenberg, D., 2020. *Commercial Development Plan (Deliverable 8.2)* (No. DOE-SSEB-0029465-58). Southern States Energy Board, Peachtree Corners, GA (United States).

Lagneau, V., Pipart, A. and Catalette, H., 2005. Reactive Transportmodelling and Long Term Behaviour of CO2 Sequestration in Saline Aquifers. *Oil & Gas Science and Technology*, *60*(2), pp.231-247. https://doi.org/10.2516/OGST:2005014.

Lasaga, A.C., 1984. Chemical kinetics of water-rock interactions. *Journal of geophysical research: solid earth*, *89*(B6), pp.4009-4025. https://doi.org/10.1029/JB089IB06P04009/FORMAT/PDF.

Lu, J., Kharaka, Y.K., Thordsen, J.J., Horita, J., Karamalidis, A., Griffith, C., Hakala, J.A., Ambats, G., Cole, D.R., Phelps, T.J. and Manning, M.A., 2012. CO2–rock–brine interactions in Lower Tuscaloosa Formation at Cranfield CO2 sequestration site, Mississippi, USA. *Chemical Geology*, *291*, pp.269-277.

Matter, J.M. and Kelemen, P.B., 2009. Permanent storage of carbon dioxide in

geological reservoirs by mineral carbonation. *Nature Geoscience*, *2*(12), pp.837-841. https://doi.org/10.1038/NGEO683.

Matter, J.M., Stute, M., Snæbjörnsdottir, S.Ó., Oelkers, E.H., Gislason, S.R., Aradottir, E.S., Sigfusson, B., Gunnarsson, I., Sigurdardottir, H., Gunnlaugsson, E. and Axelsson, G., 2016. Rapid carbon mineralization for permanent disposal of anthropogenic carbon dioxide emissions. *Science*, *352*(6291), pp.1312-1314. https://doi.org/10.1126/SCIENCE.AAD8132/FORMAT/PDF.

McGrail, B.P., Schaef, H.T., Spane, F.A., Cliff, J.B., Qafoku, O., Horner, J.A., Thompson, C.J., Owen, A.T. and Sullivan, C.E., 2017. Field validation of supercritical CO2 reactivity with basalts. *Environmental Science & Technology Letters*, *4*(1), pp.6-10. https://doi.org/10.1021/ACS.ESTLETT.6B00387/SUPPL_FILE/EZ6B00387_SI_001.PDF.

Michael, K., Allinson, G., Golab, A., Sharma, S. and Shulakova, V., 2009. CO2 storage in saline aquifers II–experience from existing storage operations. *Energy Procedia*, *1*(1), pp.1973-1980. https://doi.org/10.1016/J.EGYPRO.2009.01.257.

Mualem, Y., 1976. A new model for predicting the hydraulic conductivity of unsaturated porous media. *Water resources research*, *12*(3), pp.513-522. https://doi.org/10.1029/WR012I003P00513.

Nathenson, M. and Guffanti, M., 1988. Geothermal gradients in the conterminous United States. *Journal of Geophysical Research: Solid Earth*, *93*(B6), pp.6437-6450. https://doi.org/10.1029/JB093iB06p06437.

Gray, K., 2015. *Carbon Storage Atlas* (No. DOE-SSEB-42590-120). Southern States Energy Board, Peachtree Corners, GA (United States). https://doi.org/10.2172/1814017.

Palandri, J.L. and Kharaka, Y.K., 2004. *A compilation of rate parameters of water-mineral interaction kinetics for application to geochemical modeling*. Geological

Survey Menlo Park CA.

Pashin, J.C., Hills, D.J., Kopaska-Merkel, D.C. and McIntyre, M.R., 2008. Geological evaluation of the potential for CO2 sequestration in Kemper County. *Mississippi: Birmingham, Final Report, Southern Company Research & Environmental Affairs*.

Pfeiffer, W.T. and Bauer, S., 2015. Subsurface porous media hydrogen storage–scenario development and simulation. *Energy Procedia*, *76*, pp.565-572. https://doi.org/10.1016/j.egypro.2015.07.872.

Pruess, K., 2005. *ECO2N: A TOUGH2 fluid property module for mixtures of water, NaCl, and CO2*. eScholarship, University of California.

Qin, F. and Beckingham, L.E., 2019. Impact of image resolution on quantification of mineral abundances and accessible surface areas. *Chemical Geology*, *523*, pp.31-41. https://doi.org/10.1016/j.chemgeo.2019.06.004.

Qin, F. and Beckingham, L.E., 2021. The impact of mineral reactive surface area variation on simulated mineral reactions and reaction rates. *Applied Geochemistry*, *124*, p.104852. https://doi.org/10.1016/J.APGEOCHEM.2020.104852.

Shafeen, A., Croiset, E., Douglas, P.L. and Chatzis, I., 2004. CO2 sequestration in Ontario, Canada. Part I: storage evaluation of potential reservoirs. *Energy Conversion and Management*, *45*(17), pp.2645-2659. https://doi.org/10.1016/J.ENCONMAN.2003.12.003.

Spycher, N.F. and Reed, M.H., 1988. Fugacity coefficients of H2, CO2, CH4, H2O and of H2O-CO2-CH4 mixtures: A virial equation treatment for moderate pressures and temperatures applicable to calculations of hydrothermal boiling. *Geochimica et Cosmochimica Acta*, *52*(3), pp.739-749. https://doi.org/10.1016/0016-7037(88)90334-1.

Spycher, N., Pruess, K. and Ennis-King, J., 2003. CO2-H2O mixtures in the geological sequestration of CO2. I. Assessment and calculation of mutual solubilities from 12 to 100 C and up to 600 bar. *Geochimica et cosmochimica acta*, *67*(16), pp.3015-3031. https://doi.org/10.1016/S0016-7037(03)00273-4.

Steefel, C.I., 1994. Coupled model for transport of multiple chemical species and kinetic precipitation/dissolution reactions with application to reactive flow in single phase hydrothermal systems. *Am. J. Sci.*, *294*, pp.529-592. https://doi.org/10.2475/AJS.294.5.529.

Xu, T., Sonnenthal, E., Spycher, N. and Zheng, L., 2017. TOUGHREACT V3. 32 Reference Manual: A Parallel Simulation Program for Non-Isothermal Multiphase Geochemical Reactive Transport. *Lawrence Berkeley National Laboratory, Berkeley, CA*.

Tullis, J. and Yund, R.A., 1982. Grain growth kinetics of quartz and calcite aggregates. *The Journal of Geology*, *90*(3), pp.301-318. https://doi.org/10.1086/628681.

Wang, X. and Economides, M., 2013. *Advanced natural gas engineering*. Elsevier. https://doi.org/10.1016/C2013-0-15532-8.

Whittaker, S., Rostron, B., Hawkes, C., Gardner, C., White, D., Johnson, J., Chalaturnyk, R. and Seeburger, D., 2011. A decade of CO2 injection into depleting oil fields: monitoring and research activities of the IEA GHG Weyburn-Midale CO2 Monitoring and Storage Project. *Energy Procedia*, *4*, pp.6069-6076. https://doi.org/10.1016/J.EGYPRO.2011.02.612.

Xu, T., Apps, J.A. and Pruess, K., 2004. Numerical simulation of CO2 disposal by mineral trapping in deep aquifers. *Applied geochemistry*, *19*(6), pp.917-936. https://doi.org/10.1016/J.APGEOCHEM.2003.11.003.

Xu, T., Apps, J.A., Pruess, K. and Yamamoto, H., 2007. Numerical modeling of injection and mineral trapping of CO2 with H2S and SO2 in a sandstone

formation. *Chemical Geology*, *242*(3-4), pp.319-346. https://doi.org/10.1016/j.chemgeo.2007.03.022.

Zhang, S. and DePaolo, D.J., 2017. Rates of CO2 mineralization in geological carbon storage. *Accounts of chemical research*, *50*(9), pp.2075-2084. https://doi.org/10.1021/acs.accounts.7b00334.

Chapter 5: Impact of Aquifer Heterogeneity on Simulated CO_2 Trapping Mechanisms in Porous Saline Aquifers

Chidera O. Iloejesi; Lauren E. Beckingham*

Department of Civil and Environmental Engineering, Auburn University, Auburn, Alabama, 36849.

Corresponding Author* Tel: 334-844-6260; e-mail: leb0071@auburn.edu

Abstract

Sequestration of CO_2 is a technology that can help permanently store large-scale volumes of CO_2 in subsurface aquifers, reducing the amount of CO_2 emission to the atmosphere. The target subsurface aquifers are typically thoroughly investigated before they can be used for sequestration purposes. This site investigation process inspects aquifer properties to access storage capacity, potential environmental safety, and suitability for trapping and permanent sequestration of the injected CO_2. The suitability of an aquifer for permanent CO_2 trapping is often assessed via reactive transport models. Simulations are often constructed based on limited data, and measurements of formation properties from a limited number of core samples. As such, simulations often consider homogenous formation properties. In reality, aquifer properties are heterogeneous and the impact of these heterogeneities on simulated CO_2 trapping mechanisms and efficiency is not well understood and is the focus of this work. This study analyzes aquifer heterogeneity's impact on CO_2 trapping efficiency. Reactive transport simulations are used in this study to compare how aquifer heterogeneity impacts CO_2 evolution from gaseous to aqueous and, finally, mineralized CO_2 over varying temporal and spatial scales. Heterogeneous models that consider porosity heterogeneity, carbonate mineralogy heterogeneity, and temperature gradient are compared to a homogenous model to understand the implications of aquifer non-uniformities on predicted CO_2 sequestration efficiency in a porous aquifer. The comparison of the uniform model to the heterogeneous model result shows that

studying an aquifer as a homogeneous model will underestimate the sequestration efficiency during the injection phase of CO_2 sequestration in a porous saline aquifer. During the post-injection phase of CO_2 sequestration, homogenization of porosity and carbonate mineralogy value the aquifer properties yields an overestimation of the sequestration efficiency. Considering temperature and pressure gradient in the modeling of the aquifer to study sequestration efficiency of CO_2 in a formation consistently produced a higher sequestration efficiency than the homogenized aquifer temperature and pressure value. The maximum deviation between the homogeneous and heterogeneous model at the end of the study period is approximately 10% of the evolved supercritical CO_2.

5.1 Introduction

In recent years, the renewable energy profile is increasing in the energy portfolio(McCrone et al. 2015). Nevertheless, increasing energy demands necessitate continued energy production through hydrocarbons(Begum et al. 2015). Unfortunately, CO_2 emissions continue to increase as a consequence of hydrocarbon energy generation(Arnette 2017; Edmonds, Freund, and Dooley 2001). Carbon capture and geologic storage, however, provide a pathway for reducing CO_2 concentration in the atmosphere and eventually achieving net-zero carbon emission in the future(Ciferno et al. 2009). This technology averts the release of CO_2 into the atmosphere by capturing it and then injecting the CO_2 into subsurface geologic formations(Freund 2003). Large scale and widespread application of this technology will involve the utilization of porous saline aquifers as storage reservoirs due to their ubiquity and enormous available storage volume(IPCC 2005; NETL 2015).

Pre-injection of CO_2, the storage aquifer is expected to be geologically stable against potential tectonic activities, porous, permeable, sufficiently deep, and sealed by impermeable rocks called the caprock(Bentham and Kirby 2005). Therefore, each time the subsurface is utilized for the development of CO_2 sequestration technology, there

are myriads of potential considerations to guarantee the success of the project. Subsurface site investigation is one of the major approaches to ensure that storage aquifers meet these guidelines to guarantee the success of the project and the onsite safety of all concerned stakeholders involved in the project(Doughty et al. 2007). Hence, the site investigation process is initiated before developing a project to evaluate the several conditions that present opportunities and threats to the successful completion of the intended project(Niemi et al. 2017). An intensive subsurface site investigation is one of the major prerequisites to guaranteeing the onsite safety of all concerned stakeholders involved in the project (NETL 2015). The prohibitive cost of these site investigations implies that a select portion of the site is investigated. Hence, the suite of geological wellbore log information and core sample data used for estimating and evaluating the storage capacity and response of the entire formation to CO_2 injection is estimated from select points in the formation. Nevertheless, the borehole logging, geophysical mapping, core sample analysis, well testing, and geological mapping from these select spots still provide meaningful overall insights into the suitability of the target formation to store CO_2 storage.

However, the results from the field-scale site investigation show that the aquifer properties vary at different locations in the same aquifer (Zemke, Liebscher, and Wandrey 2010). Moreover, the heterogeneity of aquifer properties has been found to impact aquifer processes like fluid flow in aquifers (Wardlaw and Petroleum 1976; Weber 1982). Since aquifer properties have been understood to control the CO_2-brine interaction, an understanding of the impact of geologic heterogeneity encountered during the migration of the injected CO_2 away from the point of injection becomes necessary.

These formation heterogeneities are typically considered to be a result of the evolution in the grain size, geometry, and internal structure of the original sediment composition of the aquifer to the final structural features and diagenetic alterations (Morad et al. 2010). Lithological heterogeneities can result from various features like

the alternating presence of good reservoir facie with poor quality facies as seen in Stuggart formation (Förster et al. 2006), or the presence of faults in a formation (Juhlin et al. 2007) which are all critical details that inform the vicinity and depth of injecting CO_2 in the subsurface. These lithological features influence the heterogeneity of porosity and permeability of the formation. The lithological influence on the hydrogeological features affects the rate and transport of fluid in the subsurface which has been found to impact the CO_2-migration front to cause a fingering effect and ultimately impact injectivity(Lengler et al. 2010). Consequently, the micro-scale through hecto-scale heterogeneities in the formation exert influence to the formation that needs to be understood.

Numerical modeling is a tool that has been useful to provide insight into the field-scale behavior of CO_2 injected into the subsurface (Ennis-King and Paterson 2003; Xu, Apps, and Pruess 2004; Riaz et al. 2006). Numerical simulations have used to couple the complexity of various subsurface conditions that affect CO_2 storage and have been typically been used to extrapolate the experimental observations (Beckingham et al. 2016). In other cases, numerical modeling has been used independently to understand potential evolution in a storage site and the simulation results have been compared to field observation (Doughty et al. 2007; Hovorka et al. 2004). Essentially, the ability to fundamentally access a formation through field scale numerical modeling can be utilized to determine the geochemical suitability of a formation. From the geochemical evolution standpoint, a suitable site must ensure the mineralization of the injected CO_2 in a storage site (Zhang and DePaolo 2017). CO_2 mineralization is the conversion of the CO_2 to carbonate rocks to permanently sequester the CO_2. CO_2 mineralization is preceded by the trapping of the injected CO_2 by the caprock termed structural trapping and the dissolution of CO_2 in the brine through solubility trapping and residual trapping(Gaus et al. 2008).

This study seeks to understand the geochemical impact of spatial heterogeneity of aquifer properties on CO_2 trapping. The study uses numerical modeling to analyze

the CO_2 mineralization efficiency in a heterogenous aquifer by comparing it to the simulation result of a homogenous aquifer. The model used for the study will consider spatial heterogeneity of porosity in the model. The other model presented in this study will capture the spatial heterogeneity of carbonate mineralogy in the model and, the last model will capture the variation of aquifer temperature and pressure properties based on geothermal and pressure gradients. Ultimately, an equal volume of CO_2 will be injected into the homogeneous and heterogenous model to understand the role heterogeneity plays during the subsurface injection of CO_2 into the porous aquifer. Then the simulation result will be analyzed to understand how the heterogeneity associated with geothermal gradient effect on temperature, porosity, and carbonate mineralogical composition factor would impact the sequestration efficiency of a heterogeneous formation. In this study sequestration efficiency simply refers to the rate at which the supercritical CO_2 injected into the storage aquifer evolves to be dissolved into the brine or mineralized as carbonate minerals in the formation.

5.2 Method

5.2.1 System Setup

The simulation approach adopted here aims to help understand the effects of spatially heterogeneous aquifer properties on CO_2 sequestration efficiency. Here, two sets of field scale simulations are developed, one with homogeneously distributed properties and the other with variations in aquifer properties. The average properties for the two sets of simulations are equivalent such that this study evaluates the potential impact of heterogeneity on simulated site evolution even after an excellent site investigation study has been carried out.

The TOUGHREACT reactive transport simulator was used for this field-scale modeling. The simulator couples subsurface multiphase transport and reaction and uses the ECO2N fluid property module to handle the CO_2 and water thermophysical properties under the typical range of temperature and pressure conditions of a saline aquifer (Tianfu Xu, Eric Sonnenthal, Nicolas Spycher 2017; Pruess 2005). The model

presented in this study investigates the impact of aquifer heterogeneity on the extent of CO_2 trapping in porous saline aquifers using a radially symmetrical two-dimensional model.

Two sets of models were developed for this study. The first set is a homogeneous model. The homogeneous model is initialized with the aquifer properties of the Paluxy formation located in the southern region of the United States which is being considered as a potential CO_2 storage formation is used to define the condition for the homogeneous model (Jalali et al. 2021; Qin and Beckingham 2019; Kuuskraa, V., Koperna, G., & Riestenberg 2020).

The second set is the heterogeneous model. In the heterogeneous model, each aquifer property evaluated for its impact on sequestration efficiency in this study was spatially varied to create an independent heterogeneity of that property in a 2-D model. The spatial heterogeneity is developed in the grid cells by stochastic assignment of aquifer properties to the grid cells of the model. Despite the random assignment of aquifer properties to the grid cells, the average value of the aquifer properties used to initialize the entire grid cells in the heterogeneous model will match the initial condition assigned to the entire grid cells for the homogeneous model.

For instance, in the model developed to consider porosity heterogeneity, the heterogeneous simulation randomly assigned five different porosity values to the aquifer ranging from 10% to 40%. However, the average porosity value of porosity for the entire heterogeneous grid cells is 25% which is equivalent to the porosity value of the Paluxy formation which is used to initialize the homogeneous model. Similarly, the model for evaluating the impact of carbonate mineral heterogeneity in the rock matrix was developed using five different carbonate abundance. These five rock sample characterizations were randomly assigned to still maintain a carbonate mineral abundance equivalent to the homogeneous system. Lastly, a non-isothermal model setup is used to depict the subsurface temperature variation with the geothermal

gradient. The temperature at the center of the aquifer thickness is used to initialize an isothermal model for the homogeneous simulation.

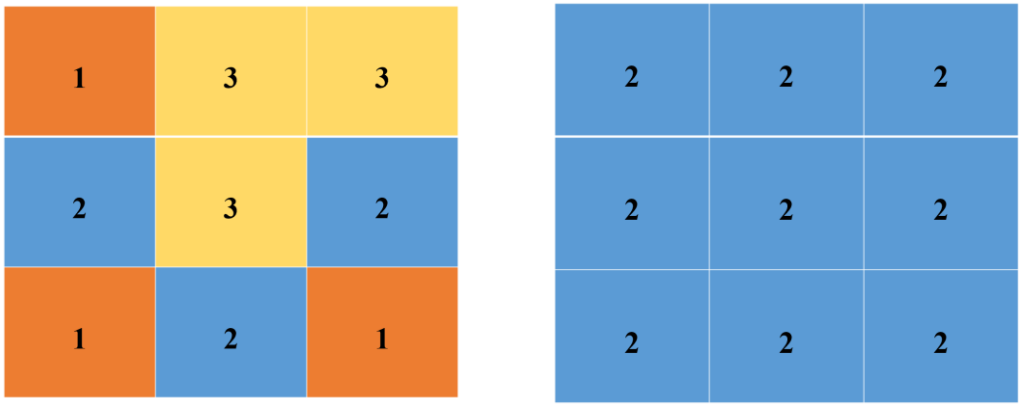

Simplified randomized grid block parameter initialization of heterogeneous formation

Simplified uniform grid block parameter initialization for the homogeneous formation

Figure 5.1: A demonstration of the difference in the model setup for the study on the effect of aquifer heterogeneity on sequestration efficiency. The heterogeneous model shows the different cases of possible aquifer values assignment for each grid cell.

Essentially, the simulation approach adopted in this study is based on using the average value of the spatially heterogeneous aquifer to define the homogeneous model. Therefore, the practical implication of this investigation is that the result of this study could be interpreted as a study that aims to explain the geochemical advantage of taking more multiple data points during site investigations over the prevalent practices of adopting parameters that define the aquifer from fewer data points. As already pointed out in the introduction, some constraints make the practicality of taking multiple data points that could be represented by thousands of grid points in numerical models unfeasible. This study tries to answer this question by evaluating the heterogeneities associated with porosity, carbonate mineralogy, and temperature and pressure condition of a formation before CO_2 injection.

Table 5.1: Simulation parameter values for each considered aquifer property. Aquifer formation properties for acting and proposed CO_2 reservoir formations were collected from the literature. The values are representative of the range of aquifer properties in these target formations and do not necessarily correspond to the exact values. The heterogenous values are chosen so that the aquifer value could be numerically the average of the homogeneous model.

Model Setup		**Porosity**	**Carbonate mineralogy**
Heterogeneous model	**Case 1**	10%	2%
	Case 2	20%	5%
	Case 3	25%	11.5%
	Case 4	30%	16%
	Case 5	40%	21%
Homogeneous model		25%	11.5%

The properties of the Paluxy formation in the southeastern region of the United States as obtained from the literature and given in Table 2 (Qin and Beckingham 2019). The mineral composition includes quartz mineral composition of 76.45% abundance, calcite at 9.63%, siderite at 1.98%, and smectite, K-feldspar, and muscovite with the mineral abundance of 8.23%, 3.50%, and 0.31% respectively. The model in this study is set up such that the mineral abundance is scaled up or down to accommodate an increase or decrease in porosity when the porosity heterogeneity is considered. The hydrostatic pressure gradient is 0.43 psi/ft (Pashin et al. 2008). The temperature was calculated based on the surface temperature of 20^{o}C and temperature gradient of 20^{o}C/km (John Warner 1993; Nathenson and Guffanti 1988). The aquifer was discretization of 20 layers is adopted. A uniform and logarithmically increasing radial discretization was adopted with the lateral boundary considered to be at infinity to mimic constant temperature, concentration, and pressure conditions at the boundaries. The quartz mineralogical composition of the formation is adjusted to accommodate the variation in carbonate mineral fraction. Quartz has been shown to minimally affect geochemical reactions because of its slow kinetics (Tullis and Yund 2015). Table 2 and Table 3 have more information on the mineral composition, the reactive surface area of primary minerals, and the reactive surface areas of secondary minerals used in this simulation.

Table 5.2: Base case mineral composition, mineral abundance, volume fraction, and reactive surface area of primary minerals(Qin and Beckingham 2019), and reactive surface areas of secondary minerals (Xu, Apps, and Pruess 2004).

Mineral	**Mineral Reaction**	**Mineral Abundance (v%)**	**Surface Area (m^2g^{-1})**
Quartz	Quartz = $SiO_{2(aq)}$	76.45	2.59E-2
Calcite	$CaCO_3 + H^+ = Ca^{2+} + HCO_3^-$	9.63	1.42E-3
K-Feldspar	K-Feldspar + $4H^+ = K^+ + Al^{3+} + SiO_{2(aq)} + 2H_2O$	3.50	1.15E-3
Smectite	Smectite + $7.8H^+ = 0.2K^+ + 1.25Al^{3+} + 3.5SiO_{2(aq)} + 4.9H_2O + 0.7Fe^{2+} + 0.1Na^+ + 0.025Ca^{2+} + 1.15Mg^{2+} + 0.05O_{2(aq)}$	8.23	1.63E+1
Muscovite	Muscovite + $10H^+ = 3SiO_{2(aq)} + 6H_2O + 3Al^{3+} + K^+$	0.31	1.10E+0
Siderite	Siderite + $H^+ = HCO_3^- + Fe^{2+}$	1.98	6.49E-4
Kaolinite	Kaolinite + $6H^+ = 5H_2O + 2Al^{3+} + 2SiO_{2(aq)}$		9.8
Gibbsite	Gibbsite + $3H^+ = 3H_2O + Al^{3+}$		9.8
Albite	Albite + $4H^+ = 2H_2O + Al^{3+} + Na^+ + 3SiO_{2(aq)}$		9.8
Ankerite	Ankerite + $2H^+ = Ca^{2+} + Mg^{2+} + 2HCO_3^-$		9.8
Chlorite	Chlorite + $10H^+ = 2Fe^{2+} + SiO_{2(aq)} + 2Al^{3+} + 7H_2O$		9.8
Chalcedony	Chalcedony = SiO2(aq)		9.8
Dolomite			9.8

Table 5.3: Fixed aquifer properties of the formation obtained from the literature. Geothermal gradient(John Warner 1993; Nathenson and Guffanti 1988). Hydrostatic gradient(Pashin et al. 2008), liquid relative permeability and capillary pressure(Van Genuchten 1980), and gaseous relative permeability(COREY and T. 1954).

Parameter	**Value/description**
Geothermal gradient	20°C/km
Hydrostatic gradient	0.43 psi/ft
Salinity (mass fraction)	0.06
CO_2 injection rate	20kg/s
Relative permeability	Liquid $K_{rl} = \sqrt{S^*}\left\{1 - \left(1 - [S^*]^{\frac{1}{m}}\right)^m\right\}^2$ $S^* = (S_l - S_{lr})/(1 - S_{lr})$ Irreducible water saturation, S_l = 0.30 Exponent, m = 0.457
	Gas $K_{rg} = (1 - S)^2 (1 - S^2)$ $S = \frac{(S_l - S_{lr})}{(S_l - S_{lr} - S_{gr})}$ Irreducible gas saturation, S_{gr} = 0.05
Capillary Pressure	$P_{cap} = -P_o([S^*]^{-\frac{1}{m}} - 1)^{1-m}$ $S^* = (S_l - S_{lr})/(1 - S_{lr})$ Irreducible water saturation, S_l = 0.30 Exponent, m = 0.457 Strength coefficient, P_o = 19.61kPa

A single CO_2 injection well of eight meters injection screen thickness is used for simulation into an initially saturated with a brine solution. Two-dimensional simulations of the injected CO_2 gas bubble used the van Genuchten function for capillary pressure and the van Genuchtem-Mualem model for water relative permeability, respectively (Mualem 1976; Van Genuchten 1980). The gas relative permeability for the two-phase system was modeled with Corey's curve (COREY and T. 1954). For this simulation, the activity of aqueous species is modeled using the extended Debye-Huckle equation (Helgeson and Kirkham 1974; Helgeson 1981).

The simulation steps included the equilibration of the formation mineral with brine, followed by constant CO_2 injection at 20 kg/s injection rate for ten years of simulation into the aquifer, and geochemical monitoring simulation of the injected CO_2

for forty years duration. The initial brine composition was determined via water-rock equilibration using a molal solution of sodium chloride until the brine-rock system attained equilibrium (Xu, Apps, and Pruess 2004).

As simulations progressed, the relative quantity of the aqueous, supercritical, and mineralized CO_2 in the system was tracked. For a given aquifer volume and porosity, the aqueous CO_2 mass is a function of water saturation, water density, and CO_2 mass fraction in water. The amount of supercritical CO_2 in the system is directly proportional to gas saturation and gas density for a given volume of the porous formation. The mass per unit volume of the carbonate precipitation over time is used to calculate the total CO_2 sequestered in the mineral phase. This result of the total sequestered CO_2 in the mineral phase is multiplied by the aquifer volume to obtain the cumulative mass of the mineralized CO_2. The degree of deviation from the homogenous aquifer and the heterogeneous aquifer is what will be determined as the impact of heterogeneity. Understanding the degree of this deviation of the heterogonous formation from the homogenous formation is necessary given that most natural aquifers have heterogeneous properties.

5.3 Result and Discussion

This section study presents the simulation results. Here we will compare the geochemical evolution of CO_2 in the homogeneous model with the heterogeneity model for each case of heterogeneity discussed here for a porous aquifer. The analysis will consider how heterogeneity in aquifer properties impacts sequestration efficiency. Where sequestration efficiency is the analysis of the amount of injected CO_2 that evolves from supercritical CO_2 to mineralized and aqueous CO_2. The term trapped CO_2 will be used here to refer to the summation of the amount of mineralized and aqueous CO_2 during the CO_2 sequestration process. Hence, the four parameters discussed here will focus on the evolution of the supercritical, mineralized, dissolved, and trapped CO_2.

5.3.1 Effect of Carbonate Mineralogy Heterogeneity

The effect of varying compositions of carbonate mineralogy at different grid cells in the model is shown here. Other aquifer properties are set as the value of the homogeneous model. The result of the simulated mass change in the amount of injected CO_2 for a carbonate-mineral heterogeneous and homogeneous formation is shown in Fig. 2. The result shows that the rate at which the injected CO_2 evolves into aqueous and mineralized CO_2 is greater during the injection phase for the heterogeneous model compared to the carbonate homogeneous model. As the reaction progresses the rate of aqueous dissolution and mineralization of CO_2 into the system becomes greater in the homogeneous model. Unlike in the aqueous CO_2 evolution where the rate of aqueous dissolution changed instantaneously, the transition happened over a prolonged period for the mineralization evolution.

The trapped CO_2 plot which combines the aqueous and mineralized CO_2 evolution shows that a heterogeneous carbonate mineralogy formation shows a higher estimation of sequestration efficiency in the early stages of the injection and sequestration phase. However, the homogenous system performed better in lowering the amount of supercritical injected CO_2 composition in a long-term perspective as depicted by the values at the end of the study period. Interestingly, the slightly over 0.2 million tons of deviation in the amount of trapped CO_2 was 75% a function of more aqueous dissolution of CO_2 in the homogenous model at 50 years.

One of the key drivers of the observation of carbonate heterogeneity is because carbonates in acidified brine undergo relatively fast dissolution to increase porosity and liberate divalent cations that encourage mineralization in the CO_2-acidified brine system(SHE et al. 2016; Smith et al. 2013). This ability to increase pore volume in a brine-saturated environment increases the brine volume available for supercritical CO_2 to dissolve into the aqueous phase. The effect of more divalent cation dissolution in brine through carbonate dissolution is a more favorable condition for the mineralization

of CO_2. The prolonged mineralization transition phase observed in figure 2 unlike the fast aqueous transition is a result of a kinetically controlled process of mineralization that is significantly slower than the transport-controlled process of aqueous dissolution. The time for this transition to occur in a particular storage site will depend on the unique kinetic and geochemical properties that characterize the formation.

The heterogeneous model has a mineral composition as high as 35% percentage carbonate composition. Therefore, the early trapping benefits of a heterogenous model over the homogenous model could be a result of the higher reactivity occurring at these high carbonate locations in the heterogeneous model. The progression of the reaction will result in a reduction of carbonate volume fraction which will eventually make the homogenous model have more number of high carbonate sites in the domain. This is the point when the observed transition in the amount of trapped CO_2 begins to favor a homogeneous system. These simulation results show that when the overall carbonate composition is equal in a domain, the domain with more sites with a higher fraction of carbonate minerals will create high reaction sites that favor mineral dissolution to liberate more positive divalent cations like calcium, magnesium, and iron which aid CO_2 mineralization.

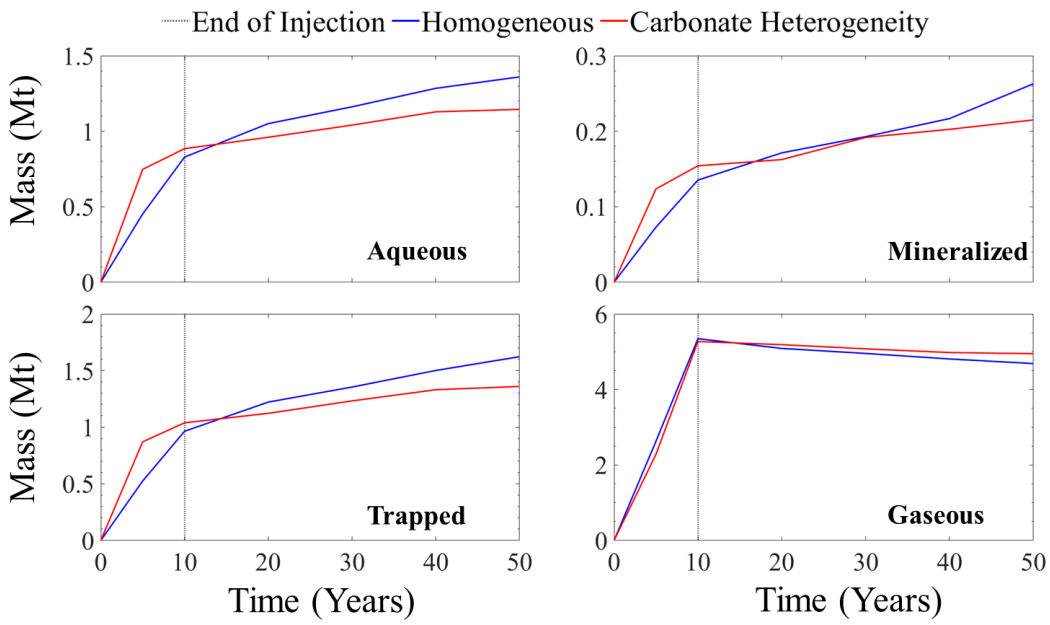

Figure 5.2: Comparison of the simulated aqueous, mineralized, trapped, and gaseous CO_2 in millions of metric tons over 50 years for simulations with varying carbonate mineral fractions. The red line represents the carbonate heterogeneity model, and the blue represents the homogeneous model.

5.3.1.2 Effect of Porosity Heterogeneity

Fig. 3 shows a higher rate of CO_2 mineralization in the porosity heterogeneous model throughout the study period. While the heterogeneous model mineralized approximately one hundred and twenty thousand more CO_2 than the homogenous model during the injection phase, the homogenous model mineralized approximately one thousand more tons of CO_2 per year relative to the heterogeneous model after the injection phase of CO_2. The aqueous CO_2 dissolution in both models reflects this trend. The heterogeneous porosity setup of the model encouraged higher aqueous CO_2 dissolution until the end of the injection phase as the mass of aqueous CO_2 at the end of injection appears to be equal. From that point of mass of aqueous CO_2 intersection, the mass of aqueous CO_2 in the homogeneous model maintains a higher rate of increase than in the heterogeneous model.

The trapped CO_2 result shows that the sequestration efficiency of the porosity heterogeneous model gives a higher estimation than the homogeneous model during the

injection phase. As the mineralization rate and the aqueous dissolution rate decrease in the heterogeneous model, the trapped CO_2 becomes higher for the homogeneous model to result in a better sequestration efficiency. Hence, there is lesser gaseous CO_2 in the homogeneous model at the end of the study period.

Here, the porosity values of the various grid cells in the domain are the only difference between the homogeneous and heterogeneous models. The observation that the variation in porosity causes initial high rate mineralization could be due to the ability of CO_2-saturated brine in grid cells with smaller porosity values to attain saturation conditions faster. Therefore the faster dissolution and mineralization in smaller pores encouraged the initial higher mineralization rate in the heterogeneous model. Typically, systems with faster dissolution conditions result in increased brine volume to accommodate more supercritical CO_2 dissolution. We see here that aqueous CO_2 was marginally higher in the heterogeneous model during the injection period when there is higher CO_2 mineralization and a faster dissolution period in the heterogeneous model. This portends the reason why the low porosity grid cells are the drivers of the mineral reactivity that favors higher mineralization in the heterogeneous model. Over time, the dominating reaction site of the heterogeneous model will be the high porosity grid cells which were initially as high as 15% more than the initial porosity of the homogeneous model. When these high porosity sites start to dominate the reaction, the mineralization rate becomes higher for the homogeneous model to indicate a faster dissolution and mineralization in the pores of the homogeneous model. In a field or experimental study, this can be similar to when precipitates have clogged the pores to preclude reaction at certain pores(Lin et al. 2021; Miri and Hellevang 2016).

The driving condition for reaction during the spatial variation in porosity is the spatial water-rock ratio in the grid blocks. Given equal availability of carbonate to mineralize the injected CO_2, more reaction sites with lower water-rock ratios will attain

faster saturation conditions which determines the model that dominates in the rate of CO_2 mineralization.

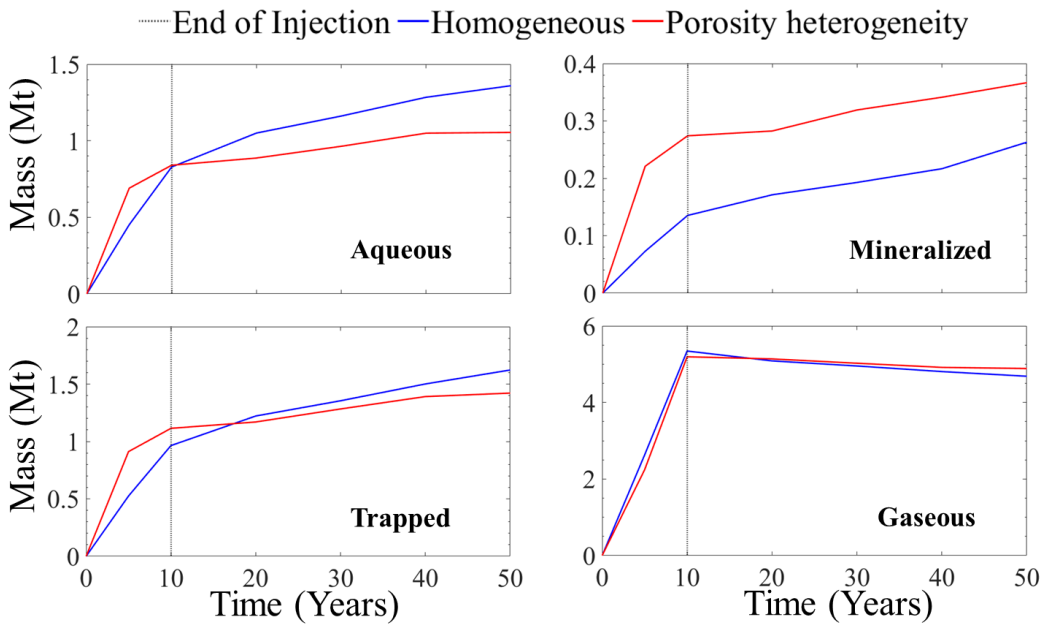

Figure 5.3: Comparison of the simulated aqueous, mineralized, trapped, and gaseous CO_2 in millions of metric tons over 50 years for simulations with varying carbonate mineral abundance. The red line represents the carbonate heterogeneity model, and the blue represents the homogeneous model.

5.3.1.3 Effect of Temperature Gradient

The homogenous simulation in this case is modeled with uniform temperature throughout the domain. The heterogeneous model considers the effect of variations in temperature with depth. The result evaluates the sequestration efficiency of injected CO_2 in the two models of the porous saline aquifer. Here, the simulation of CO_2 injection into the porous aquifer is modeled to be injected through the deepest part of the domain. Since temperature increases with depth, this also corresponds to the highest temperature region in the heterogeneous model.

The simulation result shows a similar trend in the behavior of the aqueous and mineralized CO_2 but there is a higher rate of converting the injected CO_2 to the aqueous and mineralized phase in the heterogeneous model. Consequently, the trapped CO_2 result shows that sequestration efficiency is estimated to be higher for the

heterogeneous model and the resulting mass of injected supercritical CO_2 remaining in the heterogeneous model is smaller than in the homogeneous model for the whole study period.

The homogeneous and heterogeneous models have an equal average aquifer temperature condition. The difference is that the peak temperature condition of the heterogeneous model is higher and the CO_2 injection occurs through the high-temperature zone. Since the plot of the mass comparison of CO_2 evolution shows that the heterogeneous model consistently maintained higher sequestration efficiency, this points to the importance of understanding the temperature and pressure condition of the target aquifer, especially in the vicinity of the injection zone. Poor understanding of the factors like temperature, as studied here, could lead to potential underestimation of CO_2 evolution at a storage site as the kinetic conditions that drive geochemical reactions may be significantly understimated.

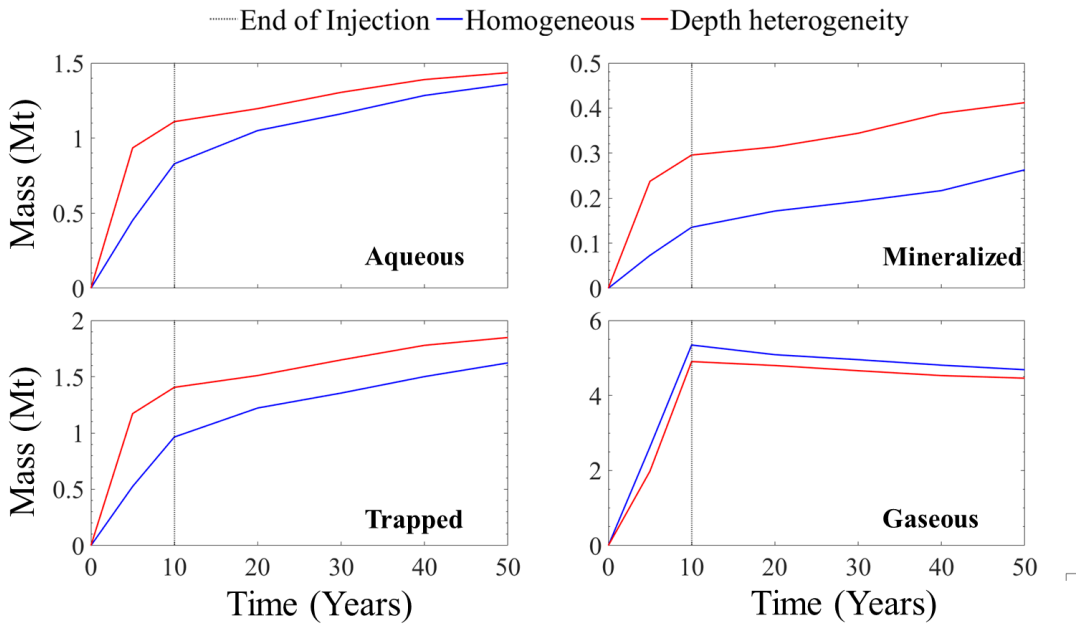

Figure 5.4: Comparison of the simulated aqueous, mineralized, trapped, and gaseous CO_2 in millions of metric tons over 50 years for simulations with varying carbonate mineral fractions. The red line represents the carbonate heterogeneity model, and the blue represents the homogeneous model.

5.4 Conclusion

The major goal of this study is to investigate the implication of aquifer heterogeneity on sequestration efficiency. A homogeneous and heterogeneous model was developed to evaluate heterogeneity in the formation. Here, the heterogeneous model was initialized with a range of aquifer properties and was randomly distributed in the grid cells of a two-dimensional model such that the average value of the aquifer property is equal to the value of a homogeneous model. The deviation in the simulation results of the homogeneous and heterogeneous models were observed over a fifty years study period that comprised of an injection phase of ten years and a CO_2 monitoring phase of forty years.

Numerical simulations have been a powerful tool to analyze the evolution in the formation. Previous studies have contributed to understanding the impact of aquifer heterogeneity on the CO_2 sequestration process. This study presents heterogeneity as it affects field-scale sequestration of CO_2 to provide the perspective on the aquifer property homogenization during the site investigation process that preceded every CO_2 sequestration development. Therefore, this study has uniquely used numerical modeling to understand if we need every detail of a well-characterized aquifer property before we can predict the evolution of gaseous CO_2 to mineralized, and solubility trapping of CO_2 as a result of changing aquifer properties.

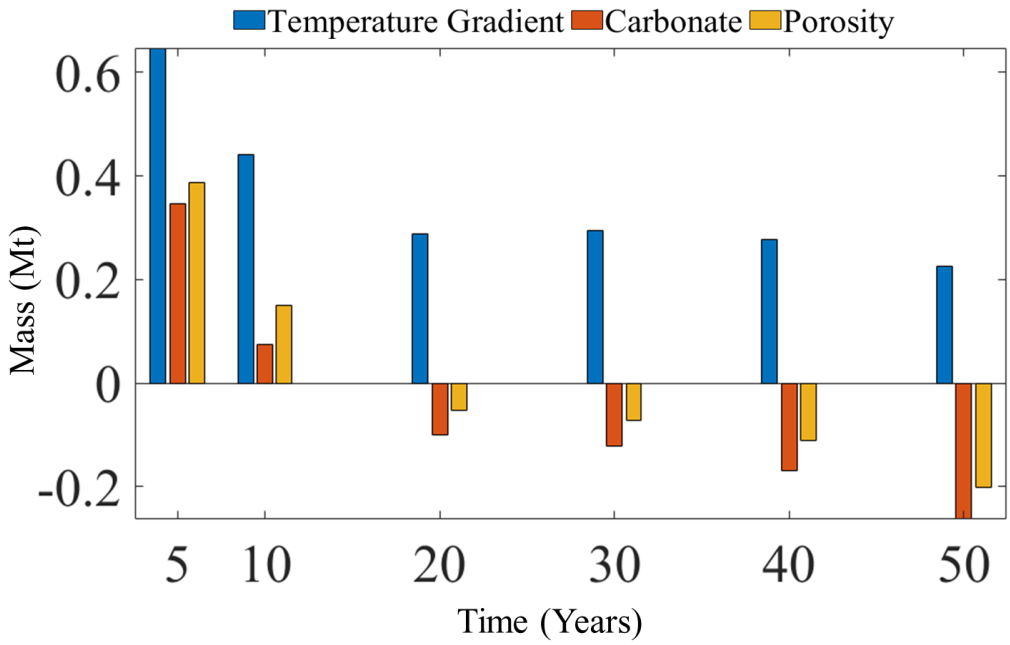

Figure 5.5: Simulated mass comparison in millions of metric tons of the difference between the trapped CO_2 in the homogeneous and heterogeneous model of the aquifer properties. The blue, orange, yellow, and purple bar represents the temperature gradient, permeability, carbonate, and porosity, respectively. A bar with a value of 2Mt means that the difference in trapped CO_2 for the homogeneous model and heterogenous is 2Mt.

Fig 5.5 shows that the homogenization of the property of an aquifer obtained from site investigation studies will yield a lower estimate of the sequestration efficiency during the injection phase of injecting CO_2 into a subsurface aquifer. However, the use of one porosity and carbonate mineralogy value to homogenize the aquifer properties yields a higher estimation of the geochemical capability of a formation to trap the injected CO_2 during the post-injection phase of CO_2 sequestration. Using the variation of aquifer temperature and pressure properties to study the trapping of CO_2 in a formation consistently produced a higher estimation of sequestration efficiency than the homogenized aquifer temperature and pressure value. Combining the differential analysis of figure 5.5 as a function of the maximum trapped CO_2 we find that based on the unique properties of the model setup in this study, the maximum deviation between the homogeneous and heterogenous formation ranges from 60% during the injection

phase of the project to 10% at the end of the study period. Hence, the result of this study shows that estimating the sequestration efficiency of a formation will largely depend at the phase of the project. The approach, however, serves as a guideline for predicting the possible range of estimating sequestration efficiency of a potential target aquifer.

5.5 Acknowledgments

Authors Iloejesi and Beckingham acknowledge support from the Southeast Regional CO_2 Utilization and Storage Acceleration Partnership (SECARB-USA) project funded by the U.S. Department of Energy and cost-sharing partners under grant number FE0031830, managed by the Southern States Energy Board.

5.6 References

Arnette, A.N., 2017. Renewable energy and carbon capture and sequestration for a reduced carbon energy plan: An optimization model. *Renewable and sustainable energy reviews*, *70*, pp.254-265. https://doi.org/10.1016/j.rser.2016.11.218.

Bachu, S., Gunter, W.D. and Perkins, E.H., 1994. Aquifer disposal of CO2: hydrodynamic and mineral trapping. *Energy Conversion and management*, *35*(4), pp.269-279. https://doi.org/10.1016/0196-8904(94)90060-4.

Beckingham, L.E., Mitnick, E.H., Steefel, C.I., Zhang, S., Voltolini, M., Swift, A.M., Yang, L., Cole, D.R., Sheets, J.M., Ajo-Franklin, J.B. and DePaolo, D.J., 2016. Evaluation of mineral reactive surface area estimates for prediction of reactivity of a multi-mineral sediment. *Geochimica et Cosmochimica Acta*, *188*, pp.310-329. https://doi.org/10.1016/j.gca.2016.05.040.

Begum, R.A., Sohag, K., Abdullah, S.M.S. and Jaafar, M., 2015. CO2 emissions, energy consumption, economic and population growth in Malaysia. *Renewable and Sustainable Energy Reviews*, *41*, pp.594-601. https://doi.org/10.1016/j.rser.2014.07.205.

Bentham, M. and Kirby, M., 2005. CO2 storage in saline aquifers. *Oil & gas science*

and technology, *60*(3), pp.559-567. https://doi.org/10.2516/ogst:2005038.

Ciferno, J.P., Fout, T.E., Jones, A.P. and Murphy, J.T., 2009. Capturing carbon from existing coal-fired power plants. *Chemical Engineering Progress*, *105*(4), p.33.

Corey, A.T., 1954. The interrelation between gas and oil relative permeabilities. *Producers monthly*, pp.38-41. https://ci.nii.ac.jp/naid/20001335630.

Doughty, C., Freifeld, B.M. and Trautz, R.C., 2008. Site characterization for CO2 geologic storage and vice versa: the Frio brine pilot, Texas, USA as a case study. *Environmental Geology*, *54*(8), pp.1635-1656. https://doi.org/10.1007/s00254-007-0942-0.

Edmonds, J.A., Freund, P.F. and Dooley, J.J., 2002. *The role of carbon management technologies in addressing atmospheric stabilization of greenhouse gases* (No. PNWD-SA-5131). Pacific Northwest National Lab., Richland, WA (US).

Ennis-King, J. and Paterson, L., 2003, October. Role of convective mixing in the long-term storage of carbon dioxide in deep saline formations. In *SPE annual technical conference and exhibition*. OnePetro.

Forster, A., Norden, B., Zinck-Jørgensen, K., Frykman, P., Kulenkampff, J., Spangenberg, E., Erzinger, J., Zimmer, M., Kopp, J., Borm, G. and Juhlin, C., 2006. Baseline characterization of the CO2SINK geological storage site at Ketzin, Germany. *Environmental Geosciences*, *13*(3), pp.145-161. https://doi.org/10.1306/EG.02080605016.

Freund, P., 2003. Making deep reductions in CO2 emissions from coal-fired power plant using capture and storage of CO2. *Proceedings of the Institution of Mechanical Engineers, Part A: Journal of Power and Energy*, *217*(1), pp.1-7. https://doi.org/10.1243/095765003321148637.

Gaus, I., Audigane, P., André, L., Lions, J., Jacquemet, N., Durst, P., Czernichowski-Lauriol, I. and Azaroual, M., 2008. Geochemical and solute transport modelling for CO2 storage, what to expect from it?. *International journal of greenhouse gas*

control, *2*(4), pp.605-625. https://doi.org/10.1016/J.IJGGC.2008.02.011.

Van Genuchten, M.T., 1980. A closed-form equation for predicting the hydraulic conductivity of unsaturated soils. *Soil science society of America journal*, *44*(5), pp.892-898.

Helgeson, H.C., 1981. Prediction of the thermodynamic properties of electrolytes at high pressures and temperatures. *Physics and Chemistry of the Earth*, *13*, pp.133-177. https://doi.org/10.1016/0079-1946(81)90009-4.

Helgeson, H.C. and Kirkham, D.H., 1974. Theoretical prediction of the thermodynamic behavior of aqueous electrolytes at high pressures and temperatures; II, Debye-Huckel parameters for activity coefficients and relative partial molal properties. *American Journal of Science*, *274*(10), pp.1199-1261.

Hovorka, S.D., Doughty, C., Benson, S.M., Pruess, K. and Knox, P.R., 2004. The impact of geological heterogeneity on CO2 storage in brine formations: a case study from the Texas Gulf Coast. *Geological Society, London, Special Publications*, *233*(1), pp.147-163. https://doi.org/10.1144/GSL.SP.2004.233.01.10.

IPCC. 2005. "Special Report on Carbon Dioxide Capture and Storage. Prepared by Working Group III of the Intergovernmental Panel on Climate Change." *Environmental Science and Technology*.

Jalali, J., Koperna, G.J., Cyphers, S., Riestenberg, D. and Esposito, R., 2021, March. Large Volume CO2 Storage and Plume Management in the Southeastern US; Reservoir Characterization and Simulation. In *Proceedings of the 15th Greenhouse Gas Control Technologies Conference* (pp. 15-18). https://doi.org/10.2139/SSRN.3867756.

Warner, A.J., 1993. *Regional geologic framework of the Cretaceous, offshore Mississippi*. Mississippi Department of Environmental Quality, Office of Geology.

Juhlin, C., Giese, R., Zinck-Jørgensen, K., Cosma, C., Kazemeini, H., Juhojuntti, N., Lüth, S., Norden, B. and Förster, A., 2007. 3D baseline seismics at Ketzin,

Germany: the CO 2 SINK project. *Geophysics*, *72*(5), pp.B121-B132. https://doi.org/10.1190/1.2754667.

Kuuskraa, V., Koperna, G. and Riestenberg, D., 2020. *Commercial Development Plan (Deliverable 8.2)* (No. DOE-SSEB-0029465-58). Southern States Energy Board, Peachtree Corners, GA (United States).

Lengler, U., De Lucia, M. and Kühn, M., 2010. The impact of heterogeneity on the distribution of CO2: Numerical simulation of CO2 storage at Ketzin. *International Journal of Greenhouse Gas Control*, *4*(6), pp.1016-1025.

Lin, Q., Akai, T., Blunt, M.J., Bijeljic, B., Iwama, H., Takabayashi, K., Onaka, Y. and Yonebayashi, H., 2021. Pore-scale imaging of asphaltene-induced pore clogging in carbonate rocks. *Fuel*, *283*, p.118871. https://doi.org/10.1016/J.FUEL.2020.118871.

McCrone, Angus, Ulf Moslener, Eric Usher, Christine Grüning, Virginia Sonntag-O'Brien, Victoria Cuming, Luke Mills, et al. 2015. "Global Trends in Renewable Energy Investment 2015." *Frankfurt School of Finance & Mangement*.

Miri, R. and Hellevang, H., 2016. Salt precipitation during CO2 storage—A review. *International Journal of Greenhouse Gas Control*, *51*, pp.136-147. https://doi.org/10.1016/J.IJGGC.2016.05.015.

Morad, S., Al-Ramadan, K., Ketzer, J.M. and De Ros, L.F., 2010. The impact of diagenesis on the heterogeneity of sandstone reservoirs: A review of the role of depositional facies and sequence stratigraphy. *AAPG bulletin*, *94*(8), pp.1267-1309. https://doi.org/10.1306/04211009178.

Mualem, Y., 1976. A new model for predicting the hydraulic conductivity of unsaturated porous media. *Water resources research*, *12*(3), pp.513-522. https://doi.org/10.1029/WR012I003P00513.

Nathenson, M. and Guffanti, M., 1988. Geothermal gradients in the conterminous United States. *Journal of Geophysical Research: Solid Earth*, *93*(B6), pp.6437-6450. https://doi.org/10.1029/JB093iB06p06437.

NETL. 2015. “Carbon Storage Atlas: Fifth Edition.” *U.S. Department of Energy-National Energy Technology Laboratory-Office of Fossil Energy*.

Niemi, A., Edlmann, K., Carrera, J., Juhlin, C., Tatomir, A., Ghergut, I., Sauter, M., Bensabat, J., Fagerlund, F., Cornet, F.H. and Vilarrasa, V., 2017. Site characterization. In *Geological Storage of CO2 in Deep Saline Formations* (pp. 309-380). Springer, Dordrecht. https://doi.org/10.1007/978-94-024-0996-3_7.

Pashin, J.C., Hills, D.J., Kopaska-Merkel, D.C. and McIntyre, M.R., 2008. Geological evaluation of the potential for CO2 sequestration in Kemper County. *Mississippi: Birmingham, Final Report, Southern Company Research & Environmental Affairs*.Pruess, Karsten. 2005. “ECO2N: A TOUGH2 Fluid Property Module for Mixtures of Water, NaCl, and CO 2.”

Qin, F. and Beckingham, L.E., 2019. Impact of image resolution on quantification of mineral abundances and accessible surface areas. *Chemical Geology*, *523*, pp.31-41. https://doi.org/10.1016/j.chemgeo.2019.06.004.

Riaz, A., Hesse, M., Tchelepi, H.A. and Orr, F.M., 2006. Onset of convection in a gravitationally unstable diffusive boundary layer in porous media. *Journal of Fluid Mechanics*, *548*, pp.87-111. https://doi.org/10.1017/S0022112005007494.

Min, S.H.E., Jianfeng, S.H.O.U., Anjiang, S.H.E.N., Liyin, P., Anping, H.U. and Yuanyuan, H.U., 2016. Experimental simulation of dissolution law and porosity evolution of carbonate rock. *Petroleum Exploration and Development*, *43*(4), pp.616-625. https://doi.org/10.1016/S1876-3804(16)30072-6.

Smith, M.M., Sholokhova, Y., Hao, Y. and Carroll, S.A., 2013. CO2-induced dissolution of low permeability carbonates. Part I: Characterization and experiments. *Advances in Water Resources*, *62*, pp.370-387.https://doi.org/10.1016/J.ADVWATRES.2013.09.008.

Xu, T., Sonnenthal, E., Spycher, N. and Zheng, L., 2017. TOUGHREACT V3. 32 reference manual: A parallel simulation program for non-isothermal multiphase geochemical reactive transport. *Lawrence Berkeley National Laboratory,*

Berkeley, CA.

Tullis, J. and Yund, R.A., 1982. Grain growth kinetics of quartz and calcite aggregates. *The Journal of Geology*, *90*(3), pp.301-318. https://doi.org/10.1086/628681.

Wardlaw, N.C. and Taylor, R.P., 1976. Mercury capillary pressure curves and the intepretation of pore structure and capillary behaviour in reservoir rocks. *Bulletin of Canadian Petroleum Geology*, *24*(2), pp.225-262. https://pubs.geoscienceworld.org/cspg/bcpg/article-abstract/24/2/225/57123.

Weber, K.J., 1982. Influence of common sedimentary structures on fluid flow in reservoir models. *Journal of Petroleum Technology*, *34*(03), pp.665-672. https://doi.org/10.2118/9247-PA.

Xu, T., Apps, J.A. and Pruess, K., 2004. Numerical simulation of CO2 disposal by mineral trapping in deep aquifers. *Applied geochemistry*, *19*(6), pp.917-936. https://doi.org/10.1016/J.APGEOCHEM.2003.11.003.

Zemke, K., Liebscher, A. and Wandrey, M., 2010. Petrophysical analysis to investigate the effects of carbon dioxide storage in a subsurface saline aquifer at Ketzin, Germany (CO2SINK). *International Journal of Greenhouse Gas Control*, *4*(6), pp.990-999. https://doi.org/10.1016/J.IJGGC.2010.04.008.

Zhang, S. and DePaolo, D.J., 2017. Rates of CO2 mineralization in geological carbon storage. *Accounts of chemical research*, *50*(9), pp.2075-2084. https://doi.org/10.1021/acs.accounts.7b00334.

Chapter 6. Conclusions and contribution to new knowledge

6.1 Assessment of Geochemical Limitations to Utilizing CO_2 as a Cushion Gas in Compressed Energy Storage Systems

Chapter 2 presents a study that evaluates the principle of the cushion gas utilized in stabilizing the cyclic pressure associated with the injection and extraction flow condition during the operation of a compressed energy storage system. Since CO_2 has been understood to have several advantages as a cushion gas, the aim of the study was to investigate the geochemical consequence associated with utilizing CO_2 as a cushion gas of a compressed energy storage system developed in a porous saline aquifer. This analysis involved developing two core-scale reactive transport simulations. One reactive transport simulation models the case of CO_2 sequestration which involves a one-directional flow of acidified through the model. The other novel reactive transport simulation model developed in this work models the cyclic flow condition of the compressed energy storage system. The advanced knowledge base for the CO_2 sequestration simulation serves as a benchmark to detect the possible deviation observed in the compressed energy storage simulation.

The simulation results yield geochemical indicators like influent and effluent species concentration, saturation indices, porosity evolution, and mineral precipitation and dissolution reactions. Comparing the results from both simulations from different stages shows that the injected CO_2 initially creates conditions that favor mineral dissolution. However, the dissolution extent becomes limited in the cyclic flow condition of the compressed energy storage after the first injection cycle. This is why the domain of the CO_2 sequestration model showed uniform increases in porosity over the length of the domain. In contrast, a non-uniform dissolution was observed in the cyclic flow condition as the porosity increase was observed at the inlet and outlet.

The new knowledge gained from the implication of this result shows that the rate and the extent of the geochemical behavior of CO_2 in a cyclic flow condition allow CO_2 to be a viable choice of cushion gas. This result shows the need for researchers to

evaluate the complete flow conditions in a system to understand the potential effect of the different flow conditions. The result of this study is informative to researchers who need more basis to explore the thermodynamic advantages of CO_2 as cushion gas as thermodynamic analysis has shown that CO_2 can improve the operational efficiency of the compressed energy system.

6.2 Effect of energy storage on geochemical reactions in porous aquifer energy storage systems

Our previous study has established that CO_2 can be used as a cushion gas in a compressed energy storage system. This study aims to utilize the novel simulation technique developed in the previous study to understand the geochemical reactivity of the system during the storage conditions of the compressed energy system. The previous work investigated a continuous cyclic condition of the cushion gas that occurs as the working gas is continuously used for injecting and extracting CO_2 from the system. However, there is another scenario where the compressed energy system could be intermittently used for energy storage. Therefore, there is a need to understand how this condition affects the viability of CO_2 as cushion gas. Here, we model an additional flow condition that comprises injection, storage, and extraction to understand how it differs from the continuous injection and extraction flow condition.

This study presented in Chapter 3, equally uses a reactive transport modeling developed in CrunchFlow to simulate the geochemical reactions induced by the injection and extraction flow regime as well as the injection, storage, and extraction flow regime for 15 years study period. The result of the study on operational schedule shows that while some reactivity might occur at the inlet of the domain, the pore structure of the inner domain is significantly preserved during the cycling of CO_2 acidified brine for both systems. Hence the geochemical indicators for both systems show that very small differences occur in the simulations for both flow conditions.

This work provides new and valuable geochemical insights on the long-term utilization of CO_2 as cushion gas under all possible operational scenarios (continuous operation and intermittent operation). It also provides the researchers the confidence to explore the other benefits of utilizing CO_2 as a cushion gas in a compressed energy system. Using CO_2 as cushion gas not only improve the operational efficiency of the system but also serves as an approach to sequestering large volume of the gas.

6.3 Field Scale Insight Towards Understanding Impact of Aquifer Properties on Extent and Timeline of CO2 Trapping.

In the third work presented in Chapter 4, we aim to understand how aquifer properties impact the sequestering of injected CO_2. This analysis takes advantage of the ability of numerical simulations to predict the evolution in the formation. Several studies have previously tried to explain the relationship between CO_2 sequestration and various factors that can affect the process. These explanations have looked at all the scales of the processes involved. However, non of the studies have taken a field-scale approach to monitoring the evolution of CO_2 mineralization, solubility trapping, and gaseous CO_2 as a result of changing aquifer properties. The aquifer properties investigated in this study include porosity, permeability, carbonate mineralogy, and depth. The values of these aquifer properties were varied systematically in a base model to understand how these aquifer properties impact sequestration efficiency. The values used to vary the aquifer properties are the maximum and minimum values of the properties reported in the literature that we research. The value of the base model is based on the Paluxy formation located in the southeastern region of the united states.

The result of the TOUGHREACT reactive transport simulation tracks the amount of gaseous, aqueous, and mineralized CO_2 after the injection and sequestration period. Therefore, the sequestration efficiency monitored here is defined as the rate at which the CO_2 injected into the aquifer is converted to aqueous or mineralized CO_2. The simulation results show that the aquifer properties impact the sequestration

efficiency. Also, the impact of aquifer properties on CO_2 evolution depends on the stage of the sequestration project.

The new knowledge provided by the analysis of the work reveals that the amount of CO_2 sequestered during the injection phase of the CO_2 sequestration project depends on understanding the amount of carbonate mineralogy of an aquifer since carbonate mineralogy has the most significant impact on predicting the evolution of injected CO_2. Post injection of CO_2 into a target aquifer, the depth of the storage reservoir has the largest impact on the evolution of CO_2. The findings from this research can be beneficial to research that aims to quantify the amount of injected CO_2 in a prospective storage site that can be sequestered. The approach used in this study can be adapted for a unique site by using precise values of aquifer properties and kinetic parameters to understand key considerations in selecting a storage site for a CO_2 project. In addition, consideration of injection and the post-injection response of the aquifer to CO_2 will help develop the best injection schedule to optimize CO_2 sequestration.

6.4 Impact of Aquifer Heterogeneity on Simulated CO_2 Trapping Mechanisms in Porous Saline Aquifers

The final work in Chapter 5 of this thesis focus on understanding heterogeneity impacts on CO_2 trapping efficiency. The site investigation process conducted before CO_2 injection into an aquifer inspects aquifer properties to access storage capacity, potential environmental safety, and suitability for trapping and permanent sequestration of the injected CO_2. The suitability of an aquifer for permanent CO_2 trapping is often assessed via reactive transport models. Simulations are often constructed based on limited data, and measurements of formation properties from a limited number of core samples. As such, simulations often consider homogenous formation properties. In reality, aquifer properties are heterogeneous and the impact of these heterogeneities on simulated CO_2 trapping mechanisms and efficiency is not well understood and is the

focus of this work. This work presents a novel study of understanding how the heterogeneity of aquifer properties in a formation impacts sequestration efficiency.

Two sets of models were developed for this study. The first set is a homogeneous model. The second set is the heterogeneous model. In the heterogeneous model, the spatial heterogeneity is developed in the grid cells by stochastic assignment of aquifer properties to the grid cells of the model. Despite the random assignment of aquifer properties to the grid cells, the average value of the aquifer properties used to initialize the entire grid cells in the heterogeneous model will match the initial condition assigned to the entire grid cells for the homogeneous model.

The output of the TOUGHREACT reactive transport simulation is used to calculate the relative gaseous, aqueous, and mineralized CO_2 for the homogenous and heterogeneous model for a 50 years study period. The result shows that the homogenization of aquifer property will relatively underestimate the sequestration efficiency during the injection phase of injecting CO_2 into a subsurface aquifer. However, the use of uniform porosity and carbonate mineralogy value to homogenize the aquifer properties yields a relative higher estimation of the geochemical capability of a formation to trap the injected CO_2 during the post-injection phase of CO_2 sequestration. Varying the aquifer temperature and pressure properties to study the trapping of CO_2 in a formation consistently produced a higher estimation of sequestration efficiency than the homogenized aquifer temperature and pressure value.

The new knowledge provided by the analysis of the work shows an approach for potential range in the estimation field-scale of CO_2 sequestration efficiency in a target formation. The deviation in the CO_2 sequestration efficiency predicted by the homogeneous and heterogeneous model shows that understanding the temperature and pressure condition of the target aquifer is necessary for the accurate prediction of sequestration efficiency. The findings from this research are beneficial to serve as a guide for the pre-injection estimation analysis of future storage sites.